Fall 12-5-2016

Memory Effects in Brownian Motion, Random Walks under Confining Potentials, and Relaxation of Quantum Systems

Matthew Chase
University of New Mexico

Recommended Citation

Matthew Chase

Candidate

Physics and Astronomy

Department

This dissertation is approved, and it is acceptable in quality and form for publication:

Approved by the Dissertation Committee:

Vasudev Kenkre

, Chairperson

Sudhakar Prasad

Dinesh Loomba

Luca Giuggioli

Memory Effects in Brownian Motion, Random Walks under Confining Potentials, and Relaxation of Quantum Systems

by

Matthew Chase

B.A, Colorado College, Colorado Springs, CO, May, 2009

M.S., Physics, University of New Mexico, Albuquerque, NM, 2014

DISSERTATION

Submitted in Partial Fulfillment of the

Requirements for the Degree of

Doctor of Philosophy

Physics

The University of New Mexico

Albuquerque, New Mexico

December, 2016

Dedication

Acknowledgments

Nitant, for your tireless efforts over the last three-plus years lighting my path. Whether or not one can be taught, I certainly learned a tremendous amount.

Satomi, for your friendship and deep ability to care. Without your prodding, I would never be finished.

Anastasia, Tzu-Cheng, Dave, for your inputs and questions. Learning physics with you all as been a blast.

To all my friends both in the department and out, here is to many more interesting drinks over a couple of conversations.

To my parents, your love and support, often met with stubbornness, was vital to all my achievements. Thank you so so much.

Memory Effects in Brownian Motion, Random Walks under Confining Potentials, and Relaxation of Quantum Systems

by

Matthew Chase

B.A, Colorado College, Colorado Springs, CO, May, 2009

M.S., Physics, University of New Mexico, Albuquerque, NM, 2014

Ph.D., Physics, University of New Mexico, 2016

Abstract

This dissertation is a report on a number of distinct topics in the field of non-equilibrium statistical mechanics including the evolution of classical as well as quantum systems.

The evolution of an object that is described by the Ornstein-Uhlenbeck process generalized through a time-nonlocal attraction is considered. The time-nonlocality is taken to be represented in the Langevin description through the presence of memory. Analysis of the Langevin equation is performed for algebraic and delay-type memories. An equivalent *bona-fide* Fokker-Planck equation is constructed.

A random walker subjected to a non-standard confining potential, taken to be a piece-wise linear function, is analyzed. Matching conditions for arbitrary joining configurations are given. Exact propagators in both the time- and Laplace-domains

are derived for the case of a 'V'-shaped potential. Two illustrative applications of such calculations are presented in the areas of chemical physics and biophysics.

The relaxation of quantum systems interacting with a thermal reservoir is studied. Calculations for specified bath spectral functions are presented. Our primary focus is the vibrational relaxation of an excited molecule and we provide a generalization of the Montroll-Shuler equation into the coherent domain. A related system, the Stark ladder, is briefly discussed.

Contents

Part 2: Simple Random Walk under Confinement

CONTENTS

Part 3: Approach to Equilibrium in Quantum Systems

Chapter 1

Introduction

In this thesis, we report on a few fundamental studies in the field of non-equilibrium statistical mechanics covering a number of distinct, unrelated, topics including the evolution of classical as well as quantum systems. The former include a Brownian particle subject to time-nonlocal memory effects and a random walker moving in a non-standard confining potential. The latter deals with the influence of an interaction with a thermal reservoir on the evolution of quantum systems. We also include the results of an additional investigation on a dimension effect in reaction-diffusion theory (Appendix A) on a topic unrelated to the rest of the thesis. As we cover a wide variety of topics, we have divided our discussion into three Parts. Each of the three Parts is divided into three Chapters. The first Chapter in the sequence serves to introduce the specific problem and provide motivation for its study; any techniques required for the analysis are introduced in this Chapter as well. The two Chapters that follow in each sequence contain the main elements of this thesis. Conclusions are presented internal to each Chapter. We provide a brief outline of the thesis here.

In the first Part (Chapters 2, 3, and 4), we discuss the effects of introducing time-nonlocality in the Ornstein-Uhlenbeck process. The time-nonlocality is taken

to be present in the Langevin description of the process. Chapter 3 proceeds with a direct analysis from the resulting Langevin equation while Chapter 4 presents a derivation of the equivalent *bona-fide* Fokker-Planck equation.

In the second Part (Chapters 5, 6, and 7), we analyze the effects of non-standard confinement on the motion of a random-walker, i.e., a diffusing particle. The confining potential is taken to be a simple piece-wise linear function consisting of joining two segments of equal and opposite slopes. In Chapter 6, we give expressions for various dynamic quantities and in Chapter 7 we describe two illustrative applications and present specific calculations relevant to their qualitative analysis.

In the third Part (Chapters 8, 9, and 10), we study the influence of a bath on the relaxation of quantum systems; a Generalized Master equation approach in the weak-coupling approximation is used. The requisite memories depend on a single bath spectral function through an integral transform. At equilibrium, the detailed balance condition is ensured by a simple restriction on the spectral function. In Chapter 9, we reproduce results for a simple, yet illustrative, system, the non-degenerate dimer analyzed earlier, and present explicit calculations of the bath spectral functions. In Chapter 10, we analyze vibrational relaxation of a molecule in a bath under conditions of high coherence. The related Stark ladder system is also briefly discussed.

Part 1: Brownian Motion with Memories

Chapter 2

Overview of Memory Effects in Brownian Motion

The Ornstein-Uhlenbeck process describes the motion of a particle under the effect of a harmonic restoring potential that is being subjected to white Gaussian noise. It arise frequently in statistical mechanics [1, 2]. In a one-dimensional system, the equation that governs the evolution of the probability density $P(x, t)$ at time t and position x, often referred to as the Smoluchowski equation, takes the form

$$\frac{\partial P(x, t)}{\partial t} = \frac{\partial}{\partial x}\left(\gamma x P(x, t) + D\frac{\partial P(x, t)}{\partial x}\right) \tag{2.1}$$

where γ gives the strength of the restoring force and D is the diffusion constant. The solution to Eq. (2.1) is well-known. It is similar to that of the simple diffusion equation provided that the time t undergoes a saturation transformation $t \to \mathcal{T}(t) = (1 - e^{-2\gamma t})/2\gamma$. In addition, an extra term that decays at the rate γ in a well known way modifies the standard initial condition term. Thus, for an initial condition $P(x, 0) = \delta(x - x_0)$,

$$P(x, t) = \frac{1}{\sqrt{4\pi D\mathcal{T}(t)}}e^{-\frac{(x - x_0 e^{-\gamma t})^2}{4D\mathcal{T}(t)}}$$

The focus in Chapters 3 and 4 is on systems in which the harmonic restoring force is time-nonlocal. One might be tempted to argue that such a generalization of the Ornstein-Uhlenbeck process could be performed directly in Eq. (2.1). The time-nonlocality would then be introduced into the potential term through a general memory function $\phi(t)$ with the simple transform,

$$\frac{d}{dx}\gamma x P(x,t) \to \frac{d}{dx}\gamma \int_0^t \phi(t-t')xP(x,t').$$

The evolution of $P(x,t)$ would then depend not only on the current time t but prior times t' as well. As will briefly be discussed in Chapter 3, however, this method leads to unphysical predictions. Our interest is in situations in which the physics of the problem introduces a memory $\phi(t)$ into the *Langevin* equation rather than in the probability equation. We have then, for the stochastic variable $x_i(t)$ (which represents the ith particle),

$$\frac{dx_i(t)}{dt} = -\gamma \int_0^t dt' \, \phi(t-t')x_i(t') + \xi_i(t), \tag{2.2}$$

where $\xi_i(t)$ is the noise. When the memory in Eq. (2.2) is a δ-function, i.e., when the equation is local in time, one reacquires the standard Langevin equation for $x_i(t)$ and the standard Smoluchowski equation for the probability density. The analysis that follows takes Eq. (2.2) as its starting point.

Newton's laws provide a simple example of how a time-nonlocal Langevin equation might arise. As should be well-known, Newton's second law of motion relates the force to an object's acceleration, i.e., the second derivative with respect to time a spatial coordinate. For many physical systems, it is standard, and appropriate, for these inertial, second-order terms to be neglected in the construction of the Langevin equation by making a high-damping approximation. This converts the second-order equations of Newton into first-order approximations that are reminiscent of Aristotle. However, one may find the high-damping approximation inappropriate in certain

physical situations. If one keeps the inertial term intact, both the coordinate x of the particle and its velocity v must be treated on an equal footing. Thus one is concerned with a probabilistic description that depend on both, i.e., one considers $P(x, v, t)$ rather than $P(x, t)$. If observables that are dependent only on the coordinate are of interest, a one-variable description can be introduced through the use of a memory function that relates the time derivative of x to an appropriate function of x, i.e., Eq. (2.2). A recent review of the mathematics of animal motion [3] discusses such a situation. In an alternative source of time-nonlocality, the physical signal related to the restoring force may propagate at a finite speed. Examples of such delays may be found in the study of Alzheimer walks [4] and a recent analysis of pairwise movement coordination [5] applicable to a system of foraging bats [6].

One is tempted to attempt the construction of a Fokker-Planck equivalent to Eq. (2.2) by defining for the ith particle the velocity at time t as $v_i(t) = dx_i(t)/dt$. Then, one performs the standard transformation from the particle description defined by $x_i(t)$ to a field description that is identified by the field variable x. Concretely, the microscopic definitions of the probability density $P(x, t)$ and its current density $j(x, t)$ are

$$P_1(x, t) = \langle \delta(x_i(t) - x) \rangle, \tag{2.3a}$$

$$j(x, t) = \left\langle \frac{dx_i(t)}{dt} \delta(x_i(t) - x) \right\rangle, \tag{2.3b}$$

where $\langle ... \rangle$ is the ensemble average. When the memory in Eq. (2.2) is a delta-function, the velocity, $v_i(t) = -\gamma x_i(t) + \xi_i(t)$, can be inserted into Eq. (2.3b) and its factor of $x_i(t)$ replaced by the field variable x due to the presence of $\delta(x - x_i(t))$ as a multiplying factor. If the noise is taken to be Gaussian, standard procedures [7] allow the averaged noise, $\langle \xi_i(t) \delta(x_i(t) - x) \rangle$, to be converted into a diffusive term. The result is the standard constitutive relation for the Ornstein-Uhlenbeck process

$$j(x, t) = -\left(\gamma x + D \frac{\partial}{\partial x} \right) P(x, t).$$

In tandem with the continuity equation,

$$\frac{\partial P(x,t)}{\partial t} + \frac{\partial j(x,t)}{\partial x} = 0,$$

one derives the Smoluchowski equation, Eq. (2.1). See the textbook by van Kampen [8] for an in-depth discussion of this procedure

If, however, the memory in Eq. (2.2) is retained, it is $x_i(t')$, not $x_i(t)$, that is present in the velocity. Thus, the velocity depends on the position of the ith particle not just at time t but for previous times as well. As the delta-functions in both of Eqs. (2.3) relate x only with the position of the particle at time t and not t', i.e., $x_i(t)$ and not $x_i(t')$, the conversion used in the Markoffian situation can not be performed. This technical failure to derive non-Markoffian field equations is a direct consequence of the time-nonlocal nature of the potential term in Eq. (2.2). A derivation of the Fokker-Planck representation equivalent to Eq. (2.2) requires the additional manipulation discussed in Chapter 4.

Our focus in Chapter 3 is on the Langevin description. We consider two explicit forms of the memory, algebraic and single delay, and compare their respective results with the well-understood exponential memory. Two quantities of potential experimental interest are discussed. In Chapter 4, we give a derivation of what is referred to in the literature as a *bona fide* Fokker-Planck description for the Ornstein-Uhlenbeck process by construction of a conditional probability distribution. We find the conditioned distribution to retain dependence on its history and contrast the resultant evolution with that of the propagator for an exponential memory.

We note that discussions in Chapters 3 and 4 should find applicability in systems far from equilibrium. These might include movement of animals that have a preference to places visited in the past [9] and, as in Alzheimer-related investigations [10], various versions of the concept of 'self-reinforced random walks'. The complexity of the biological nature of the systems involved necessitates a memory description

and the fact that we are not necessarily near equilibrium suggests that a fluctuation-dissipation relationship between the memory and the noise need not apply. Thus, we take the noise to be Gaussian and white noise as a useful first step.

Chapter 3

Langevin Analysis: Algebraic and Delay Memories

Langevin equations with memories have often been investigated in the past, but modern work on the topic appears to have begun with Budini and Cáceres [11]. However, their investigations were restricted primarily to the exponential memory with a focus on various kinds of non-Gaussian noise (radioactive, Poisson, Abel, etc.). Algebraic memories were touched upon in the context of fractional derivatives but no dissipation was assumed in their analysis. A more recent study of theirs analyzed stationary properties of memory-possessing Langevin equations of the algebraic and delay type [12]. Fractional derivatives have been used [13] to introduce what are in essence memory effects into fractional probability density equations. An interesting report in the literature by Fiscina et. al. [14] found that a Langevin equation with fractional derivatives accurately described the observed asymptotic spectral density of vibrated granular material. Drozdov [15] analyzed the stationary properties of Langevin equations using characteristic functionals for various noise distributions. Bolivar [16] reported on work that explored the dynamic behavior of a non-Markoffian Langevin equation for arbitrary Gaussian noise correlation functions through a focus

on the differentiability of the displacement. A Langevin equation with an exponential memory has also been analyzed with a path integral approach [17].

In a manner analogous to the work highlighted above, in the following Chapter we focus on the Langevin description of the time-nonlocal Ornstein-Uhlenbeck process. In Section 3.1, we derive general results for the average displacement and size of a particle whose motion is described by Eq. (2.2). To facilitate calculations, we have taken the noise to be white, i.e., δ-correlated. The processes we consider are far from equilibrium and do not obey a fluctuation-dissipation relation between the noise and the memory. Sections 3.2 and 3.3 of this Chapter focus on two memories of both conceptual and physical interest. Respectively, they are the algebraic and single delay memories. We find that, in the case of an algebraic memory, the Green function is the Mittag-Leffler function while for a single delay process the Green function is related to the Lambert function As in the well-understood case of the exponential memory, both Green functions display a regime in which they decrease monotonically and one in which they oscillate while they decay.

Section 3.4 discusses potential applications of our results through two specific experiments. The first discusses motional narrowing in the frequency-dependent susceptibility of our system. The particle is charged and a time-periodic electric field is applied. A measurement of the steady-state mean square displacement of the particle is discussed in the second. We conclude in Section 3.5 with four short interesting remarks. In the first, we compare the results for the three memories, the algebraic, the single delay, and the simple exponential, highlighting intriguing simi-larities and differences. The second discusses a natural but incorrect generalization of the Smoluchowski equation. Remarkably, its predictions are correct in the context of the first of the two experiments. In the third, we remark upon an apparent vio-lation of the Balescu-Swenson theorem, an important theorem in the understanding of the effects of memory. Lastly, we contrast the two-time correlation functions for

each of the three memories with its equivalent in the Markoffian limit.

3.1 A Route for the Description of Memory Effects

With our attention restricted to the Langevin equation, Eq. (2.2), we drop the label i and consider a single particle without loss of generality as the particles do not interact. With $\lambda(t)$ being the Green function of the homogenous (without noise) part of Eq. (2.2), an immediate consequence is

$$\widetilde{\lambda}(\epsilon) = \frac{1}{\epsilon + \gamma\widetilde{\phi}(\epsilon)}. \tag{3.1}$$

Here, tildes denote Laplace transforms and ϵ is the Laplace variable. This result leads to the solution of Eq. (2.2) in the time domain as

$$x(t) = \lambda(t)x(0) + \int_0^t dt'\lambda(t - t')\xi(t'). \tag{3.2}$$

An explicit calculation along these lines was given by San Miguel and Sancho in ref. [18]. From here onwards, we only consider systems in which the noise $\xi(t)$ has zero mean, $\langle\xi(t)\rangle = 0$, and is white, which means that $\langle\xi(t)\xi(s)\rangle = 2D\delta(t - s)$ where the constant D describes the strength of the noise. If one makes the reasonable assumption that the noise is uncorrelated with the initial value of the observation, the expectation values of arbitrary powers of x at a specified time can be calculated explicitly. The average displacement and the average squared displacement are

$$\langle x(t)\rangle = x_0\lambda(t), \tag{3.3}$$

$$\langle \Delta x^2(t)\rangle = \langle x(t)^2\rangle - \langle x(t)\rangle^2 = 2D\int_0^t ds\lambda^2(s), \tag{3.4}$$

where we take a localized initial condition, $x(0) = x_0$. In light of the fact that Eq. (2.2) already has $t = 0$ as a special instant at which the memory is initialized, we observe that there are now two, generally different, times 0 and t_0, the latter being the time at which $\langle x(t_0) \rangle$ is first measured, e.g., the initial observation time. For the sake of simplicity, we take $t_0 = 0$ though, generally, the two times can be different. This general case, for which the two times are different, leads to interesting subtleties which we discuss in Chapter 4. In the second line we have displayed the difference of the average of the square of the displacement and the square of its average. We represent it by the symbol $\langle \Delta x^2 \rangle$ and refer to it, rather than to $\langle x^2 \rangle$, as the mean square displacement (MSD). Expectation values of two-time quantities such as the correlation function $\langle x(t)x(s) \rangle$ can also be obtained straightforwardly:

$$\langle x(t)x(s) \rangle = x_0^2 \lambda(t)\lambda(s) + 2D \int_0^s dt' \lambda(t-t')\lambda(s-t'), \tag{3.5}$$

$$f(t,s) \equiv \langle x(t)x(s) \rangle - \langle x(t) \rangle \langle x(s) \rangle = 2D \int_0^s dt' \lambda(t-t')\lambda(s-t'). \tag{3.6}$$

The above results do *not* require that the noise be Gaussian. If, however, it is known to be Gaussian we can also write, for arbitrary powers of the displacement,

$$\langle x^n(t) \rangle = \begin{cases} \sum_{m=0}^{p} \frac{(2p)!}{(2m)!(p-m)!} [x_0\lambda(t)]^{2m} \left(D \int_0^t ds\, \lambda^2(t) \right)^{p-m} & \text{even n } (p \equiv \frac{n}{2}), \\ \sum_{m=0}^{p} \frac{(2p+1)!}{(2m+1)!(p-m)!} [x_0\lambda(t)]^{2m+1} \left(D \int_0^t ds\, \lambda^2(t) \right)^{p-m} & \text{odd n } (p \equiv \frac{n-1}{2}), \end{cases}$$

and thereby solve the entire problem on the basis of the Gaussian property.

3.2 Algebraic Memories in the Langevin Equation

The family of algebraic functions provides a useful case study of the class of memories that cannot be approximated via a Markoffian procedure. The latter means the

replacement of $\phi(t)$ for long times by a delta-function in t of strength $\int_0^\infty dt\phi(t)$. We consider such memories as our starting point for the present section:

$$\phi(t;\nu) = \frac{\alpha(\alpha t)^{\nu-1}}{\Gamma(\nu)}. \tag{3.7}$$

Here α is a positive constant with units of inverse time and the Gamma function, $\Gamma(\nu)$, provides the appropriate normalization. We analyze the Green function $\lambda(t)$.

The Laplace transform[1] of Eq. (3.7), and insertion into Eq. (3.1), gives the Laplace domain Green function as,

$$\widetilde{\lambda}(\epsilon;\nu) = \frac{1}{\epsilon + \frac{\gamma\alpha^\nu}{\epsilon^\nu}} = \frac{\epsilon^\nu}{\epsilon^{\nu+1} + \gamma\alpha^\nu} = \frac{1}{\epsilon\left(1 + \frac{\gamma\alpha^\nu}{\epsilon^{\nu+1}}\right)}, \tag{3.8}$$

the Laplace-domain representation of the Mittag-Leffler function of one parameter, which is written in usual notation as $E_{\nu+1}(-\gamma\alpha^\nu t^{\nu+1})$ [19]. In the time domain, setting $\gamma\alpha^\nu \equiv \zeta^{\nu+1}$, this results in the series,

$$\lambda(t;\nu) = \sum_{n=0}^\infty \frac{\left[-(\zeta t)^{(1+\nu)}\right]^n}{\Gamma(n(1+\nu)+1)}. \tag{3.9}$$

This expression is derived through a binomial expansion of the denominator in Eq. (3.8). One obtains a formal series in increasing powers of $(\zeta/\epsilon)^{1+\nu}$. A term-by-term inverse Laplace transform of this formal series results in Eq. (3.9) for all $\nu > -1$. The resulting series converges for all finite times.

For the parameter range of interest, the Green function we have calculated shows three interesting types of behavior. The first is an overdamped decay, $\nu \in (-1,0)$, the second is underdamped oscillations, $\nu \in (0,1)$, and the third unstable oscillations, $\nu \in (1,\infty)$. We depict $\lambda(t)$ for the cases of overdamped decay (left) and underdamped oscillations (right) in Fig. 3.1 over 16 dimensionless time units ζt.

---

[1]The Laplace transform of Eq. (3.7) only exists for $\nu > 0$. However, the form of the Laplace-domain Green function, Eq. (3.8), suggests extending the domain of validity to $\nu \geq -1$. In this range, the Green function is unity when $t = 0$ (except for $\nu = -1$ where $\lambda(t) = 1/2$).
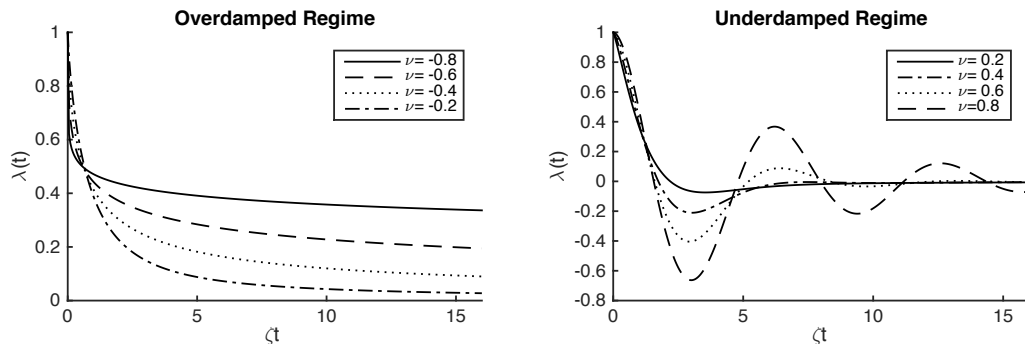
Figure 3.1: The Green function, $\lambda(t)$, is displayed for varying ν in Eq. (3.9) over the overdamped (left) and underdamped (right) regimes in the range $[-0.8, -0.2]$ and $[0.2, 0.8]$ in steps of 0.2. Time is plotted in units of $1/\zeta$. A more negative ν leads to $\lambda(t)$ approaching 0 more slowly, while a more positive ν results in the increased amplitude and persistence of the oscillations.

The overdamped regime exhibits sharper initial decays, but longer tails, as the value of ν is made more negative. The amplitude of oscillation and the time for which they persist both increase for increasing ν in the underdamped regime. The derivative of $\lambda(t)$ at $t = 0$ changes discontinuously when ν approaches 0 from either direction. For positive values of ν it vanishes. For negative values it tends to infinity. This behavior is sharply different from that in the case of the simple exponential memory characteristic of the damped harmonic oscillator. For the latter, the derivative of $\lambda(t)$ at $t = 0$ always vanishes. Not shown are the unstable oscillations for values of $\nu > 1$. Three special values of ν correspond with standard processes. For $\nu = -1$, we have standard Brownian diffusion, i.e., a Wiener process or an unconfined random walk. For $\nu = 0$, we have the standard Smoluchowski equation, and the time-local Ornstein-Uhlenbeck process. For $\nu = 1$, we have pure oscillations with no damping.

A second representation of $\lambda(t)$ is found by explicitly closing the Bromwich contour. For all non-integer values of ν, Eq. (3.8) has at least two singularities of interest: branch points at zero and infinity. Simple poles exist for all relevant values of ν at the points $\ln(\epsilon) = \pm i(1 + 2m)\pi/(\nu + 1)$ where m is an integer greater than zero.

By choosing the branch cut to be along the negative real axis, the domain of ϵ is restricted to $|\arg(\epsilon)| < \pi$. This limits the number of poles that fall on the relevant Riemann sheet, i.e., when $\nu < 0$, there are no simple poles while two additional poles move on to the Riemann sheet as ν passes through each successive even integer. The Bromwich integral of Eq. (3.8) can be performed to quadrature and results in

$$\lambda(t;\nu) = -\frac{\sin \nu\pi}{\pi} \int\limits_0^\infty dr \; e^{-r\zeta t} \frac{r^\nu}{r^{2(\nu+1)} - 2r^{\nu+1}\cos\nu\pi + 1}$$

$$+ \begin{cases} 0 & -1 < \nu \leq 0 \\ \frac{2}{\nu+1} e^{-\zeta t \cos\frac{\nu\pi}{\nu+1}} \cos(\zeta t \sin\frac{\nu\pi}{\nu+1}) & 0 < \nu \leq 2 \\ \frac{2}{\nu+1}\left[e^{-\zeta t \cos\frac{\nu\pi}{\nu+1}}\cos(\zeta t \sin\frac{\nu\pi}{\nu+1}) + e^{-\zeta t \cos\frac{3\nu\pi}{\nu+1}}\cos(\zeta t \sin\frac{3\nu\pi}{\nu+1})\right] & 2 < \nu \leq 4 \end{cases} \quad (3.10)$$

where $\lambda(0;\nu)$ equals 1 for all ν. The integral in Eq. (3.10) is the Laplace transform of a positive definite function and, for non-integer values of ν, is therefore non-negative at all times. As mentioned previously, additional exponential terms become relevant as ν is increased further.

We have given two separate representations of $\lambda(t)$ in the time domain: the series, Eq. (3.9), and the integral expression, Eq. (3.10). These are compared in Fig. 3.2, over a range of approximately 30 dimensionless time units for 2 values of ν in each regime, ± 0.1 and ± 0.9. The two representations match up well over shorter time periods. However, at longer times, the numerical implementation of the series leads to divergent results as a consequence of round-off errors.

The integral in Eq. (3.10) is not reducible in terms of known functions for arbitrary ν. For the particular case of $\nu = m + 1/2$, where m is an integer, a transform of $u = r^{1/2}$ simplifies the integrand to

$$(-1)^{m+1}\frac{2}{\pi} \int\limits_0^\infty du \; e^{-u^2\zeta t} \frac{u^{2(m+1)}}{u^{2(2m+3)} + 1}.$$

The denominator of this integral is easily factorable into the $(2m + 3)$th roots of
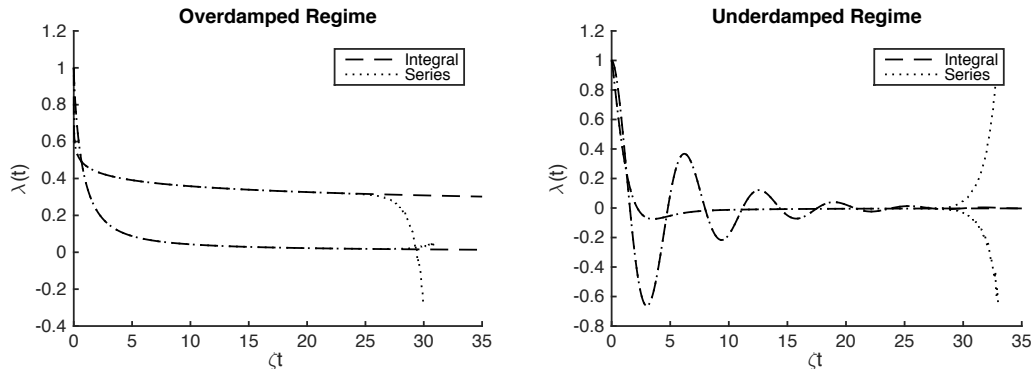
Figure 3.2: Depicts both the integral representation and the series representation of the Green function, $\lambda(t)$ for two values of $\nu = \pm 0.2, \pm 0.8$ each in the overdamped regime (left) and the underdamped regime (right). The series representation is indicated by dots and the integral representation by solid lines. At approximately 30 dimensionless time units ζt, the series begins to diverge as a result of numerical round-off results.

1. This results in the standard integral representation of the Faddeeva function, $w(iz) = \mathrm{erfcx}(z)$, which corresponds to the scaled error functions with complex arguments [20]. We give here the $\nu = -1/2 \ (m = -1)$ and $\nu = 1/2 \ (m = 0)$ cases:

$$\lambda\left(t; -\frac{1}{2}\right) = e^{\zeta t} \mathrm{erfc}\left((\zeta t)^{\frac{1}{2}}\right), \tag{3.11}$$

$$\lambda\left(t; \frac{1}{2}\right) = e^{-\frac{\zeta t}{2}} \cos\frac{3^{\frac{1}{2}}\zeta t}{2} + w\left(i\sqrt{\zeta t}\right) - w\left(i\sqrt{\zeta t}e^{\frac{i\pi}{3}}\right) - w\left(i\sqrt{\zeta t}e^{-\frac{i\pi}{3}}\right). \tag{3.12}$$

The long-time behavior of the Mittag-Leffler function, valid for non-integer values of ν in the region $(-1, 1)$, is well known [19],

$$\lambda(t \to \infty; \nu) = -\sum_{n=1}^{p} \frac{1}{\Gamma\left[1 - n(\nu+1)\right]} \left[\frac{-1}{(\zeta t)^{(\nu+1)}}\right]^{n} + \mathcal{O}(t^{-p(\nu+1)}). \tag{3.13}$$

We see that an algebraic memory results in an algebraic time-dependence of $\lambda(t)$ at long times. The dominant term in the series, proportional to $1/(\zeta t)^{1+\nu}$, leads to a decay which is stronger when ν is larger. In the underdamped regime, the leading

16
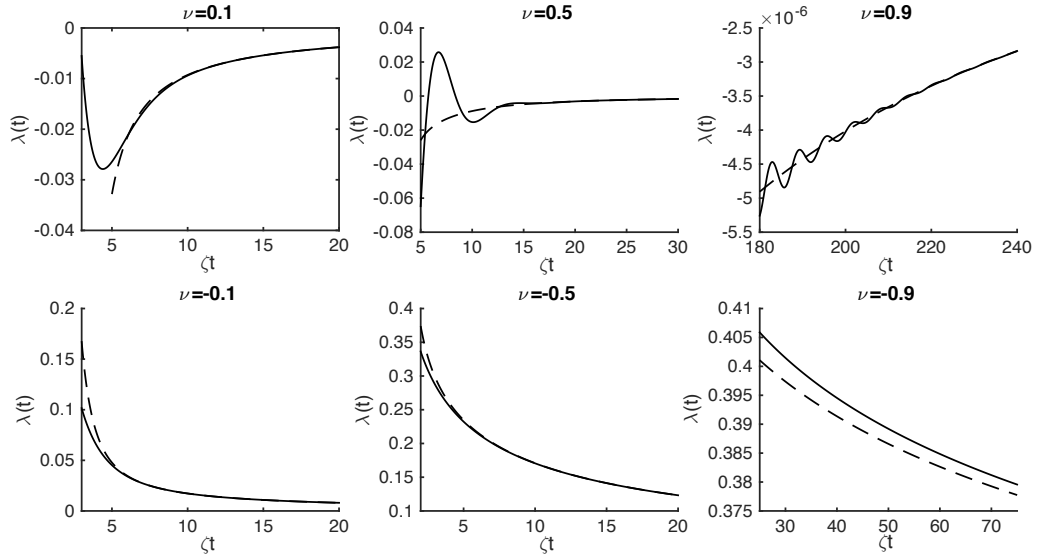
Figure 3.3: Long-time comparison of two expressions of the Green function: the integral expression, Eq. (3.10), shown with solid lines and its series approximation, Eq. (3.13), shown with dashed lines. The latter consists of the first 5 terms for 3 values of ν, 0.1 (left), 0.5 (center), and 0.9 (right) over differing time ranges.

term of Eq. (3.13) is negative. Therefore, at long times, $\lambda(t)$ approaches zero from below, confirming the existence of at least one minimum. This term is positive for the overdamped regime. The correspondence between the long-time approximation, Eq. (3.13) with 5 terms, and the full propagator is depicted in Fig. 3.3 for 6 values of ν: ± 0.1, ± 0.5, ± 0.9. The long-time approximation does not lead to oscillations, rather to an overall decay towards 0. For smaller values of $|\nu|$, the approximation becomes valid at earlier times.

Thus, the algebraic memory leads to a noiseless Green function that corresponds exactly to the Mittag-Leffler function. Three separate regimes emerge: overdamped decay, $-1 < \nu \leq 0$, underdamped oscillations, $0 < \nu < 1$, and unstable oscillations, $\nu \geq 1$.

3.3 Memories that Represent Delay Processes

We now briefly outline memories that represent delay processes [4, 5, 21–25]. A full discussion of such memories can be found in works by McKetterick and Giuggioli [5, 25]. Our focus here is on a memory with only a single time delay τ. Thus, we have

$$\phi(t) = \delta(t - \tau). \tag{3.14}$$

A complete analysis [5, 21] of delay processes requires an extension of the Eq. (2.2) to the time $-\tau < 0$ to avoid dealing with a piece-wise process with Wiener dynamics for $0 \leq t < \tau$ and delayed dynamics for $t \geq \tau$. The evolution of x then depends on the prior history of x during $-\tau \leq t \leq 0$. We refer the reader to [5] for a thorough discussion and treat here the simplest case in which the history is neglected. Thus, the delay process is defined by its Green function $\lambda(t)$, the Laplace-domain expression of which is

$$\tilde{\lambda}(\epsilon) = \frac{1}{\epsilon + \gamma e^{-\epsilon \tau}}. \tag{3.15}$$

Two equivalent time-domain expressions for Eq. (3.15) highlight properties of $\lambda(t)$ over different time scales. In the first, Eq. (3.15) is expanded in a formal power series and inverted term-by-term. This gives the following expression [4, 22–24]

$$\lambda(t) = \sum_{k=0}^{\infty} \frac{(-\gamma)^k}{k!} (t - k\tau)^k \Theta(t - k\tau), \tag{3.16}$$

where $\Theta(x)$ is the Heaviside step function. Eq. (3.16) is useful for short time calculations as only a finite number of terms are required to calculate $\lambda(t)$ for any finite time. Its functional dependence is a kth degree polynomial in the interval $k\tau \leq t \leq (k + 1)\tau$. An alternative functional form for $\lambda(t)$, found with the use of Cauchy's residue theorem, is given by

$$\lambda(t) = \sum_{\text{Res}} \frac{e^{\epsilon t}}{\epsilon + \gamma e^{\epsilon \tau}}, \tag{3.17}$$
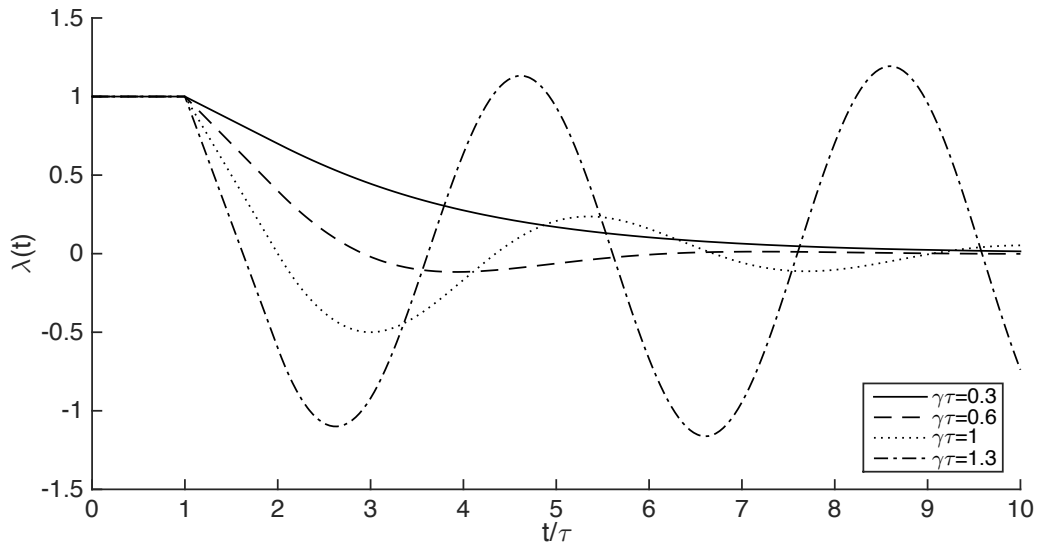
Figure 3.4: The single delay Green function $\lambda(t)$ for four values of $\gamma\tau = 0.3, 0.6, 1, 1.6$ are shown. The first represents the stable non-oscillatory regime, the next two represent the stable oscillatory regime and the last the unstable oscillatory regime.

where the summation is over the residues. The poles of Eq. (3.15) are the the roots of the characteristic equation, $\epsilon + \gamma\exp-\epsilon\tau = 0$. These poles are defined through the Lambert function [23,26] and, in particular, provide information about the long-time evolution of the system. Thus, the single delay process has three distinct behavioral regimes: monotonic decay, oscillatory decay, and unstable oscillations [21]. Fig. 3.4 displays illustrative examples of $\lambda(t)$ for each of the parameter regimes.

3.4 Application to Experiments and Comparison of Consequences of Different Memories

We discuss our predictions for the three cases of algebraic, single delay, and exponential memory in the context of two experiments that can, in principle, be performed.

The first involves motional narrowing of spectral lines and the second the spatial extension of the particle in the steady-state. The expression for the exponential memory is given by

$$\phi(t) = be^{-bt}, \tag{3.18}$$

with the b obeying $\gamma b = \omega^2$, the square of the oscillator frequency.

Eq. (3.18) appears not only in the damped harmonic oscillator analyzed by San Miguel and Sancho [18], but in numerous other contexts, including a description of transport with an arbitrary degree of quantum mechanical coherence given in the Frenkel exciton context by Kenkre [27–29]. Despite its introduction in the latter reference being in the context of site-to-site motion of a quasiparticle rather than of attraction towards a center, many of the expressions obtained, and much of the intuition, can be ported here. The Green function $\lambda(t)$ is well-known to be given by the simple expression

$$\lambda(t) = e^{-bt/2} \left[\cos \Omega t + (b/2\Omega) \sin \Omega t\right], \tag{3.19}$$

where $\Omega = \sqrt{\omega^2 - b^2/4}$. Eq. (3.19) displays standard features including the reduction of the original undamped oscillator frequency ω to Ω when damping is introduced via the damping exponent $b/2$ and passage from the damped oscillatory to the over-damped regime when $b/2 > \omega$. In the latter, trigonometric functions change into their hyperbolic counterparts leading to the phenomenon of motional narrowing of spectral lines.

3.4.1 Motional Narrowing of Spectral Lines

In the first experiment, the particles are charged and a time-varying electric field is applied (the particles do not interact among themselves). Thus, a forcing term is

added to Eq. (2.2), the label i being suppressed, to give

$$\frac{dx(t)}{dt} = -\gamma \int\limits_0^t dt'\, \phi(t - t')x(t') + \mathrm{E}(t) + \xi(t), \qquad (3.20)$$

This allows for the measurement of the polarization and, thus, the susceptibility. The latter is the ratio of the Fourier transforms of the polarization and the applied electric field. The term $\mathrm{E}(t)$ has absorbed unimportant proportionality constants and is essentially the electric field. The spectral line at frequency f is proportional to $\frac{\langle \hat{x}(f) \rangle}{\hat{\mathrm{E}}(f)}$ where the circumflexes denote Fourier transforms and f is the frequency. We use f rather than the more usual ω to distinguish it from the oscillator frequency that we have already used in our treatment.

A well-known phenomenon that occurs in systems with a simple exponential memory is motional narrowing. The spectral lines, narrow if the damping in the system is vanishing or small, broaden as the damping is increased. However, after a critical value of the damping is exceeded, separate lines coalesce and increased damping leads to a *narrowing* of the line. This effect, expected for the damped harmonic oscillator also occurs for the algebraic and single delay cases. One sees from Eq. (3.20) that the the frequency-dependent susceptibility is proportional to $\frac{\langle \hat{x}(f) \rangle}{\hat{\mathrm{E}}(f)}$ and, thus, that the one-sided Fourier transform of the Green function $\lambda(t)$ is required. From Eq. (3.19) for the exponential memory and Eq. (3.9) and Eq. (3.16) for the algebraic and single delay memories, respectively, we have

$$\hat{\lambda}(f) = \begin{cases} \dfrac{\sqrt{f^2 + b^2}}{\sqrt{(f^2 - \omega^2)^2 + f^2 b^2}} & \text{Exponential,} \quad (3.21a) \\[4mm] \dfrac{1}{\sqrt{f^2 - 2f\tau\mu^2 \sin f\tau + \tau^2\mu^4}} & \text{Single Delay,} \quad (3.21b) \\[4mm] \dfrac{(|f|)^\nu}{\sqrt{|f|^{2(\nu+1)} - 2\left(|f|\zeta\right)^{\nu+1} \sin \frac{\pi\nu}{2} + \zeta^{2(\nu+1)}}} & \text{Algebraic,} \quad (3.21c) \end{cases}$$

where we have given the absolute value of the Fourier transforms. In Eq. (3.21b)
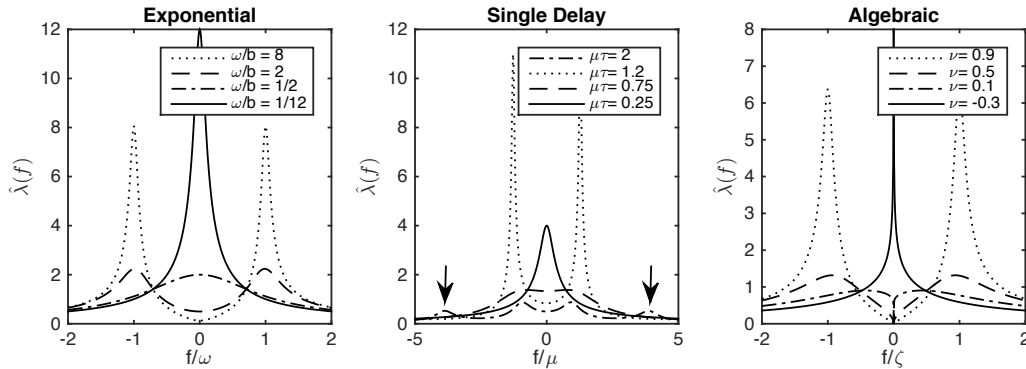
Figure 3.5: Susceptibility on the frequency f of the applied electric field for the three cases, exponential, single delay, and algebraic, in the left, center, and right panels, respectively. Motional narrowing is seen as each displays two peaks in the coherent limit which, as damping is increased, initially broaden and move towards each other (to the center, i.e., the region $f = 0$). An increase in the damping beyond a critical value in each case, however, leads to a *narrowing* rather than a broadening. Frequency is plotted on the horizontal axis in units of the coherent parameter ω, μ and ζ for the three respective cases. The vertical axis units are arbitrary. Two arrows in the central panel locate the additional peaks that develop for the single delay process. The sharp transition at $f = 0$ for the algebraic memory, which is a jump from a vanishing to an infinite value, can be seen when comparing the $\nu = -0.3$ case with the $\nu = 0.1$ case.

we have introduced the coherence parameter $\mu = \sqrt{\gamma/\tau}$ for the delay case and is analogous to ω in the exponential case and ζ in the algebraic case.

We show the results of Eq. (3.21) in Fig. 3.5 for the exponential (left), single delay (center) and algebraic (right) memories. Units along the vertical axis are arbitrary. The left panel depicts motional narrowing for the exponential memory: two peaks broaden and then coalesce into a single peak as the damping is increased. Similar transitions are seen for both the single delay memory (coherence measured by the value $\mu\tau$) and the algebraic memory (coherence measured by the value ν). The single delay process is quite similar with the exception that it develops additional symmetric peaks, indicated by the arrows. The algebraic process, while also similar in the overall aspects, exhibits sharp differences for small values of f. The source

of this peculiar behavior is the fact that the integral of $\lambda(t)$ over all time changes drastically as one crosses from the oscillatory to the monotonic region. The integral is 0 for positive ν and infinite for negative values of ν.

The motional narrowing phenomenon [30] appears in magnetic resonance observations [31], neutron scattering experiments [32–37], and in other contexts whenever the underlying dynamics of a system undergo spectral diffusion. Such spectral diffusion arises not only from thermal motion in an inhomogeneous medium but from a variety of sources that includes changes in the bath fluctuation rate [38]. For example, the simple exponential memory case can be seen to arise explicitly in the magnetic resonance context.

3.4.2 Spatial Extent in the Steady State

The competition between the spread due to diffusion the attraction to the center often leads to a steady-state spatial extent of the particle. A number of experimental techniques could be devised in principle to measure this size. The size in the steady-state is given by the saturation value of the MSD $\langle \Delta x^2 \rangle$. The time-dependent MSD for the exponential memory is given by,

$$\langle \Delta x^2 \rangle(t) = \frac{D}{\omega}\left[\frac{\omega}{b} + \frac{b}{\omega} - \frac{be^{-bt}}{\omega}\left(\frac{\omega^4}{b^2\Omega^2} + \frac{4\Omega^2 - \omega^2}{4\Omega^2}\cos 2\Omega t + \frac{3\omega^2 - 4\Omega^2}{2b\Omega}\sin 2\Omega t\right)\right]. \quad (3.22)$$

Although any two of the three parameters ω, b and Ω uniquely determine the third, we have used all three here and elsewhere to avoid cumbersome square roots in the display. In the overdamped limit, i.e., when $b > 2\omega$, the above trigonometric functions turn into hyperbolic functions as Ω becomes imaginary.

The MSD for the case of the single delay is

$$\langle \Delta x^2 \rangle(t) = 2D\left(\Theta(k)\sum_{l=0}^{k-1}\int_{l\tau}^{(l+1)\tau} ds\, g_l(\gamma s) + \int_{k\tau}^{t} ds\, g_k(\gamma s)\right), \quad (3.23)$$

where $g_k(t)$ is defined as

$$g_k(\gamma t) = \sum_{m=0}^{k} \sum_{n=0}^{k} \frac{(-1)^{(m+n)}}{m!n!}(\gamma t - m\gamma\tau)^m(\gamma t - n\gamma\tau)^n,$$

in any interval, $k\tau \le t \le (k+1)\tau$.

The MSD for the algebraic case is given by,

$$\langle \Delta x^2 \rangle(t) = 2D \int_0^t ds \begin{cases} \left[\int_0^\infty \frac{dr}{\pi} e^{-r\zeta s} C(r) \right]^2 & -1 < \nu \le 0, \quad (3.24a) \\[4mm] \left[\frac{2}{\nu+1} e^{-\Lambda\zeta s} \cos \kappa\zeta s - \int_0^\infty \frac{dr}{\pi} e^{-r\zeta s} C(r) \right]^2 & 0 < \nu \le 2, \quad (3.24b) \end{cases}$$

with

$$\Lambda = \cos\left(\frac{\nu\pi}{\nu+1}\right), \qquad \kappa = \sin\left(\frac{\nu\pi}{\nu+1}\right),$$

$$C(r) = \frac{r^\nu \sin\nu\pi}{r^{2(\nu+1)} - 2r^{(\nu+1)}\cos\nu\pi + 1}.$$

Our interest lies in the steady-state size of the particle given by these expressions in the limit $t \to \infty$. Calling the saturation value of the MSD as the particle size S (in units of area for our 1-dimensional system), we have

$$S = \begin{cases} \dfrac{D}{\omega}\left(\dfrac{\omega}{b} + \dfrac{b}{\omega}\right), & (3.25a) \\[4mm] \dfrac{D}{\mu}\left(\dfrac{1 + \sin\mu^2\tau^2}{\mu\tau\cos\mu^2\tau^2}\right), & (3.25b) \\[4mm] \dfrac{D}{\zeta}\displaystyle\iint_0^\infty \dfrac{dr\,dq}{\pi^2}\dfrac{2C(r)C(g)}{r+q}, & (3.25c) \\[4mm] \dfrac{D}{\zeta}\left[\dfrac{2}{(\nu+1)^2}\left(\Lambda + \dfrac{1}{\Lambda}\right) - \dfrac{8}{\nu+1}\displaystyle\int_0^\infty \dfrac{dr}{\pi}\dfrac{C(r)(\Lambda+r)}{r^2+2\Lambda r+1} + 2\displaystyle\iint_0^\infty \dfrac{dr\,dq}{\pi^2}\dfrac{C(r)C(q)}{r+q}\right], & (3.25d) \end{cases}$$

where Eq. (3.25c) is for $-0.5 < \nu \le 0$ and Eq. (3.25d) is for $0 < \nu \le 1$. For the parameter range $\nu \le -0.5$, the MSD diverges as,

$$\lim_{t\to\infty} \langle \Delta x^2 \rangle(t) \propto \begin{cases} \ln t & \nu = -0.5, \\ t^{2|\nu|-1} & -1 \le \nu < -0.5. \end{cases}$$
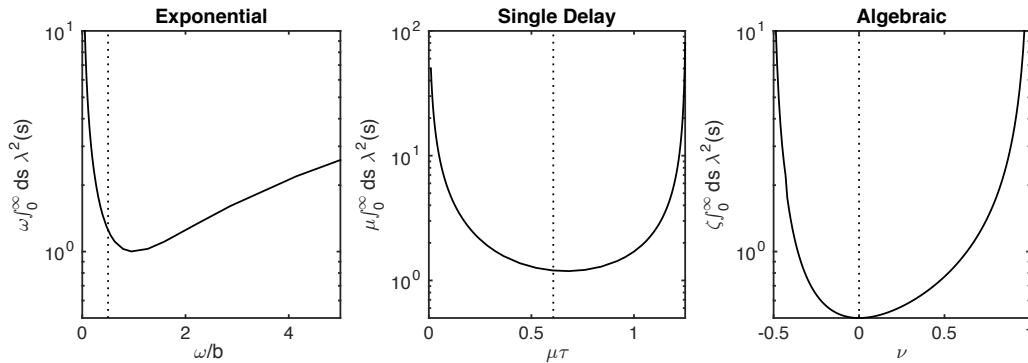
Figure 3.6: Spatial extent of the particle in the steady-state as determined from the saturation value of the MSD. The left, center, and right panels display the MSD for an exponential memory, single delay memory, and algebraic memory, respectively. The vertical axis is the steady-state size normalized to the size for the time-local case, $\phi(t) = \delta(t)$. We set γ equal to the coherent parameter for each case: ω for the exponential memory, μ for the single delay memory and ζ for the algebraic memory. Dotted lines indicate the location of the transition from monotonic (overdamped) to oscillatory (underdamped) regimes.

The MSD for the single delay memory, Eq. (3.25b), is known to have the analytic expression shown above. It can be obtained after solving [22] the differential equation governing the evolution of the covariance at long times.

Plots of the long-time expressions in Eq. (3.25) are shown in Fig. 3.6 for the exponential, single delay, and algebraic memories in the left, center, and right panels, respectively. We normalize the MSD for all three memories using the respective coherent parameters: ω, μ and ζ. An increase in D results in a monotonic increase in the MSD in all three cases. The exponential memory has a symmetric dependence on ω and b, with a minimum for $b = \omega$. Only in the stable regime, $\mu^2\tau^2 < \pi/2$, is the expression valid for the single delay memory. As expected, the MSD diverges as the unstable limit is approached. The saturation value of the MSD diverges as either of ω/b and $\mu\tau$ approach zero because γ vanishes and, therefore, there is no attractive center.

At long times, the MSD for the algebraic case diverges when $\nu \to -0.5$ from the right and when $\nu \to 1$ from the left. The divergence at the lower limit occurs due to the long-time algebraic dependence of the Green functions, Eq. (3.13). The value of ν for which the steady-state size is minimum depends on the ratio of time constants, γ/α. When this ratio is equal to 1, the minimum is at $\nu = 0$. This is obvious in Fig 3.6. For an arbitrary γ/α, the value of ν at the minimum is given by the transcendental equation,

$$\ln \frac{\gamma}{\alpha} = -(\nu_{min} + 1)^2 \left[\frac{d}{d\nu} \ln F(\nu) \right]_{\nu=\nu_{min}}, \tag{3.26}$$

where $F(\nu)$ is the functional form of the curve plotted in the right panel of Fig. 3.6. An increase in the ratio of γ/α shifts the minimum rightwards, a decrease shifts it to the left.

A comparison of the MSD dynamics can be done by setting the parameters such that, $\varrho \int_0^\infty ds \, \lambda_d^2(s) = V$, where ϱ is the appropriate coherent parameter, is identical for all three cases. The saturation value of the three memories are not comparable over the entire parameter space. The single-delay process has a minimum MSD saturation when $2\mu^2\tau^2 = \cos(\mu^2\tau^2)$, i.e., a value $V = 1.19$, while the exponential memory process has a minimum value, $V = 1$ exactly when $b/\gamma = 1$. For these parameter values, the algebraic memory has a minimum value of $V = 1/2$ located at $\nu = 0$.

We select values of $V > 1.19$ from the algebraic long-time MSD, Eqs. (3.25c) and (3.25d), and solve the exponential and single delay memory expressions in Eqs. (3.22) and (3.23) to obtain

$$\omega/b = V \pm \sqrt{V^2 - 1}, \qquad \sin\left((\mu\tau)^2\right) = \frac{(2V\mu\tau)^2 - 1}{(2V\mu\tau)^2 + 1},$$

respectively. For the exponential memory we choose the negative branch, $\omega/b = V - \sqrt{V^2 - 1}$, for the monotonic regime and the positive branch, $\omega/b = V + \sqrt{V^2 - 1}$, in the oscillatory regime.
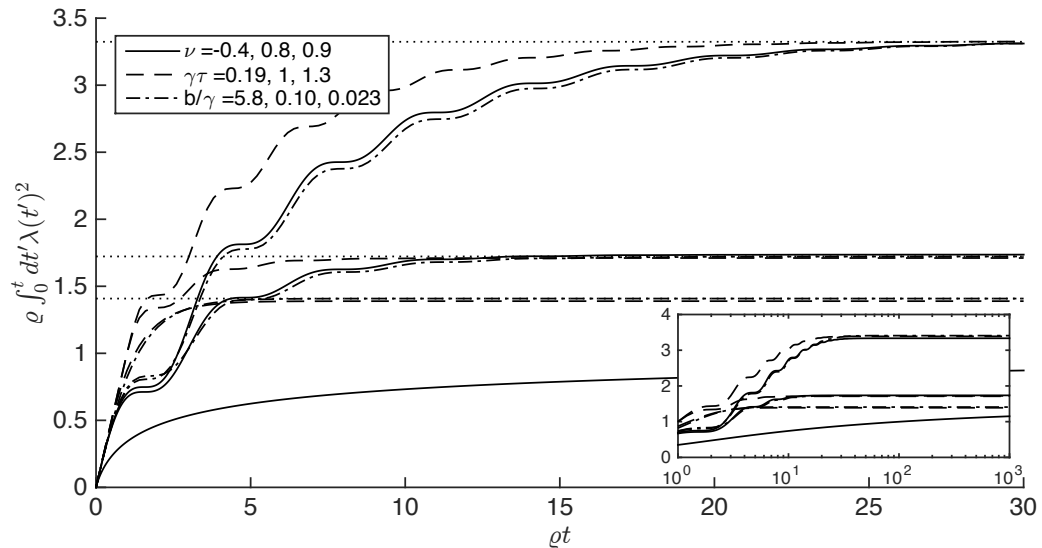
Figure 3.7: Comparing the dynamics of the MSD for the algebraic, exponential memory, and single delay memories when their MSD have a mutual saturation value with solid, dot-dashed, and dashed lines, respectively. We hold constant ϱ which is equal to the coherent parameter for each of the memories (ω for exponential, μ for the single delay, and ζ for the algebraic. The MSD is normalized in units ϱ/D. Two curves for each memory depict dynamics in the underdamped regime and one for each memory in the overdamped regime. The inset plot shows that same figure with logarithmic axes.

Using these values of V, ω/b and $\mu\tau$ we plot in Fig. 3.7 the dynamics of the three memories. In the oscillatory regime, all three memories exhibit the apparent saturation behavior associated with the oscillations of their respective Green functions. The single delay memory clearly saturates the fastest. The exponential and algebraic memories have very similar MSD, with the exponential memory initially larger. In the overdamped regime, the algebraic memory saturates much slower due to its heavy tail.

3.5   Discussion

This Chapter focused on an investigation into the dynamics of a time-nonlocal generalization of the Ornstein-Uhlenbeck process. The time-nonlocality is achieved through the presence of a memory function, which we have denoted by the symbol $\phi(t)$, in the harmonic restoring force. For the time-local case, i.e., where $\phi(t)$ is a simple δ-function in time, the result is text-book material and leads to solutions of the corresponding Smoluchowski equation. We have investigated here two memories that may be applicable to certain biological systems: the algebraic memory, Eq. (3.7), and a delay case, Eq. (3.14). They are compared with the standard exponential memory, Eq. (3.18), the consequences of which are well-known. Similarities across the three cases as well as some distinguishing characteristics of each have been found. The connection to the time-local case, for which $\phi(t) = \delta(t)$, is trivial for both the delay and the exponential memories as the memory is finite when integrated over all time. For the algebraic case this is not true and leads to some peculiar behavior.

3.5.1   Similarities and dissimilarities in the consequences of the three memories

Eq. (2.2) convolves the displacement $x(t)$ with $\gamma\phi(t)$ in all three cases. The strength of the confinement to the attractive center may be said to be described by γ while the specific manner by which the particle is confined may be attributed to $\phi(t)$. The three memories, exponential, single delay, and algebraic, are found in Eqs. (3.18), (3.14) and (3.7), respectively. We label the coherence parameter ω in the exponential case, $\mu = \sqrt{\gamma/\tau}$ for the delay case and $\zeta = \sqrt{\gamma\alpha}$ in the algebraic case while the loss of coherence occurs at the rate b, $1/\tau$ (equal to the reciprocal of the delay time), and α, respectively.

The basic quantity that determines the behavior of the system is the Green function $\lambda(t)$. It is given generally in the Laplace domain by Eq. (3.1). In the time domain it takes the form given in Eq. (3.19) for the exponential memory, Eq. (3.16) for the delay memory, and Eq. (3.9) for the algebraic case. An additional result shown in this Chapter is the alternate form, Eq. (3.10) that we have derived. We use it along with its asymptotic form, Eq. (3.13), well known to the literature [19]. Both provide considerable computational convenience. While Fig. 3.1 shows the Green function for the algebraic case in the underdamped and overdamped regimes, Figs. 3.2 and 3.3 display the usefulness of the alternate forms we provide for the computations.

The behavior of the algebraic case is determined by a single parameter ν. Positive values result in oscillations while negative values lead to monotonic decay. Whereas for the other two memories, where a transition in the system from the oscillatory to the overdamped regimes occurs when the coherence parameter (ω or μ) is held constant and the damping (b or $1/\tau$ respectively) is varied, variation of α with ζ held constant does not do anything similar in the algebraic case. The scaling behavior of the power-law dependence results in the damping parameter α introduced in the algebraic memory, Eq. (3.7), completely drops out of the picture in the Green function as seen in Eq. (3.9). This despite being introduced in a manner analogous to the exponential case Eq. (3.18). Instead, the coherence parameter merely serves to scale time. The exponent ν determine the oscillatory-decaying transition. This remarkable feature of the algebraic memory stems from its scale-free nature.

The time-integral of the Green function from zero to infinity, i.e., $\int_0^\infty \lambda(t)dt$ given by $1/\gamma\widetilde{\phi}(0)$, is of direct relevance for several observables. This presents no problems for the exponential and the delay memories but for the algebraic case one runs into the peculiarity that $\widetilde{\phi}(0)$ may not exist. Indeed, $\int_0^\infty \lambda(t)dt$ vanishes for positive ν but becomes infinite provided $\nu \in [-1, 0)$. One of the direct consequences of this feature

is the drastic jump from 0 to ∞ observed in the spectral line at zero frequency f noted in Fig. 3.5 which depicts motional narrowing of the a.c. susceptibility.

For algebraic and delay memories there is also the regime of unbounded oscillations that occurs for $|\nu| > 1$ and $\gamma\tau > \pi/2$ respectively. Because the regime is seldom physical, we have shown it only passingly in Fig. 3.4 and only for the delay case, with an effect in the central panel of Fig. 3.5 where additional peaks in the spectral line result.

3.5.2 Non-local attractive term in the Smoluchowski equation

We leave to Chapter 4 a complete discussion of the Fokker-Planck equivalent to Eq. (2.2). As was mentioned in Chapter 2, the direct generalization of Eq. (2.1) itself through the inclusion of a memory in its attraction term can not be deduced from Eq. (2.2). Such a generalized Smoluchowski equation is given by

$$\frac{\partial P(x,t)}{\partial t} = \frac{\partial}{\partial x}\left(\gamma \int_0^t dt'\, \phi(t-t')xP(x,t')\right) + D\frac{\partial^2 P(x,t)}{\partial x^2}. \tag{3.27}$$

One may be tempted by the self-evident naturalness of Eq. (3.27) to observe the consequences of its assumption despite its incorrectness. By multiplying Eq. (3.27) by x^n, integrating over x from $-\infty$ to $+\infty$, and performing the requisite integration by parts one obtains the equations for the moments. The equation for an arbitrary moment is thus given by

$$\frac{d\langle x^n(t)\rangle}{dt} + n\gamma \int_0^t dt'\, \phi(t-t')\langle x^n(t')\rangle = \frac{n!}{(n-2)!}D\langle x^{n-2}\rangle. \tag{3.28}$$

Upon particularization of Eq. (3.28) to the first moment ($n = 1$), we have

$$\langle x(t)\rangle = \lambda(t)x_0. \tag{3.29}$$

While a comparison with the equation for the *true* average displacement, given in Eq. (3.3), for the correctly generalized Langevin equation finds that Eq. (3.29) is correct, higher moments are not. For the case of $n = 2$, the average square displacement, the solution to Eq. (3.28) becomes

$$\langle x^2 \rangle(t) = \lambda_{\gamma \to 2\gamma}(t)x_0^2 + 2D \int_0^t dt' \, \lambda_{\gamma \to 2\gamma}(t'), \tag{3.30}$$

where by $\lambda_{\gamma \to 2\gamma}$ we mean the expression for the Green function $\lambda(t)$ that is obtained when γ is replaced by 2γ. A comparison with the correct moment, given in Eq. (3.4), shows that the higher moment prediction of the inappropriate generalization is always inaccurate except for when $\phi(t) = \delta(t)$, i.e., the time local case, in which case $\lambda(t)$ is exponential and the relation required for equivalence, $\lambda_{\gamma \to 2\gamma}(t) = \lambda^2(t)$, is accidentally correct.

Occasions where approximate descriptions accurately reproduce the lower moments but not the higher moments are frequently encountered in transport theory [39]. While the inappropriate generalization of the Smoluchowski equation accurately reproduces the motional narrowing phenomenon because it depends completely on the first moment, we display in the next subsection that the size of the particle, time-dependent or steady-state, can not be reproduced because the size is determined by the *second* moment.

3.5.3   Apparent violation of the Balescu-Swenson Theorem

A theorem in the field of non-equilibrium statistical mechanics, first enunciated by Balescu [40] and Swenson [41], relates the dynamical and steady-state observables that can be calculated from non-Markoffian equations to those of their Markoffian equivalent. The Balescu-Swenson theorem clarifies that non-Markoffian equations are unnecessary for a steady-state description. This is true despite the fact that they
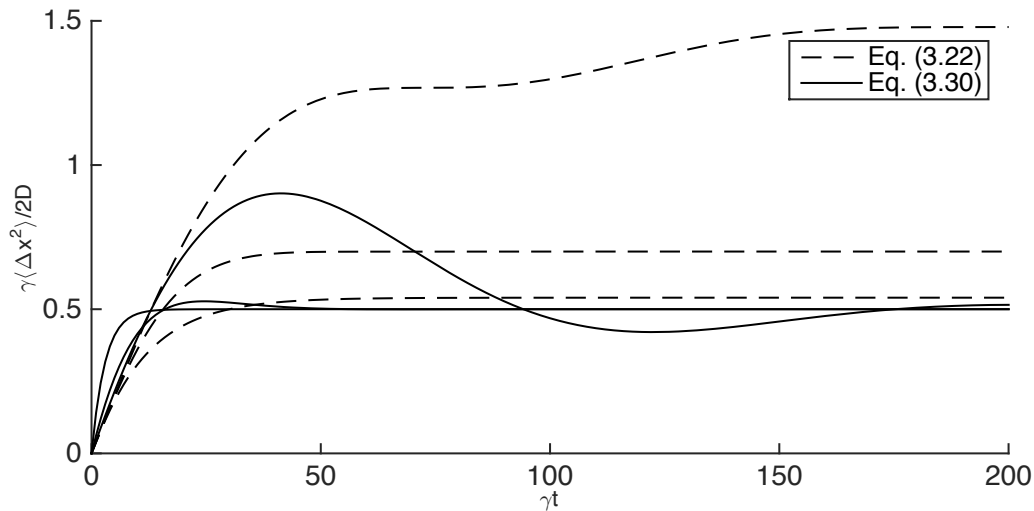
Figure 3.8: Apparent violation of the Balescu-Swenson theorem in the mean squared displacement. We plot with dashed lines the MSD of our theory for the exponential memory, Eq. (3.22), for a constant γ and three values of the damping parameter b/γ: 0.5, 2.5 and 12.5. Their saturation values increase when b/γ is increased signifying a violation of the Balescu-Swenson theorem as γ is being held constant. By contrast, all three predictions of the incorrect generalization of the Smoluchowski equation, Eq. (3.30), saturate to the same single value the difference in the values of b/γ.

incorporate the microscopic dynamics, which provides a more accurate description of the approach to equilibrium. Thus, while non-Markoffian equations differ from their Markoffian equivalents in their predictions for the values of ac observables, the values of dc observables are reproduced by Markoffian equations with perfect accuracy. One may find an intuitive understanding of the theorem through the explicit consideration of the Markoffian approximation in the Laplace-domain. The approximation requires the replacement of the Laplace variable by zero in the Laplace transforms of the memories. This exact replacement occur as well in the Tauberian theorems used to calculate asymptotic, i.e., steady state, results.

Fig. 3.8 displays the time-dependence and the saturation value of the mean square displacement (MSD) for the simple case of exponential memory. We hold γ constant and vary the damping parameter over three values $b/\gamma = 0.5$, 2.5 and 12.5. The

exact results, Eq. (3.22), are depicted with dashed lines and indicate a dependence of the saturation size on b despite no change to γ. This result certainly conflicts with the statement of the Balescu-Swenson theorem if we assume the saturation value of the MSD to be a steady-state observable applicable to the theorem. We also display in Fig. 3.8 (solid lines) that the incorrectly generalized Smoluchowski equation, Eq. (3.27), predicts a MSD that does follow the Balescu-Swenson theorem. Although one should not take the predictions of the incorrect generalization of the Smoluchowski equation too seriously as physical parameter ranges exist for which the MSD takes negative values, all do approach the same saturation value of the MSD that is obtained for the time-local situation.

For a fuller understanding of the apparent violation of the Balescu-Swenson theorem, consideration of the theorem in the context of its time may be of import. First Balescu [40] and then Swenson [41] enunciated the theory when the generalized master equation (GME) was initially being developed by various investigators [42–47]. While the GME can accurately describe the short-time dynamics that are not accessible to the Master equation, the latter's importance to the understanding of central tenets in statistical mechanics necessitated an awareness of which properties required the use of a GME for an accurate model and which could be accurately modeled by a Master equation. The Balescu-Swenson theorem provides this understanding. Its apparent violation here (see Eq. (3.25)) thus necessitates an answer to the query: what underlies Eq. (2.2) such that its predicted steady-state quantities have a dependence on the memory?

Other cases [28, 48] for which the Balescu-Swenson theorem does not apply have been identified earlier. For example, an apparent violation has been shown [28] to occur when the particle under consideration has a finite lifetime. However, the process under discussion here incorporates no finite lifetime effects. The simple answer to the above question is that the memory we consider here appears only in

the systematic term of Eq. (2.2). The Balescu-Swenson theorem requires that the memory describe the whole process.

3.5.4   A Comment on Two-Time Correlation Functions

For many practical situations, only two times are of physical significance: an initialization time and what one might term an observation time. In these cases, only single-time quantities (such as $\langle x(t) \rangle$) are of experimental interest. In some physical situations, however, a third (and fourth, etc.) time can play a physical role in the process. For example, in Section 3.4 we discuss an experiment in which one measures the polarization of a charged particle that experiences both the time non-local attraction to a center expressed in Eq. (2.2) and an applied time-varying electric field. Initially, we assume that the electric field is turned on concurrent with the initialization time t_0 of the system. If, instead, the field is turned on at the later time s and the position of the particle is measured at a time t, two-time correlations such as $\langle x(t)x(s) \rangle$ are of experimental importance. These two-time correlations have appeared previously in the context of aging [49,50] and, when the quantity of interest is the velocity, in [51].

We have provided general expressions for $\langle x(t)x(s) \rangle$ and $f(t,s)$, the antisymmetrized combination of the former, in Eqs. (3.5) and (3.6) respectively in terms of the Green function $\lambda(t)$. For the case of an exponential memory, for instance, we have

$$f(t,s) = \frac{D}{\omega}\left\{ e^{-\frac{b}{2}(t-s)}\left(\left[\frac{b}{\omega}+\frac{\omega}{b}\right]\cos\left[\Omega(t-s)\right] + \frac{b^2-\omega^2}{2\Omega\omega}\sin\left[\Omega(t-s)\right] \right) \right.$$

$$\left. -\frac{be^{-\frac{b}{2}(t+s)}}{\omega}\left(\frac{\omega^4}{\Omega^2 b^2}\cos\left[\Omega(t-s)\right] + \frac{4\Omega^2-\omega^2}{4\Omega^2}\cos\left[\Omega(t+s)\right] + \frac{b^2-\omega^2}{2\Omega b}\sin\left[\Omega(t+s)\right] \right) \right\} \tag{3.31}$$

The Markoffian counterpart, obtained by taking the limit $b \to \infty$, $\omega \to \infty$, such that
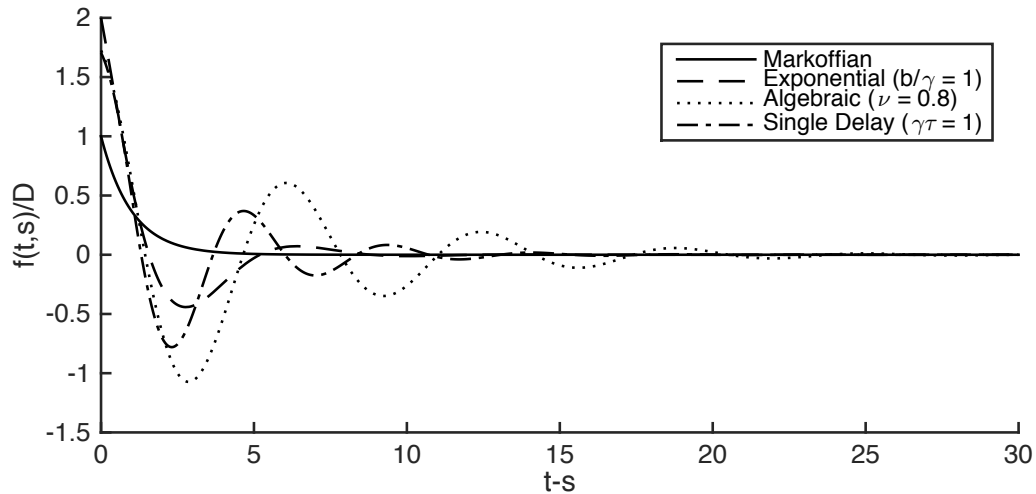
Figure 3.9: Plotted are the antisymmetrized two-time correlation $f(t, s)$ as a function of the difference of the times t and s for all three cases of the memory functions, exponential, algebraic, and single delay, in dashed, dotted, and dot-dashed lines respectively. The solid line plots $f(t, s)$ in the limit of no memory. Parameters have been chosen so that the same Markoffian limit is obtained for all three memories. The horizontal axis is the difference in time and the vertical axis is $f(t, s)/D$, both being normalized by $1/\gamma$. We have held the sum of the times constant at a reasonably large value, $\gamma(t + s) = 30$ while the difference $\gamma(t - s)$ is varied over the range $[0, 30]$. Only the underdamped case is displayed.

$\omega^2/b = \gamma$, is

$$f(t, s) = \frac{D}{\gamma} \left(e^{-\gamma(t-s)} - e^{-\gamma(t+s)} \right). \tag{3.32}$$

Neither the exponential memory, Eq. (3.31), nor its Markoffian limit, Eq. (3.32), results in $f(t, s)$ being solely a function of the difference in time $t - s$. As expected, the non-Markoffian two-time correlation function differs from its Markoffian counterpart at short values of the difference $t - s$ but tends to the latter for large values. We depict this behavior for the underdamped case graphically in Fig. 3.9 for all three cases of the memory by fixing the sum of the two times and varying the difference. Two features are clear, one at short and one at long $t - s$. As expected, all cases tend to the Markoffian limit at large values of $t - s$. At short times, on the other hand,

they all are different. This is so because there they depict the (dimensionless) mean square displacements which we have seen indeed differ, representing the violation of the Balescu-Swenson theorem.

The work in this Chapter was done in collaboration with co-investigators external to UNM, and has been published as M. Chase, T. J. McKetterick, L. Giuggioli and V. M. Kenkre, "Langevin analysis for time-nonlocal Brownian motion with algebraic memories and delay interactions", *European Physics Journal B*, **89**, 1-15 (2016).

Chapter 4

Fokker-Planck Analysis

Attempts [18, 52–54] to derive the probability density approach to the time-nonlocal Ornstein-Uhlenbeck process have been the subject of a number of articles [55–58] over the years. The aim is to construct the deterministic equation for the probability distribution corresponding to Eq. (2.2). A *bona-fide* equation of this type, referred to as a Fokker-Planck equation, describes the evolution of a conditional probability distribution, i.e., the probability density that the particle is located at position x at time t conditioned on it being at the position x' at the prior time t'. In the case of the familiar Smoluchowski equation, Eq. (2.1), and more generally any time-homogeneous Markov process, this requirement is met implicitly by an equation for the single-time probability density. The presence of memory in the Langevin equation, however, requires the explicit construction of the *conditional* probability distribution. Despite this, discussions in the literature generally focus on the one- and two-time probability distributions [18,52,53,55,59], the practical utility of which remain untested, e.g., the sign of the mean of the distribution can change in certain parameter regions, which leads to the coefficients of both the restoring force and the diffusive term being undefined [60].

We extend these procedures [18, 52, 53, 55, 59], developed for the one- and two-time probability distributions, to processes for which the initial condition of the stochastic variable is taken to be non-local in *time* (see the discussion by Giuggioli in ref. [61]). Of particular interest when the memory is of the delay type [62–66], an extended history of the stochastic variable, however, may play a role for any memory. Questions remain, however, on the appropriateness of the label Fokker-Planck for these equations [53, 55–58]. We do not attempt to settle the matter here. Despite these questions, we present our results for their interesting nature as well as their potential application in extensions to recent work.

Two examples illustrate concrete issues in which a *bona-fide* Fokker-Planck description for the conditional probability distribution may be of importance. Observations of a particular stochastic process may be limited by external or internal constraints to a subspace of the allowable motion space. In these situations, the results are inherently conditioned on the object being in the observational space. In combination with memory effects, a restricted observation space limits one to only a partial characterization of the process. Physical boundaries lead to similar conceptual issues even with full access of the observer to the motion space. Inferences about the underlying stochastic process are complicated by boundary effects. Recent work [67, 68] has found the time-local Smoluchowski equation, Eq. (2.1), applicable to trapping situations [67] and to the spread of epidemics [68]. The latter leads to an interesting description of the transmission of infection in diseases such as the Hantavirus [69]. If, through further observation, memory effects are found to be important, what has been called in the literature a *bona-fide* Fokker-Planck description may be of use.

We divide this Chapter into five Sections as follows. In Section 4.1, we define in detail the relations between joint and conditional probability distributions. We briefly discuss the specialization of those relations to the context of Markov and

time-homogeneous processes. Section 4.2 introduces a method devised by San Miguel and Sancho [18] to construct a form of the memory-possessing Langevin equation, Eq. (2.2), without a convolution. This form is useful in the present context because the non-Markoffian effects have been translated into time-dependent, but time-local, coefficients. Using the proscription described in Chapter 2, Section 4.3 presents the probability density description of the Ornstein-Uhlenbeck process, which is fully characterized by the one- and two-time joint probability distributions. In Section 4.4, the conditional probability distribution is discussed and a Markov condition on the memories is derived. We compare the twice-conditioned version to the simple one-time propagator, a special case of the one-time joint probability. We conclude in Section 4.5 with final remarks and briefly note the equation that defines the conditional probability distribution.

4.1 Discussions on Joint and Conditional Probability Distributions and Their Relations

We begin with a review of the basic concepts necessary to understand the derivation. The full description of the stochastic variable $x_i(t)$, taken to be one-dimensional as in Chapter 3, requires knowledge of the entire set of the n-time joint probability distributions, identified by $P_n(x_n, t_n; x_{n-1}, t_{n-1}; ...; x_1, t_1)$. This expression defines the probability density that the particle takes the value x_1 at time t_1 *and* x_2 at time t_2 *and* x_3 at time t_3, etc. Physically, this corresponds the observation of the position of a single object at multiple different times. Henceforth, we take the times to be ordered such that $t_n \geq ... \geq t_1$. The joint probability distributions are constructed from a microscopic description by extending Eq. (2.3a) to multiple variables. We define

$$P_n(x_n, t_n; ...; x_1, t_1) = \langle \delta(x_i(t_n) - x_n)\delta(x_i(t_{n-1}) - x_{n-1})...\delta(x_i(t_1) - x_1)\rangle, \quad (4.1)$$

where $\langle ... \rangle$ is the ensemble average. It is, of course, essential that the δ-functions in Eq. (4.1) are all for the ith particle. Eq. (4.1) allows [70] for the construction of any m-time averaged observable, for $n \geq m$, by multiplication with the desired observable and then integrating each variable, x_n, x_{n-1}, etc., over all space.

Three properties relate the joint probability distributions of different indices. The first property reduces P_n when two of its times are identical:

$$P_n(x_n, t_n; ...; x_p, t_p; x_q, t_q; ...; x_1, t_1) = \delta(x_p - x_q) P_{n-1}(x_n, t_n; ...; x_p, t_p; ...; x_1, t_1). \quad (4.2)$$

That is, when $t_p = t_q$ the positions associated with those times must be identical as well, i.e., $x_p = x_q$. There are no additional conditions on P_n. The marginal P_{n-1} of P_n is found by integration over one of its variables, i.e.,

$$P_{n-1}(x_1, t_1; ..; x_{s-1}, t_{s-1}; x_{s+1}, t_{s+1}..; x_n, t_n) = \int_{-\infty}^{\infty} dx_s \, P_n(x_1, t_1; ..; x_s, t_s; ..; x_n, t_n). \quad (4.3)$$

The m-time joint probability distribution can then be constructed from the n-time one for $n \geq m$. Bayes' theorem [71] relates the n- and m-joint probability distributions for $n, m \geq 1$ to the *conditional* probability distribution. We have

$$Q_{n|m}(x_{n+m}, t_{n+m}; ..; x_{m+1}, t_{m+1} | x_m, t_m; ..; x_1, t_1) = \frac{P_n(x_{n+m}, t_{n+m}; ..; x_1, t_1)}{P_m(x_m, t_m; ..; x_1, t_1)}, \quad (4.4a)$$

$$= \frac{Q_{n+r|m-r}(x_{n+m}, t_{n+m}; ..; x_{m-r+1}, t_{m-r+1} | x_{m-r}, t_{m-r}; ..; x_1, t_1)}{Q_{r|m-r}(x_m, t_m; ..; x_{m-r+1}, t_{m-r+1} | x_{m-r}, t_{m-r}; ..; x_1, t_1)}, \quad (4.4b)$$

where $Q_{n|m}$ gives the probability density of the particle being at x_{n+m} at time t_{n+m} and ... and x_{m+1} at time t_{m+1} *conditioned* on it previously being at x_m at time t_m and ... and x_1 at time t_1. Thus, the conditioned distribution describes the probability density that the stochastic variable takes on certain values given its *particular* history.

The single-time conditional probability distribution $Q_{n|1}$ is often referred to as the n-time propagator, $\Pi_{n|1}(x_n, t_n; ...; x_1, t_1 | x_0, 0)$. It can be related to the n-time joint probability distribution through the appropriate marginalization of Eq. (4.4a).

One takes $m = 1$ and rearranges Eq. (4.4a) such that $P_1(x_1, t_1)$ is on the left hand side. By then taking $t_1 = 0$ and marginalizing over x_1, we have

$$P_n(x_n, t_n; ...; x_1, t_1) = \int_{-\infty}^{\infty} dz \, \Pi_n(x_n, t_n; ...; x_1, t_1 | x_1, 0) P_1(x_1, 0), \qquad (4.5)$$

where we have used the equivalence between $Q_{n|1}$ and the propagator P_n. As $t = 0$, however, $P_1(x_1, 0)$ is simply the initial condition ($P_0(z)$) and the standard relation between the propagator and the joint probability distributions is recovered. When the particle is taken to be initially localized, P_n reduces to the propagator Π_n and becomes explicitly dependent on the P_0.

As is evident from Eq. (4.5), the joint probability distributions retain this dependence on initial conditions in the case of initially delocalized particles as well. Despite this, we use the standard notion for the joint probability distributions, which leaves as implicit their dependence on the initial condition (again excepting the propagator). However, as the conditional probability distributions can be constructed from the joint ones, they may retain the latter's dependence on the initial condition. Unfortunately, this can lead to confusion in the notation for $Q_{n|m}$. The ambiguity becomes clear by considering Eq. (4.4b) for the case of a localized initial condition at x_0, i.e., $P_0(z) = \delta(z - x_0)$. The *implicit* dependence of the joint probability distributions, labeled P_n and P_m in Eq. (4.4a), becomes *explicit* in the propagators Π_n and Π_m. If the conditional probability distribution retained the formers implicit dependence on the initial condition, the transition to the explicit dependence in the propagators leads to its own transition. The result is $Q_{n|m}$, implicitly dependent on $P_0(z)$, becoming $Q_{n|m+1}$, with explicit dependence on the initial location x_0. To avoid ambiguity, when the conditional probability distribution is dependent on the initial condition, it is written explicitly, i.e., $Q_{n|m}(...|...; P_0)$. However, the notation that we have used, in which the index m in $Q_{n|m}$ counts only the number of points on which it is conditioned, is retained. Thus, $Q_{n|m}(...|...; P_0)$ becomes $Q_{n|m+1}(...|...; x_0)$ if P_0 becomes a δ-function.

As is well-known [8], an important subclass of stochastic processes are the Markov processes. They are defined by the fact that the conditional probability depends only on its most recent conditioned time [8]. Thus, satisfying the equality

$$Q_{n|m}(x_{n+m}, t_{n+m}; ..; x_{m+1}, t_{m+1} | x_m, t_m; ..; x_1, t_1)$$
$$= Q_{n|1}(x_{n+m}, t_{n+m}; ..; x_{m+1}, t_{m+1} | x_m, t_m). \quad (4.6)$$

The combination of the reduction in the number of conditioned times and Bayes' theorem, Eq. (4.4a), implies that $P_n = Q_{1|1}P_{n-1}$ for any n. Thereafter, repeated use of Bayes' theorem shows that P_n can be written solely in terms of $Q_{1|1}$ and P_1. As the complete set of joint probability distributions specify a stochastic process, P_2 therefore completely characterizes Markov processes. One recovers P_1 following a marginalization of P_2 using Eq. (4.3) and recovers $Q_{1|1}$ from both with the use of Bayes' theorem. A Markov processes is time-homogenous if $Q_{1|1}(x_1, t_1 | x_0, t_0)$ can be rewritten with shifted times, i.e., as $Q_{1|1}(x_1, t_1 - t_0 | x_0, 0)$.

For non-Markoffian processes, the complete set of P_n is generally needed for its characterization. However, for the special case of Gaussian noise, the process is specified by just the one- and two-time averages [72]. We reiterate that, as in Chapter 4, we take the noise to be white and Gaussian and, thus, focus on P_1 and P_2 in the remainder of the Chapter.

4.2 An Equivalent Langevin Equation without Convolutions

The derivation that we present here reproduces one that was first elucidated by San Miguel and Sancho [18]. As our starting point, we take Eq. (2.2) and generalize it to a process in which the initial condition is time-nonlocal, i.e., $x_i(t) = \beta(t)$ is known

for $-t_0 \leq t \geq 0$ $(t_0 \geq 0)$. Thus, we have

$$\frac{dx_i(t)}{dt} = -\gamma \int_{-t_0}^{t} dt' \, \phi(t - t') x_i(t') + \xi_i(t). \tag{4.7}$$

When t_0 is taken to be 0 (or $\beta(t) = 0$), Eq. (2.2) is recovered. Similar to the derivation presented in Section 3.1, Eq. (4.7) is formally solved using Laplace transforms. The result is

$$x_i(t) = x_0 \lambda(t) + \int_{0}^{t} dt' \lambda(t - t') \xi_i(t') + \Phi(t), \tag{4.8}$$

where

$$\Phi(t) = -\int_{0}^{t} dt' \, \lambda(t - t') \int_{-t_0}^{0} dt'' \, \gamma\phi(t' - t'')\beta(t''), \tag{4.9}$$

$x_0 = \beta(0)$ is the value of the extended initial condition at $t = 0$, and $\lambda(t)$ is the Green function of the process. The Laplace-domain expression of the latter is given in Eq. (3.1) of Chapter 3. In contrast with the similar result for a time-local initial condition, Eq. (3.2), the effect of an extended deterministic history is simply the addition of the forcing term $\Phi(t)$.

While the analysis in Chapter 3 proceeds directly with the related formal solution, Eq. (3.2) which is recovered from Eq. (4.8) when $t_0 = 0$, here we construct a Langevin equation without a time convolution that is equivalent to Eq. (4.7). The benefit of such a Langevin equation lies in it being local-in-time. Thus, one may use it, per the proscription briefly outlined in Chapter 2, to derive the equivalent probability distribution equation.

Developed by San Miguel and Sancho [18], the method used to convert Eq. (4.8) into an equivalent equation without a convolution is rather elegant. One simply takes the temporal derivative of Eq. (4.8), resulting in the equation

$$\frac{dx_i(t)}{dt} = x_0 \frac{d\lambda(t)}{dt} + \frac{d}{dt}\left[\int_{0}^{t} dt' \, \lambda(t - t')\xi_i(t')\right] + \dot{\Phi}(t), \tag{4.10}$$

and then removes the explicit dependence on x_0. The latter is performed by solving Eq. (4.8) for x_0 and inserting it into Eq. (4.10). The equivalent to Eq. (4.7) is then given by

$$\frac{dx_i(t)}{dt} = \frac{\dot{\lambda}(t)}{\lambda(t)} x_i(t) + \lambda(t) \frac{d}{dt} \left[\int_0^t dt' \, \frac{\lambda(t-t')}{\lambda(t)} \xi_i(t') \right] + \lambda(t) \frac{d}{dt} \left[\frac{\Phi(t)}{\lambda(t)} \right], \qquad (4.11)$$

where $\dot{\lambda}$ indicates a temporal derivative. The modified noise, which we label with $\iota_i(t)$, obeys the twin relations

$$\langle \iota_i(t) \rangle = 0, \qquad \langle \iota_i(t) \iota_i(t') \rangle_{t>t'} = D\lambda(t)\lambda(t') \frac{d}{dt} \frac{d}{dt'} \left[\int_0^{t'} ds \, \frac{\lambda(t-s)}{\lambda(t)} \frac{\lambda(t'-s)}{\lambda(t')} \right]. \quad (4.12)$$

The proscription outlined here has converted the explicit non-Markofficity of the memory-possessing Langevin equation, Eq. (4.7), into a implicit dependence in Eq. (4.11). Though time-local, Eq. (4.11) displays the effects of non-Markofficity through the time-dependence of the potential strength, $\dot{\lambda}(t)/\lambda(t)$, the addition of color to the noise, and the driving force.

4.3 Solutions to Joint Probability Equations

In a generalization similar to that performed to construct Eq. (4.1), the generalized current density for two times is defined as

$$j_2(x_2, t_2; x_1, t_1) = \left\langle \frac{dx_i(t_2)}{dt_2} \delta(x_i(t_2) - x_2) \delta(x_i(t_1) - x_1) \right\rangle. \qquad (4.13)$$

With Eqs. (4.1) and (4.13), in combination with the continuity equation, the construction of implicit equations for the one- and two-time joint probability distribu-

tions can be performed. They are given as

$$\frac{\partial}{\partial t} P_1(x,t) = -\frac{\partial}{\partial x} \left\langle \frac{dx_i(t)}{dt} \bigg|_{x_i(t') = x} \delta(x_i(t) - x) \right\rangle, \tag{4.14a}$$

$$\frac{\partial}{\partial t} P_2(x,t;x',t') = -\frac{\partial}{\partial x} \left\langle \frac{dx_i(t)}{dt} \bigg|_{x_i(t) = x} \delta(x_i(t) - x)\delta(x_i(t') - x') \right\rangle. \tag{4.14b}$$

Here, we replace numerical indices on the variables x_1 and x_2 with primed and un-primed variables, respectively. Eqs. (4.14a) and (4.14b) are closed by replacing the time derivatives of the stochastic variable with Eq. (4.11). This is followed by an exchange of the stochastic variables for their equivalent field variables as mediated by the δ-functions. The result trivially gives both the attraction coefficients and the forcing term. However, the diffusion coefficients require the use of Novikov's theorem [7]. The complete derivation of both the one- and two-time joint probabilities is given in Appendix B.

The closed equations are given by

$$\frac{\partial}{\partial t} P_1(x,t) = \frac{\partial}{\partial x} \left[\left(A(t)x - B(t) + D(t)\frac{\partial}{\partial x} \right) P_1(x,t) \right], \tag{4.15a}$$

$$\frac{\partial}{\partial t} P_2(x,t;x',t') = \frac{\partial}{\partial x} \left[\left(A(t)x - B(t) + C(t,t')\frac{\partial}{\partial x'} + D(t)\frac{\partial}{\partial x} \right) P_2(x,t;x',t') \right], \tag{4.15b}$$

with the coefficients defined as

$$A(t) = -\frac{\dot{\lambda}(t)}{\lambda(t)}, \qquad (4.16a) \qquad B(t) = -\lambda(t)\frac{d}{dt}\left[\frac{\Phi(t)}{\lambda(t)}\right], \qquad (4.16b)$$

$$C(t,t') = 2D\lambda(t)\frac{d}{dt}\int_0^{t'} ds \, \frac{\lambda(t-s)\lambda(t'-s)}{\lambda(t)}, \tag{4.16c}$$

$$D(t) = D\lambda^2(t)\frac{d}{dt}\int_0^{t} ds \, \frac{\lambda^2(s)}{\lambda^2(t)}. \tag{4.16d}$$

Both of Eqs. (4.15) contain terms that represent the attraction to a center and

diffusion expected in a description of a Ornstein-Uhlenbeck process. However, as Eqs. (4.15) represent the time-nonlocal process, the coefficients of both terms are time-dependent, being $A(t)$ and $D(t)$, respectively. The time-nonlocality also contributes through a driving term, proportional to $B(t)$, dependent on the deterministic history of the particle. The final term, which is only present in the equation for the two-time probability distribution (Eq. (4.15b)), is similar to a cross diffusion term, derivatives with respect to both x and x' begin present. The evolution of $P_2(x, t; x', t')$ therefore depends not only on a single location in the past but on the entire probability distribution. As expected, $C(t, t')$ goes to zero when $t' \to 0$ so that Eq. (4.15b) reduces to Eq. (4.15b).

Expressions similar to Eqs. (4.15) have been given in by Fox [53] and Hernandez [73] for the case in which the memory and the noise in the a Langevin equation obey a fluctuation-dissipation theorem. Unfortunately, there is no direct method that either reduces their result to Eqs. (4.15), or vice versa, except in the trivial limit of a Markoffian process.

4.3.1   Brief Note on Divergent Coefficients

When the process under consideration is in an oscillatory parameter regime, the coefficients Eqs. (4.16) diverge. They diverge because the Green function $\lambda(t)$ crosses zero when the average position of the particle is at the origin. See examples of this crossing in the right panel of Fig. 3.1 and Fig. 3.4 in Chapter 3 for algebraic and single delay memories, respectively. At these divergences, the coefficients, Eqs. (4.16), also happen to switch signs. Thus, Eqs. (4.15) describe a process that converts from a diffusive one $(D(t) > 0)$ to anti-diffusive one $(D(t) < 0)$ and, concurrently, from an attractive one $(A(t) > 0)$ to being repulsive $(A(t) < 0)$. Remarkably, as one might expect from the well-behaved averaged quantities that were discussed in Chapter 3,

these divergences do not cause issues in the solutions to Eqs. (4.15). However, they can be removed through the redefinition of time first proposed by Giuggioli in [61]. The redefined time is given by the monotonically increasing function

$$T(t) = \int\limits_0^t ds \lambda^2(s), \tag{4.17}$$

which, we note, is essentially the mean squared displacement given in Chapter 3 by Eq. (3.4).

4.3.2 Solution for the One- and Two-Time Probability Distributions

Analytic solutions to the one- and two-time joint probability equations can be found using either Eqs. (4.15) or the transformed expressions in terms of $T(t)$. In either case, the standard method of solving Smoluchowski-type equations with harmonic potentials is used. We outline the method here (see Appendix C for a complete derivation). A Fourier transform with respect to x of both Eqs. (4.15a) (and a second with respect to x' for Eq. (4.15b)) results in first-order partial differential equations. Both transformed equations are driven by diffusive terms while in the latter there is the additional cross-diffusive one proportional to $C(t, t')$. The method of characteristics then converts the partial differential equations to ordinary ones. Following an inverse transform, the real-space expressions for the two propagators

are

$$\Pi_1(x,t|x_0,0) = \frac{1}{\sqrt{4\pi DT(t)}} \exp\left\{ -\left(\frac{x - x_0\lambda(t) - \Phi(t)}{\sqrt{4DT(t)}} \right)^2 \right\}, \qquad (4.18a)$$

$$\Pi_2(x,t;x',t|x_0,0) = \frac{1}{4\pi D\sqrt{T(t)T(t')[1-N^2(t,t')]}} \exp\left\{ \frac{-1}{1-N^2(t,t')} \right. \qquad (4.18b)$$

$$\left[\left(\frac{x - x_0\lambda(t) - \Phi(t)}{\sqrt{4DT(t)}} \right)^2 + \left(\frac{x' - x_0\lambda(t') - \Phi(t')}{\sqrt{4DT(t')}} \right)^2 \right.$$

$$\left. \left. - N(t,t')\left(\frac{x - x_0\lambda(t) - \Phi(t)}{\sqrt{2DT(t)}} \right)\left(\frac{x' - x_0\lambda(t') - \Phi(t')}{\sqrt{2DT(t')}} \right) \right] \right\},$$

where x_0 is the (localized) initial condition and

$$N(t,t') = \frac{1}{\sqrt{T(t)T(t')}} \int_0^{t'} ds\, \lambda(t-s)\lambda(t'-s) \quad t \geq t',$$

is the two-time correlation function or covariance. As expected from the Markof-fian Smoluchowski equation, both propagators remain Gaussians for all times with Eq. (4.18b) being bivariate. In agreement with the results derived in Chapter 3, the mean displacement and the MSD are

$$\langle x \rangle = x_0\lambda(t) + \Phi(t), \qquad (4.19a) \qquad\qquad \langle \Delta x^2 \rangle = 2DT(t). \qquad (4.19b)$$

The MSD is defined here as the difference between the average of the squared displacement and the square of its average. The two-time correlation function $N(t,t')$ approaches 0 when $t' \to 0$ and when $t \to \infty$. It is identically 1 for $t = t'$. When the memory is taken to be a time-local δ-function, i.e., the Ornstein-Uhlenbeck process, it simplifies to $\lambda(t-t')\sqrt{T(t')/T(t)}$.

From Eqs. (4.18), the joint probability distributions for the arbitrary initial condition $P_0(z)$ is derived in the standard manner $P_n(...) = \int_{-\infty}^{\infty} dz\, \Pi_n(...|z,t)P_0(z)$. We

have then

$$P_1(x,t) = \frac{1}{\sqrt{4\pi DT(t)}} \int\limits_{-\infty}^{\infty} dz\, P_0(z) \exp\left\{ -\left(\frac{x - z\lambda(t) - \Phi(t)}{\sqrt{4DT(t)}} \right)^2 \right\}, \qquad (4.20a)$$

$$P_2(x,t;x',t') = \frac{1}{4\pi D\sqrt{T(t)T(t')[1-N^2(t,t')]}} \int\limits_{-\infty}^{\infty} dz\, P_0(z) \exp\left\{ -\left(\frac{x' - z\lambda(t') - \Phi(t')}{\sqrt{4DT(t')}} \right)^2 \right\}$$

$$\times \exp\left\{ \frac{-1}{1-N^2(t,t')} \left[\left(\frac{x - z\lambda(t) - \Phi(t)}{\sqrt{4DT(t)}} \right) - N(t,t') \left(\frac{x' - z\lambda(t') - \Phi(t')}{\sqrt{4DT(t')}} \right) \right]^2 \right\}. \quad (4.20b)$$

Eqs. (4.20a) and (4.20b) are written to highlight their similarities and differences. The integrand of the single-time joint probability distribution, Eq. (4.20a), occurs identically (modulo a change from t to t') in the integrand of the two-time joint probability. However, the complete integrand of Eq. (4.20b) incorporates a second Gaussian with dependence on both the time t and the two-time correlation function.

4.4 The Solution to a Fokker-Planck Equation

The one- and two-time joint probability distributions, Eq. (4.20) can be combined using Bayes' theorem, Eq. (4.4a), to construct the conditional probability distribution $Q_{1|1}$. It is given by

$$Q_{1|1}(x,t|x',t';P_0) = \left[\int\limits_{-\infty}^{\infty} dz\, P_0(z) \exp\left\{ -\left(\frac{x' - z\lambda(t') - \Phi(t')}{\sqrt{4DT(t')}} \right)^2 \right\} \right]^{-1} \qquad (4.21)$$

$$\times \frac{1}{\sqrt{2\pi DT(t)[1-N^2(t,t')]}} \int\limits_{-\infty}^{\infty} dz\, P_0(z) \exp\left\{ -\left(\frac{x' - z\lambda(t') - \Phi(t')}{\sqrt{4DT(t')}} \right)^2 \right\}$$

$$\times \exp\left\{ \frac{-1}{1-N^2(t,t')} \left[\left(\frac{x - z\lambda(t) - \Phi(t)}{\sqrt{4DT(t)}} \right) - N(t,t') \left(\frac{x' - z\lambda(t') - \Phi(t')}{\sqrt{4DT(t')}} \right) \right]^2 \right\}.$$

The initial condition $P_0(z)$ is carried through both of Eqs. (4.20) such that it appears in both the denominator and the numerator of Eq. (4.21), being convolved with the

one- and two-time propagators, respectively. Therefore, generally the evolution of $Q_{1|1}$ depends not only on the single conditioned time t' but on its history as well. Processes for which this dependence is retained are said to display aging dynamics. This type of dynamics clearly complicates observational or experimental analysis using Eq. (2.2) because a single measurement at time t', or even multiple measurements at times t', t'', etc., do not accurately inform about the future.

Processes that lack this historical dependence satisfy the criteria for a Markov process given in Eq. (4.6). Eq. (4.21) allows for the derivation of the corresponding conditions on $\lambda(t)$ and, therefore, the related memories. As the construction of P_3, and the general $Q_{1|2}$ is non-trivial, we avoid such complications by considering Eq. (4.21) for the case of a localized initial condition in both space and time. As discussed in Section 4.2, for an initially localized particle $Q_{1|1}(x, t | x', t'; P_0)$ becomes $Q_{1|2}(x, t | x', t'; x_0, 0)$ exactly. Thus, by taking P_0 to be a δ-function and $\beta(t) = 0$, a special case of the twice-conditioned conditional probability distribution is constructed. The result is

$$Q_{1|2}(x, t | x', t'; x_0, 0) = \frac{1}{\sqrt{4\pi DT(t)[1 - N^2(t, t')]}} \exp\left\{\frac{-1}{4DT(t)[1 - N^2(t, t')]}\right.$$
$$\left.\left[x - N(t, t')\frac{T(t)}{T(t')}x' - x_0\left(\lambda(t) - \lambda(t')N(t, t')\frac{T(t)}{T(t')}\right)\right]^2\right\} \quad (4.22)$$

Eq. (4.22) retains the Gaussian form of both propagators. The calculations of the mean displacement and the mean squared displacement (MSD) are trivial and result in the expressions

$$\langle x \rangle_Q = N(t, t')\frac{T(t)}{T(t')}x' - x_0\left(\lambda(t) - \lambda(t')N(t, t')\frac{T(t)}{T(t')}\right), \quad (4.23a)$$

$$\langle \Delta x^2 \rangle_Q \equiv \langle x^2 \rangle_Q - \langle x \rangle_Q^2 = 2DT(t)[1 - N^2(t, t')]. \quad (4.23b)$$

As indicated by the average displacement, Eq. (4.23a), at short times the particle may move in either direction. This contrasts with that of the propagator Π_1 which

displays a delay for all non-Markov processes (see our discussion on the moments in Chapter 3). The MSD is modified by a simple dependence on the covariance. Both of Eqs, (4.23) converge with the equivalent expressions for the propagator, Eqs. (4.19) at long-times.

From inspection, $Q_{1|1}(x, t; x', t'; P_0)$ is not generally equal to $Q_{1|2}(x, t; x', t'; x_0, 0)$ for $t' > 0$. As expected, the Markov criteria are therefore not generally satisfied. Only when the factor that multiples x_0 is identically zero is Eq. (4.22) independent of the initial time. This condition is met when

$$\frac{\lambda(t)}{\lambda(t')} = N(t, t')\frac{T(t)}{T(t')}.$$

Following the insertion of the definitions of $N(t, t')$ and $T(t)$ into the above relation, the derivative with respect to t is taken. This results in the simple condition for a Markov process on the Green function:

$$\lambda(t)\frac{d}{dt'}\lambda(t') = \lambda(t')\frac{d}{dt}\lambda(t). \tag{4.24}$$

This condition is met only when $\lambda(t) = \exp(-Gt)$ with a constant G. An exponential Green function occurs for time-local Langevin equations, i.e., when the memory is a time-local δ-function. From further inspection, the condition for time-homogeneity is $\lambda(t - t')\lambda(t') = \lambda(t)$, which is again only satisfied for an exponential Green function. Thus, Eq. (2.2) describes a time-inhomogenous, non-Markov process. The Smoluchowski equation represents the only Ornstein-Uhlenbeck processes that are time-homogeneous and Markoffian. Pure diffusion, i.e., the Wiener process, is a special case when $G = 0$.

4.4.1 Effect of non-Markofficity on the Conditional Probability

To give a concrete example of the evolution of the twice-conditioned distribution, Eq. (4.22), we use the exponential memory that we introduced in Chapter 3. We reproduce its Green function here for clarity (see Chapter 3 for details),

$$\lambda(t) = e^{-bt/2}\left[\cos\sqrt{\omega^2 - \frac{b^2}{4}}t + \left(\frac{b}{\sqrt{4\omega^2 - b^2}}\right)\sin\sqrt{\omega^2 - \frac{b^2}{4}}t\right],$$

where b is the damping parameter and $\omega = \sqrt{\gamma b}$ is the coherence parameter.

We have used the Green function for an exponential memory, with $b/\gamma = 1/4$, in the construction of Fig. 4.1. Its left panel depicts the propagator $\Pi_1(x, t|x_0, 0)$ as defined by Eq. (4.18a). The right panel displays the corresponding conditional probability distribution $Q_{1|2}(x, t|x_0, t'; x, 0)$ as in Eq. (4.22). The particle is taken to be initialized at $x = x_0$ for both cases (with no additional history dependence, i.e., $\beta(t) = 0$), with the latter being also conditioned on the particle being at x_0 at time $t' = \omega/2$. Thus, $Q_{1|2}(x, t|x_0, t'; x, 0)$ gives the probability density that the particle is located at x at time t given that it was at x_0 at both $t = 0$ and $t = \omega/2$. We set $D = \omega x_0^2/4$. Both probability densities are shown for five dimensionless times: for the propagator they are $\omega t = 0.1, 0.2, 0.3, 0.4, 2$ and for the conditional probability distribution we use $\omega t = 0.6, 0.7, 0.8, 0.9, 2.5$. We have, therefore, that the differences between the last conditioned time and the observation time Δt are identical for both cases (namely, $\Delta t = 0.1, 0.2, 0.3, 0.4, 2$). The initial condition, which normalizes the horizontal axis, is identified with arrows in both panels. The arrows also serve to highlight the difference between the two distributions for small values of Δt. Both the propagator and the twice-conditioned distribution immediately start to spread from diffusion. The propagator's average motion is initially delayed due to inertial effects. In contrast, the twice-conditioned distribution displays an *immediate* average motion towards the center due to the memory of its history. At long times
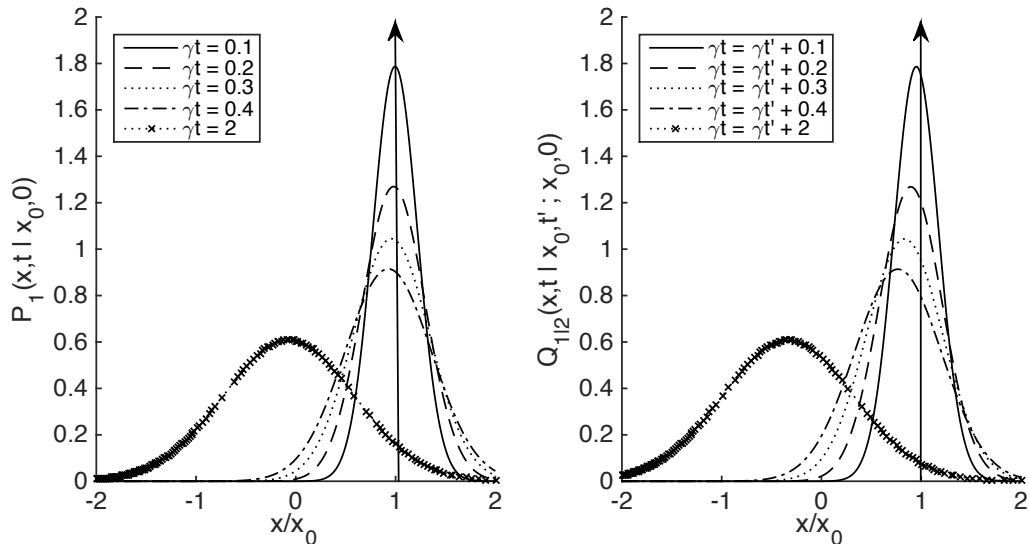
Figure 4.1: Time-dependence of the propagator $\Pi_1(x, t|x_0, 0)$ (left panel) and the twice-conditioned probability distribution $Q_{1|2}(x, t|x_0, t'; x_0, 0)$ (right panel). The history function $\beta(t)$ is taken to be 0 for both. The later condition for $Q_{1|2}$ is $t' = \omega/2$ (see text for further elaboration on the conditions). The positional dependence (horizontal axis) is normalized with x_0. We plot both distributions for five dimensionless times: $\omega t = 0.1, 0.2, 0.3, 0.4, 2$ and $\omega t = 0.6, 0.7, 0.8, 0.9, 2.5$, respectively. The latter being, respectively, $0.1\omega, 0.2\omega, 0.3\omega, 0.4\omega, 2\omega$ time units after t'. Arrows indicate the initial condition for both. Shortly after their respective final conditioned time, Π_1 is delayed prior to its motion towards the attractive center while $Q_{1|2}$ moves immediately. At long times the two distributions converge. We set $D = \omega x_0^2/4$ in both panels.

the two converge as the memory effects are damped.

4.5   Conclusion

We have presented in this Chapter a derivation of the conditional probability distribution, given in Eq. (4.21), for the time-nonlocal Ornstein-Uhlenbeck process. This derivation began with Langevin equation representation of the process, Eq. (2.2), from which an equivalent Langevin equation without convolutions is constructed [18].

From there, standard procedures [8] allow one to derive the one- and two-time joint probability distributions and, therefore, the conditional probability distribution. The conditioned distributions tend to be dependent on their full history, with the exception being Markov processes represented by the Smoluchowski equation. This includes the special case of pure diffusion, i.e., the Wiener process. See Giuggioli et. al. [61] for further discussions on the complications when the system contains a memory of the delay type.

With conditional probability distributions, processes that are governed by time-nonlocal harmonic forces can be analyzed. Two situations in which they may find application are observations that are limited to a subspace of the full motion space and systems that are subject to boundary conditions. The latter already presents issues in attempts to describe time-*local* processes that are not spatially-invariant. The one- and two-time joint distributions are generally not sufficient. For example, the method of images is inapplicable in the presence of boundary conditions [67, 74]. One suggested solution involves supplementing the Fokker-Planck equations, Eqs. (4.20), with terms that account for the boundaries. The reliance of many boundary techniques on the propagator, and not the joint distributions, may make an equation for the conditional probability distribution itself be of interest.

We close by briefly noting this equation. It can be derived from Eqs. (4.15) using $P_2 = Q_{1|1}P_1$, a rearrangement of Eq. (4.4a). When we substitute the second into the first, we have

$$\frac{\partial}{\partial t}Q_{1|1}(x,t|x',t';P_0) = \frac{\partial}{\partial x}\left[\left(A(t)x + +B(t)+C(t,t')\frac{\partial}{\partial x'}+D(t)\frac{\partial}{\partial x}\right)Q_{1|1}(x,t|x',t';P_0)\right]$$
$$+ \frac{\partial}{\partial x'}\left[\ln P_1(x',t)\frac{\partial}{\partial x}Q_{1|1}(x,t|x',t';P_0)\right]. \tag{4.25}$$

The first term on the right-hand side of Eq. (4.25) is identical to the equation for the two-time joint probability, Eq. (4.15b). The second term; however, explicitly depends on the P_1 and, therefore, the initial condition of $Q_{1|1}$. For processes dependent

on boundary conditions, additional terms may need to be added into Eqs. (4.20a) and 4.25.

The work described in this Chapter was done in collaboration with co-investigators external to UNM, and has been accepted for publication as L. Giuggioli, T. J. McKetterick, V. M. Kenkre, and M. Chase, "Fokker-Planck description for a linear delayed Langevin equation with additive Gaussian noise", *Journal of Physics A*, (2016).

Part 2: Simple Random Walk under Confinement

Chapter 5

Overview of Confinement in Random Walks

Systems that perform random walks are ubiquitous in both natural and artificial contexts. They arise in disciplines as diverse as reaction-diffusion theory [75–81], immunology [82–86], animal motion [3,87–90], and epidemiology [67,68,91–94]. True to the term "random walker", these systems often describe the spatial dependence of a particle or excitation. Such objects may experience an additional forcing term which acts to confine the particle to a particular region of space. The often-used starting point to model such systems, with confinement at the probability level of description, is the general Smoluchowski equation. In a continuous one-dimensional space, it is given by

$$\frac{\partial P(x,t)}{\partial t} = \frac{\partial}{\partial x}\left(\frac{dU(x)}{dx}P(x,t)\right) + D\frac{\partial^2 P(x,t)}{\partial x^2},\tag{5.1}$$

Here $P(x,t)$ is the probability density of the particle being located at position x at time t, $U(x)$ is the confining potential and D is the diffusion constant. Eq. (5.1) can arise from a Langevin description [1,2] for a particle in a highly-damped environment that experiences white noise. The derivation of Eq. (5.1) from its underlying

Langevin description, and, more generally, the relation between the Langevin and Fokker-Planck descriptions, is sketched in Appendix B.

The term 'Smoluchowski equation' usually is made in reference to a confining potential proportional to x^2, i.e., quadratic. This follows from the standard usage of the harmonic oscillator as the first-order model for any system with a potential minimum. A recent study of the transmission of infection on the basis of Eq. (5.1) has been carried out by Sugaya and Kenkre [68, 95]. Our interest lies in potentials that confine but are *not* quadratic in the spatial coordinate. Higher powers of x are not analytically tractable; however a linear potential, i.e., one proportional to $|x|$, can be solved exactly. The particularization of Eq. (5.1) for such a potential is

$$\frac{\partial P(x,t)}{\partial t} = \mathcal{E}\frac{\partial}{\partial x}\left(\frac{|x|}{x}P(x,t)\right) + D\frac{\partial^2 P(x,t)}{\partial x^2},\tag{5.2}$$

where $\mathcal{E}$ is the strength of the potential with units of velocity. The solution to these potentials can be found using Laplace transforms. This is followed by applying the appropriate boundary conditions at the points of discontinuity and is applicable to *any* piecewise linear potential.

In Chapter 6, we present the exact solution of the V-potential equation. Its evolution is then compared with that of the Smoluchowski equation with a quadratic potential. Chapter 7 discusses two illustrative applications in the disciplines of condensed matter, the motion of excitations on doped molecular crystals, and immunology, the motion of receptor clusters on the cell surface.

Chapter 6

Piecewise Linear Potentials: Matching Analysis

We first introduce a method of solving the general Smoluchowski equation, Eq. (5.1), for an arbitrary piece-wise linear potential. Solutions are found in each region of space complementary to the segmentation of the potential and are then joined across the boundaries. Thus, the solution to *any* linear potential can be constructed. Matching conditions for the most general boundary, a discontinuous jump between two segments each with an arbitrary slope, are presented and then particularized to two special cases: a discontinuous jump between purely diffusive spaces and a 'V-potential', i.e., two linear pieces of equal and opposite slopes on the two sides of an attractive center taken to lie at $x = 0$.

In the second section, we apply these matching conditions to the case of a V-potential. Dynamics of a particle in this sub-quadratic potential have been known in part earlier, a partial solution having been given by Smoluchowski [96] for the case of a reflecting boundary at $x = 0$ and extended by Lamm and Schulten [97–99] to absorbing boundary conditions. Here, we give the full solution for arbitrary initial

condition and no boundary. The solutions are simple but their behavior is rich. In particular, a striking feature, found when the initial condition is a δ-function, is a change in the shape of the solution from a Gaussian to a decaying exponential. The change in the shape leads to interesting consequences on the time evolution of ensemble averaged quantities such as the position and velocity. We conclude with a comparison between the solutions for the standard quadratic potential and the V-potential. In particular, the variance in the shape of the V-potential solution is contrasted with the invariant solution for the quadratic potential, which remains Gaussian for a δ-function initial condition.

6.1 Matching Conditions for a General Boundary

When the potential $U(x)$ present in Eq. (5.1) is piece-wise linear Laplace-domain results can be simply obtained. An illustrative example of such a potential is shown in the left-most panel of Fig. 6.1. Within each linear segment, and for the moment neglecting the initial condition, the dynamics are described by the standard Laplace-domain convective-diffusive equation

$$D\frac{d^2\widetilde{P}(x,\epsilon)}{dx^2} + \mathcal{E}_S\frac{d\widetilde{P}(x,\epsilon)}{dx} = \epsilon\widetilde{P}(x,\epsilon). \tag{6.1}$$

Here $\mathcal{E}_S$ is the potential strength appropriate to that segment.

As a second order linear equation with constant coefficients, Eq. (6.1) possesses two linear independent solutions. They are of the form $\widetilde{P}(x,\epsilon) \sim e^{\lambda x}$ where λ is found using the characteristic polynomial of Eq. (6.1). Within each segment, this leads to solutions of the form,

$$\widetilde{P}(x,\epsilon) = \mathcal{A}e^{\frac{-\mathcal{E}_S+\sqrt{\mathcal{E}_S^2+4D\epsilon}}{2D}x} + \mathcal{B}e^{\frac{-\mathcal{E}_S-\sqrt{\mathcal{E}_S^2+4D\epsilon}}{2D}x},$$

Here $\mathcal{A}$ and $\mathcal{B}$ are constants that will be determined by matching the solutions of each joined pair of segments at their respective 'joint', i.e., the point of discontinuity.
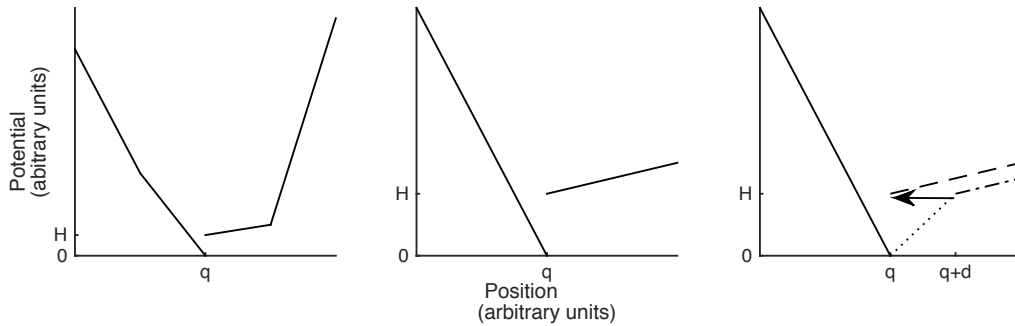
Figure 6.1: Depicts an example of a piece-wise linear potential and illustrates the method of solving for a general point of discontinuity. Both distance, on the horizontal axis, and the potential, on the vertical axis, are in arbitrary units. The left frame shows an arbitrary four-segment potential. In the center frame, a close-up of the discontinuity between the central two segments L and R is shown. The method used to solve for the matching conditions is shown in the right frame. The related potential, for which segment R is shifted rightwards a distance d (the dash-dotted line) and connecting segment C (the dotted line) is inserted. Using segment C as a mediator, the matching conditions between the original segments R and L is derived. The matching conditions for the original discontinuous potential is found by taking the limit $d \to 0$ indicated by the arrow.

With the matching conditions for a general joint, the full solution (when the initial condition is included) is found by chaining together successive segments.

The derivation of the general matching conditions between the coefficients of the solution for each segment proceeds as follows. The general joint, shown in the central frame of Fig 6.1, consists of a discontinuous jump, at point q and of height H, between segments, which we label I and II, of potential strengths α_{I} and α_{II} respectively. The potential is thus given by

$$U_G(x) = \alpha_I(x - p)\Theta(p - x) + (\alpha_{II}(x - p) + H)\Theta(x - p), \qquad (6.2)$$

where $\Theta(x)$ is the Heaviside step function. The derivation is complicated by the discontinuity in $U_G(x)$ which leads to a discontinuity in $\widetilde{P}(x)$. Instead of the potential given in Eq. (6.2), we consider a simpler potential which has the segments I and II separated a distance d and connected by a third segment, C, of potential strength

H/d. Thus, the modified potential is

$$U_M(x) = \alpha_I(x-p)\Theta(p-x) + \frac{H}{d}(x-p)(\Theta(x-p) + \Theta(d+p-x))$$
$$+ (\alpha_{II}(x-p-d) + H)\Theta(x-p-d), \qquad (6.3)$$

With the addition of segment C, $U_M(x)$ is continuous. The derivation of the matching conditions between segments I and II is simplified. As indicated by the arrow in the right-frame of Fig. 6.1, the matching conditions for $U_G(x)$ are then found by taking the limit $d \to 0$.

To start, we consider one a continuous joints of the type found in $U_M(x)$. The segments are joined at point p with potential strengths of α_L and α_R on the left and right segments respectively. This potential is given by

$$U_C(x) = \alpha_L(x-p)\Theta(p-x) + \alpha_R(x-p)\Theta(x-p),$$

Within each region the solution $\widetilde{P}(x, \epsilon)$ for the segments becomes

$$\widetilde{P}_L(x, \epsilon) = \mathcal{A}_L e^{\frac{-\alpha_L + \sqrt{\alpha_L^2 + 4D\epsilon}}{2D}x} + \mathcal{B}_L e^{\frac{-\alpha_L - \sqrt{\alpha_L^2 + 4D\epsilon}}{2D}x},$$
$$\widetilde{P}_R(x, \epsilon) = \mathcal{A}_R e^{\frac{-\alpha_R + \sqrt{\alpha_R^2 + 4D\epsilon}}{2D}x} + \mathcal{B}_R e^{\frac{-\alpha_R - \sqrt{\alpha_R^2 + 4D\epsilon}}{2D}x}.$$

Here, $\widetilde{P}_L(x, \epsilon)$ $(\widetilde{P}_R(x, \epsilon))$ is for the left (right) segment and $\mathcal{A}_R$, etc., are the coefficients. The two boundary conditions across the joint are

$$\widetilde{P}_R(q, \epsilon) = \widetilde{P}_L(q, \epsilon), \quad (6.4\text{a}) \qquad \left.\frac{d\widetilde{P}_R(x, \epsilon)}{dx}\right|_{x=p} = \left.\frac{d\widetilde{P}_L(x, \epsilon)}{dx}\right|_{x=p} + \frac{\alpha_L - \alpha_R}{D}\widetilde{P}_L(p, \epsilon). \quad (6.4\text{b})$$

Eq. (6.4a) ensures the continuity of $\widetilde{P}(x, \epsilon)$ across the joint. The discontinuity in the derivative of $\widetilde{P}(x, \epsilon)$, as seen in Eq. (6.4b), follows from requiring the integral of Eq. (6.1) around the joint go to zero as the integral limits approach the discontinuity.

That is,

$$\lim_{\kappa \to 0} \int_{p-\kappa}^{p+\kappa} \left[D\frac{d^2\widetilde{P}(x,\epsilon)}{dx^2} + \frac{d}{dx}\left([\alpha_L \Theta(p-x) + \alpha_R \Theta(x-p)]\, \widetilde{P}(x,\epsilon) \right) - \epsilon \widetilde{P}(x,\epsilon) \right] = 0.$$

From Eq. (6.4a), we have the relation

$$\mathcal{B}_R(p) = \mathcal{A}_L(p) + \mathcal{B}_L(p) - \mathcal{A}_R(p). \tag{6.5}$$

where we have introduced the notational shorthand $\mathcal{A}_R(p)$ defined by

$$\mathcal{A}(p) = \mathcal{A}e^{\frac{-\alpha+\sqrt{\alpha^2+4D\epsilon}}{2D}p}, \qquad \mathcal{B}(p) = \mathcal{B}e^{\frac{-\alpha_L-\sqrt{\alpha^2+4D\epsilon}}{2D}p},$$

for all coefficients. The condition on the derivative, Eq. (6.4b), results in the relation

$$\left(\alpha_R - \sqrt{\alpha_R^2 + 4D\epsilon} \right) \mathcal{A}_R(p) + \left(\alpha_R + \sqrt{\alpha_R^2 + 4D\epsilon} \right) \mathcal{B}_R(p) = \tag{6.6}$$

$$\left(2\alpha_R - \alpha_L - \sqrt{\alpha_L^2 + 4D\epsilon} \right) \mathcal{A}_L(p) + \left(2\alpha_R - \alpha_L + \sqrt{\alpha_L^2 + 4D\epsilon} \right) \mathcal{B}_L(p).$$

Eqs. (6.5) and (6.6) are combined into the dual matching conditions that give the coefficients of the segment R in terms of those of segment L and vice versa

$$2\sqrt{\alpha_R^2 + 4D\epsilon}\,\mathcal{A}_R(p) = \left(\alpha_L - \alpha_R + \sqrt{\alpha_R^2 + 4D\epsilon} + \sqrt{\alpha_L^2 + 4D\epsilon} \right) \mathcal{A}_L(p) \tag{6.7a}$$

$$+ \left(\alpha_L - \alpha_R + \sqrt{\alpha_R^2 + 4D\epsilon} - \sqrt{\alpha_L^2 + 4D\epsilon} \right) \mathcal{B}_L(p),$$

$$2\sqrt{\alpha_R^2 + 4D\epsilon}\,\mathcal{B}_R(p) = \left(\alpha_R - \alpha_L + \sqrt{\alpha_R^2 + 4D\epsilon} - \sqrt{\alpha_L^2 + 4D\epsilon} \right) \mathcal{A}_L(p) \tag{6.7b}$$

$$+ \left(\alpha_R - \alpha_L + \sqrt{\alpha_R^2 + 4D\epsilon} + \sqrt{\alpha_L^2 + 4D\epsilon} \right) \mathcal{B}_L(p).$$

The coefficients of segment L in terms of those of R are found by exchanging L and R.

For the modified potential given in Eq. (6.3), segments I and II can be connected by applying Eqs. (6.7) twice. The first application is across the I-C joint, located at

q, and the second application is across the *C-II* joint, located at $q + d$. In the limit $d \to 0$ the matching conditions for the discontinuous joint in Eq. (6.2) are then

$$\mathcal{A}_{II} = \frac{\alpha_I + \sqrt{\beta_I} - e^{-\frac{H}{D}}\left(\alpha_{II} - \sqrt{\beta_{II}}\right)}{2\sqrt{\beta_{II}}}\mathcal{A}_I e^{\frac{\alpha_{II} - \alpha_I + \sqrt{\beta_I} - \sqrt{\beta_{II}}}{2D}q} \tag{6.8a}$$

$$+ \frac{\alpha_I - \sqrt{\beta_I} - e^{-\frac{H}{D}}\left(\alpha_{II} - \sqrt{\beta_{II}}\right)}{2\sqrt{\beta_{II}}}\mathcal{B}_I e^{\frac{\alpha_{II} - \alpha_I - \sqrt{\beta_I} - \sqrt{\beta_{II}}}{2D}q},$$

$$\mathcal{B}_{II} = \frac{e^{-\frac{H}{D}}\left(\alpha_{II} + \sqrt{\beta_{II}}\right) - \alpha_I - \sqrt{\beta_I}}{2\sqrt{\beta_{II}}}\mathcal{A}_I e^{\frac{\alpha_{II} - \alpha_I + \sqrt{\beta_I} + \sqrt{\beta_{II}}}{2D}q} \tag{6.8b}$$

$$+ \frac{e^{-\frac{H}{D}}\left(\alpha_{II} + \sqrt{\beta_{II}}\right) - \alpha_I + \sqrt{\beta_I}}{2\sqrt{\beta_{II}}}\mathcal{B}_I e^{\frac{\alpha_{II} - \alpha_I - \sqrt{\beta_I} + \sqrt{\beta_{II}}}{2D}q}.$$

where $\beta_I = \alpha_I^2 + 4D\epsilon$ and $\beta_{II} = \alpha_{II}^2 + 4D\epsilon$. The coefficients of segment I can be found in terms of those of segment II by the combination of a label switch and the transform $H \to -H$. As expected, Eqs. (6.8) reduce to Eqs. (6.7) when the height of the discontinuity is zero, $H \to 0$.

The effects of the discontinuity are highlighted in the simple potential that consists of a step of height $H > 0$ at point $q = 0$ between two purely diffusive regions. In this straightforward case, Eqs. (6.7) are simplified as

$$\mathcal{A}_{II} = \frac{1 + e^{-\frac{H}{D}}}{2}\mathcal{A}_I + \frac{e^{-\frac{H}{D}} - 1}{2}\mathcal{B}_I, \quad (6.9a) \qquad \mathcal{B}_{II} = \frac{e^{-\frac{H}{D}} - 1}{2}\mathcal{A}_I + \frac{1 + e^{-\frac{H}{D}}}{2}\mathcal{B}_I. \quad (6.9b)$$

As expected from the similarities of this problem to that of the quantum mechanical barrier, the potential wall couples the coefficients both on a single segment and between the two segments. An increase in the height of the potential wall leads to a pronounced increase in this coupling.

When normalization requirements are applied, $\mathcal{A}_{II}$ is equal to 0, and the particle is initialized on the left segment (I), Eqs. (6.9) lead to the simple relations

$$\mathcal{B}_{II} = \frac{2}{1 + e^{\frac{H}{D}}}\mathcal{B}_I, \qquad \mathcal{A}_I = \tanh\frac{H}{2D}\mathcal{B}_I.$$

The wall leads to an exponential suppression of the transmission. In the limit $H \rightarrow \infty$, there will be no coupling between the segments. Somewhat counter-intuitively, however, when H becomes negative there is a limit to how fast the particle spills over into the low-potential region. Effectively, a particle that starts in the high potential regime does not immediately detect the drop in potential.

In preface to the analysis performed in Section 6.2 we provide Eqs. (6.7) for a V-potential. The matching conditions

$$\mathcal{A}_{II} = \frac{\sqrt{\mathcal{E}^2 + 4D\epsilon} - \mathcal{E}}{\sqrt{\mathcal{E}^2 + 4D\epsilon}} \mathcal{A}_I - \frac{\mathcal{E}}{\sqrt{\mathcal{E}^2 + 4D\epsilon}} \mathcal{B}_I, \tag{6.10a}$$

$$\mathcal{B}_{II} = \frac{\mathcal{E}}{\sqrt{\mathcal{E}^2 + 4D\epsilon}} \mathcal{A}_I + \frac{\mathcal{E} + \sqrt{\mathcal{E}^2 + 4D\epsilon}}{\sqrt{\mathcal{E}^2 + 4D\epsilon}} \mathcal{B}_I. \tag{6.10b}$$

Here we have taken $\alpha_{II} = -\alpha_I = \mathcal{E}$ where $\mathcal{E}$ is positive and set both the discontinuity H and the location q to zero.

6.2 Solutions and their Behavior

We return our focus to the confining V-potential, the expression for which is given by

$$U_V(x) = \mathcal{E}|x|,$$

$\mathcal{E}$ being the potential strength with units of velocity. The full solution to the corresponding Smoluchowski equation, Eq. (5.2) is found through deriving the propagator $\Pi(x, x_0, t)$ which is the solution for the probability density at x at a time t later given that the initial density is localized at x_0. This is due to the linearity of the problem which allows the general solution for an arbitrary initial condition to be found using the standard Greens' function formalism whereby the propagator is multiplied by

the initial probability distribution $p(x_0)$ and integrated over all space

$$P(x,t) = \int\limits_{-\infty}^{\infty} dx_0\, p(x_0)\Pi(x,x_0,t).$$

As the essence of the solution to Eq. (5.2) is given by the propagator we focus our attention on analyzing its behavior.

We first examine the steady state distribution, $P_{SS}(x)$, which is obtained by putting the left hand side of Eq. (5.2) equal to zero:

$$P_{SS}(x) = \lim_{t\to\infty} P(x,t) = \frac{1}{2\ell}e^{-\frac{|x|}{\ell}} \tag{6.11}$$

where $\ell = D/\mathcal{E}$ is the characteristic width of the distribution. When the particle is initialized far from the center the short-time behavior of the solution is essentially given by the diffusion equation with a simple convective term; the effect of the discontinuity is minimal. The requirement that the long-time behavior of the V-potential equation is given by Eq. (6.11) already shows that the full-time solution will change shape.

The full Laplace-domain expression for Eq. (5.2), with a localized initial condition $P_0(x) = \delta(x - x_0)$ is

$$\epsilon\widetilde{P}(x,\epsilon) - \delta(x-x_0) = \mathcal{E}\frac{d}{dx}\left(\frac{|x|}{x}\widetilde{P}(x,\epsilon)\right) + D\frac{d^2\widetilde{P}(x,\epsilon)}{dx^2}. \tag{6.12}$$

We initially consider the case of $x_0 > 0$, the case of $x_0 < 0$ being solved by symmetry and consequently by a simple $x \to -x$ transformation. We note that the domain of x naturally breaks up into three different regions separated by two points of discontinuity: the first, at $x = 0$, due to the potential and the second, at $x = x_0$, due to the initial condition. As mentioned in Section 6.1, within each region there are two independent solutions of the form $\exp((\pm 1 \pm \sqrt{1 + \frac{4\ell\epsilon}{\mathcal{E}}})/(2\ell)x)$.

In addition to the matching conditions across the first discontinuity, Eqs. (6.10a) and (6.10b), there are four other boundary conditions. Two conditions relate the

behavior of the probability as $x \to \pm\infty$, and require that $\widetilde{P}(x \to \pm\infty, x_0, \epsilon)$ vanish. The second pair, similar in form to Eqs. (6.4), match across the initial condition . They are

$$\widetilde{P}_L(x_0, \epsilon) = \widetilde{P}_R(x_0, \epsilon), \quad (6.13a) \qquad \frac{d\widetilde{P}_L(x_0, \epsilon)}{dx}\bigg|_{x=x_0} = \frac{d\widetilde{P}_R(x, \epsilon)}{dx}\bigg|_{x=x_0} + \frac{1}{D}. \quad (6.13b)$$

where L (R) refers to the region to the left (right) of the initial condition. As in Eq. (6.4a), the first condition, Eq. (6.13a), ensures continuity of the probability. The second, Eq. (6.4b) follows from the requirement that the integral of Eq. (6.12) around the initial condition go to zero as the integral limits approach the discontinuity, i.e.,

$$\lim_{\kappa \to 0} \int_{x_0-\kappa}^{x_0+\kappa} \left[D\frac{d^2\widetilde{P}(x, \epsilon)}{dx^2} + \mathcal{E}\frac{d}{dx}\left(\frac{x}{|x|}\widetilde{P}(x, \epsilon)\right) - \epsilon\widetilde{P}(x, \epsilon) + \delta(x - x_0) \right] = 0.$$

Application of these conditions, along with the removal of the requirement that $x_0 > 0$, yields the propagator $\widetilde{\Pi}(x, x_0, \epsilon)$ in the Laplace domain:

$$\widetilde{\Pi}(x, x_0, \epsilon) = \frac{e^{-\frac{|x|-|x_0|}{2\ell}}}{\mathcal{E}\sqrt{1 + \frac{4\ell\epsilon}{\mathcal{E}}}} \left[e^{-\sqrt{1+\frac{4\ell\epsilon}{\mathcal{E}}}\frac{|x-x_0|}{2\ell}} + \frac{e^{-\sqrt{1+\frac{4\ell\epsilon}{\mathcal{E}}}\frac{|x|+|x_0|}{2\ell}}}{\sqrt{1 + \frac{4\ell\epsilon}{\mathcal{E}}} - 1} \right]. \quad (6.14)$$

Inversion of the Laplace-domain propagator into the time-domain is possible either through explicit Bromwich contour integrations or by reference to tables [100]. The time domain propagator is a combination of error functions, exponentials and the Gaussian diffusion propagator modified appropriately for convection:

$$\Pi(x, x_0, t) = \frac{1}{\sqrt{4\pi Dt}}e^{-\frac{(x-x_0)^2+\mathcal{E}^2t^2}{4Dt}}e^{-\frac{|x|-|x_0|}{2\ell}} + \frac{e^{-\frac{|x|}{\ell}}}{4\ell}\left(1-\mathrm{erf}\left(\frac{|x|+|x_0|-\mathcal{E}t}{\sqrt{4Dt}}\right)\right). \quad (6.15)$$

Our analytic results Eq. (6.15) can be verified easily through a numerical solution of Eq. (5.2). The latter can be thought of as the continuum limit of

$$\frac{dP_n(t)}{dt} = F\left(P_{n+1} + P_{n-1} - 2P_m\right) + f\left(\frac{|n+1|}{n+1}P_{n+1} - \frac{|n-1|}{n-1}P_{n-1}\right) \quad (6.16)$$
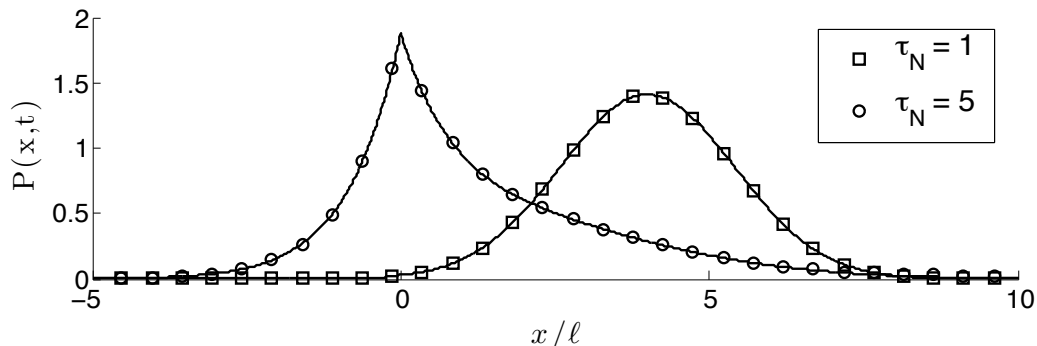
Figure 6.2: Comparison of our analytic solution in Eq. (6.15) with numerically obtained counterparts showing excellent agreement at two different dimensionless times $\tau_N = 1$ and $\tau_N = 5$. Here τ_N is Ft in units of 4×10^6, there are 1200 sites in the chain and $f/F = 0.25 \times 10^{-3}$. The walker location was at a distance $x_0/\ell = 5$ initially. The shape-shifting of the solution is also clear from an early time Gaussian to a late time mod exponential.

where $P_n(t)$ is the probability of occupation of the nth site at a time t in a discrete 1-d lattice, F is the nearest neighbor hopping rate, and f is the rate of motion towards the attractive center at $n = 0$. If a is the lattice spacing, the continuum limit

$$a \to 0, \; F \to \infty, \; f \to \infty, \; Fa^2 \to D, \; 2fa \to \mathcal{E}$$
$$na \to x, \; P_n(t)/a \to P(x,t)$$

converts Eq. (6.16) into the V-potential equation. We use $n_0 = x_0/a$ and the above discretized forms of $\mathcal{E}$ and D to represent Eq. (6.15), the propagator derived analytically in its discrete version, as

$$\Pi_{n,n_0}(t) = \frac{1}{\sqrt{4\pi Ft}} e^{-\frac{(n-n_0)^2 + 4f^2 t^2}{4Ft}} e^{-\frac{|n|-|n_0|}{F/f}} \tag{6.17}$$
$$+ \frac{f}{2F} e^{-\frac{2|n|}{F/f}} \left[1 - \mathrm{erf}\left(\frac{|n|+|n_0|-2ft}{\sqrt{4Ft}} \right) \right].$$

The analytic solution given by Eq. (6.17) (solid lines) is compared to the numerical solution (markers) of the discretized differential equation which we have obtained using standard Matlab procedures such as ODE45. We have displayed in Fig. 6.2 the

spatial distribution at two widely different times. The first depicts an early situation close to the initial distribution and the second a late situation near the steady state. The dimensionless time τ_N is Ft in units of 4×10^6. It has the respective values 1 and 5 for the two cases shown in Fig. 6.2. The value of f/F we have taken is 0.25×10^{-3} and the number of lattice sites 1200. Agreement is excellent given that the size of the region is taken to be large compared with the equilibrium width ℓ and that the potential is not too steep. Much of the interesting behavior found in our solutions is provided by the transition between an initial Gaussian and the eventual cusped steady-state distribution (a decaying exponential).

The analysis that we have discussed here for the V-Potential can in principle be performed for any piece-wise linear confining potential using the results derived in Section 6.1. Generally, however, there is no simple inverse Laplace-transform of the Laplace-domain propagator into the time-domain. Results in the time-domain would require a numerical inverse transform method.

6.2.1   Shape-shifting of the Solutions

Insight into the solutions of our Fokker-Planck equation, Eq. (5.2), can be gained by analyzing the two terms in Eq. (6.15). The first term, essentially a Gaussian, is characteristic of diffusion. The second term has the spatial form of an exponential decay required by the steady state distribution. The peak of the Gaussian travels ballistically in the manner of the case when the potential is a simple bias, i.e. $U(x) = \pm \mathcal{E} x$. The bias respects the potential experienced on either side of the confining center and reflects the peak of the Gaussian term moving through the center. Thus, at long times, only the tail contributes to the probability distribution. Note that the long-time behavior of the propagator is determined by the decaying exponential term, which is modified by a complementary error function.
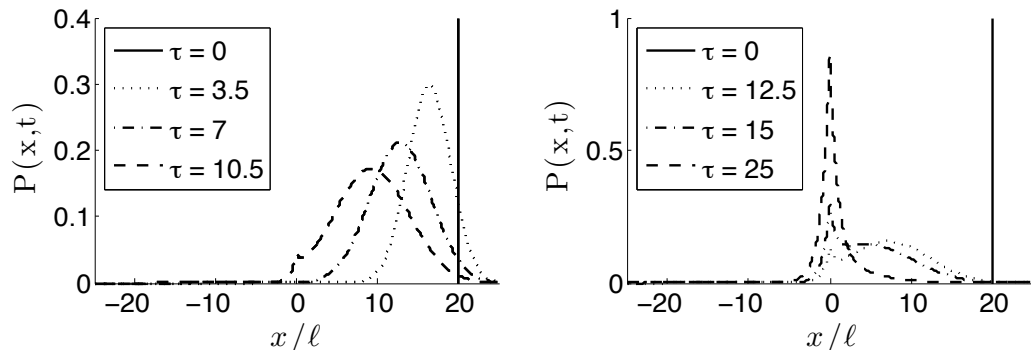
Figure 6.3: Time evolution of the probability density for a walker localized initially at $x_0/\ell = 20$. The dimensionless time is measured as the ratio of t to $\sqrt{2}D/\mathcal{E}^2$. The left panel depicts three early values (3.5, 7, 10.5) while the right depicts three late values (12.5, 15, 25). Both panels display the initial value for comparison. In the left panel, the distribution changes from localized to Gaussians as the walker moves ballistically towards the attractive center and diffuses simultaneously. The last curve shows a little peak at the attractive center as the walker begins to settle at the attractive center. In the right panel the peak grows as the shape changes clearly into the mod exponential. Shape shifting is particularly clear in this figure.

In order to examine more closely the passage from the initial shape through the Gaussian intermediate to the final exponential form, we display Fig. 6.3. Initially, the probability distribution travels ballistically maintaining the shape of a Gaussian. However, when the probability of the walker being at the potential center reaches an appreciable value, the distribution begins to form a cusp, reflecting the approach towards the steady state distribution. Following the formation of the cusp, the distribution rapidly transitions into an intermediate state reflecting both the traveling Gaussian and the exponential. During this transition period there are two local maxima. Finally, the long-term steady state distribution is attained.

6.2.2 Average Position and Velocity

Additional insight into the consequences of the random walker moving in a V-potential can be obtained by exploring its average position $\langle x \rangle$ and its average velocity $\langle v \rangle \equiv d\langle x \rangle / dt$. Choosing a positive value for x_0, the former is obtained by simply calculating the moment of the propagator as given by our Eq. (6.15):

$$\langle x \rangle = \left(\frac{x_0 - \mathcal{E}t}{2} \right) \left[1 + \mathrm{erf} \left(\frac{x_0 - \mathcal{E}t}{\sqrt{4Dt}} \right) \right] + \left(\frac{x_0 + \mathcal{E}t}{2} \right) \left[1 - \mathrm{erf} \left(\frac{x_0 + \mathcal{E}t}{\sqrt{4Dt}} \right) \right] e^{\frac{x_0}{\ell}}. \quad (6.18)$$

The expression for the average position consists of a term showing ballistic motion to the left and a term showing ballistic motion to the right, both at speed $\mathcal{E}$, and both modified by error function factors representative of simultaneous diffusion with diffusion constant D. At long times, the combination of the two terms results in $\langle x \rangle \to 0$. Time differentiation gives

$$\frac{d\langle x \rangle}{dt} = \langle v \rangle = -\frac{\mathcal{E}}{2} \left[1 + \mathrm{erf} \left(\frac{x_0 - \mathcal{E}t}{\sqrt{4Dt}} \right) - \left(1 - \mathrm{erf} \left(\frac{x_0 + \mathcal{E}t}{\sqrt{4Dt}} \right) \right) e^{\frac{x_0}{\ell}} \right]. \quad (6.19)$$

Both Eqs. (6.18) and (6.19) apply for $x_0 > 0$. The average velocity obviously begins as the slope of the V-potential at the position of initial placement, i.e., has the value $-\mathcal{E}$. If there were no diffusion, i.e., if $D = 0$, the average velocity would jump to zero when the walker reaches the attractive center as a consequence of the reverse sign of the V-potential slope on the other side of the center. Diffusion smooths the jump. The sum of the first two terms inside the square brackets in Eq. (6.19) starts at the value 2 and drops to 0 while the third term vanishes both initially and finally. The error functions ensure that there is dormant behavior at small times during which the velocity is essentially at the original constant value until diffusion kicks in and the velocity starts dropping.

In Figs. 6.4 and 6.5, we explore the effect of varying each of the parameters, D, $\mathcal{E}$, and x_0, on the average velocity of the confined random walker. The time scale is chosen separately in the case of each parameter and the plots are parametrized by
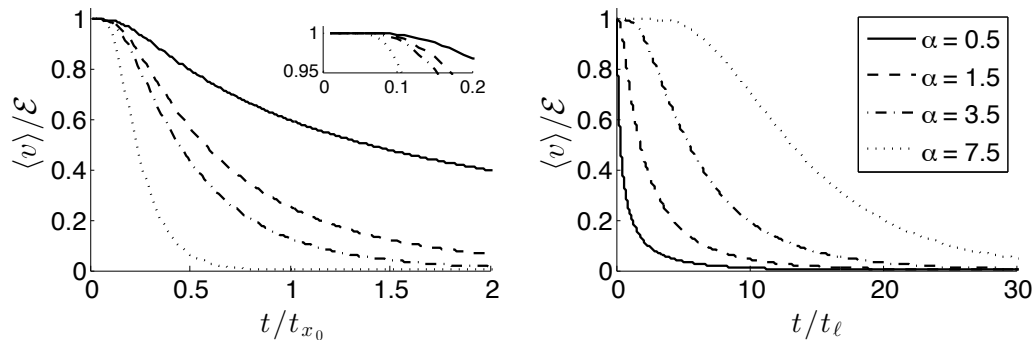
Figure 6.4: Dependence of the velocity of the random walker on time showing the effect of changing the potential slope $\mathcal{E}$ (left panel) and the initial location x_0 (right panel). The parameter that is varied and shown in the legend in the right panel, $\alpha \equiv x_0/\ell$, applies to given line styles in both panels. The dimensionless time used is t/t_{x_0} in the left panel and t/t_ℓ in the right. Here $t_{x_0} = x_0^2/2D$ and $t_\ell = \ell^2/2D$ are times taken by a pure diffusive walker to cover distances x_0 and ℓ respectively. The left panel includes an inset showing the short-term ballistic behavior where a dormant stage is followed by a velocity decrease.

$\alpha \equiv x_0/\ell$, the ratio of the initial position to the steady state width of the distribution. The effect of changing $\mathcal{E}$ is shown on the left in Fig. 6.4, where an increase in $\mathcal{E}$ corresponds to an increase in α. In the short term, shown in the inset, the walker travels ballistically for a longer time when the potential steepness is decreased. The long term decay into the steady state probability distribution, indicated by $\langle v \rangle/\mathcal{E} \to 0$, occurs more slowly for a decreased potential strength. These results match with the intuitive effect of a steeper potential in that the walker will initially travel towards the potential center at a larger velocity, experiencing the effects of confinement earlier allowing it to more quickly settle into the steady state distribution. Overall, increasing the potential strength will decrease the transition time from initial ballistic motion to the final steady state distribution.

The effect of changing the initial position of the particle, x_0, is shown in the right panel of Fig. 6.4. While the behavior appears similar to that shown in the left panel, we note that the time spent in the initial ballistic motion increases as the random
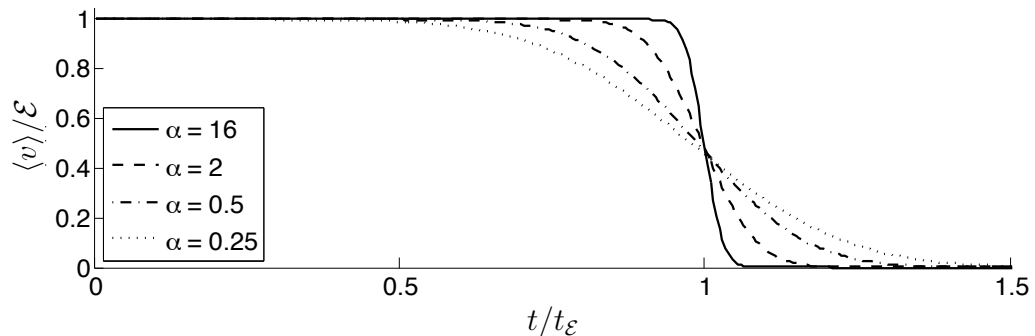
Figure 6.5: Effect of the diffusion constant D, in the form of the dimensionless parameter $\alpha \equiv x_0/\ell = x_0\mathcal{E}/D$, on the time evolution of the velocity of the random walker. The dimensionless time used here, $t/t_\mathcal{E}$ where $t_\mathcal{E} \equiv x_0/\mathcal{E}$ is the time in takes a purely ballistic walker with velocity $\mathcal{E}$ to travel a distance x_0. Note that all curves intersect at the same point when t equals $t_\mathcal{E}$.

walker is initially placed further from the potential center. The walker approaches its steady state distribution more slowly when initialized further away. The α values displayed in the right panel apply to both panels with their associated line types; so we see that that an increase in α moves one in opposite order among the curves in the two panels. The effect of changing the diffusion constant, where an increase in D corresponds to a decrease in α, is displayed in Fig. 6.5. A larger diffusion constant allows the walker to sense the confinement earlier but makes it spend less time relatively moving ballistically. This combination has the consequence that the decay into the steady state is slower. In effect, a large diffusion constant extends the time under which the walker transitions from the initial ballistic motion into the steady state. Note that all the curves in Fig. 6.5 intersect in a single point at $t = t_\mathcal{E}$.

We also show the relation between $\langle x \rangle$ and $\langle v \rangle$ in part because observations have been reported in that manner in the study of immunological synapse formation, a subject we passingly address in Section 7.2. Although we have not obtained such a relation by analytic means, eliminating the time dependence is possible numerically. The results for changing $\mathcal{E}$ is depicted in Fig. 6.6 (effect of changing x_0 is identical).

...lity distribution travels ballistically maintaining the shape of a Gaussian.

...hen the probability of the walker being at the potential center reaches ...ble value, the distribution begins to form a cusp, reflecting the approach ...e steady state distribution. Following the formation of the cusp, the dis-...pidly transitions into an intermediate state reflecting both the ...nd the exponential. During this transition period there are ...nally, the long-term steady state distribution is attained.

Average Position and Velocity

Figure 6.6: Relation between the velocity (time derivative of average displacement) and the displacement of the random walker. Plotted is $\langle v \rangle / \mathcal{E}$ versus $\langle x \rangle / x_0$ when $\mathcal{E}$ (left) and D (right) is varied, both in the form of the dimensionless parameter $\alpha \equiv x_0 / \ell = x_0 \mathcal{E}/D$. Note the change in the convexity of the curves in the left panel. Increasing x_0, corresponding to an increase in either $\mathcal{E}$ or in x_0, leads to the walker traveling ballistically for a longer distance before slowing down into the steady state. As α is decreased, this plunge has qualitatively different shapes, with curve convexity increasing, and indicates a sharper initial slowdown followed by a more leisurely approach to the steady state.

The effect of changing D is depicted in Fig. 6.6, where an increase in D corresponds to a decrease in α. Decreasing the diffusion constant makes the walker travel a larger distance ballistically before reaching the $\langle x \rangle = 0$ region. The plunge occurring closer to the confining center for larger D suggests that diffusion acts as a sensing mechanism for the walker, allowing it to interact with the potential discontinuity while further away.

...insight into the consequences of the random walker ...an be obtained by exploring its average position $\langle x \rangle$ and its average veloc-...$x\rangle/dt$. Choosing a positive value for x_0, the former is obtained by simply ...the moment of the propagator as given by Eq. (6.15):

$$\langle x \rangle = \left(\frac{x_0 - \mathcal{E}t}{2}\right)\left[1+\mathrm{erf}\left(\frac{x_0-\mathcal{E}t}{\sqrt{4Dt}}\right)\right]+\left(\frac{x_0+\mathcal{E}t}{2}\right)\left[1-\mathrm{erf}\left(\frac{x_0+\mathcal{E}t}{\sqrt{4Dt}}\right)\right]e^{\frac{x_0}{\ell}}\cdot t/t_{\mathcal{E}}$$
(6.18)

...sion for the average position consists of a term showing ballistic motion ...and a term showing ballistic motion to the right, both at speed $\mathcal{E}$, and ...ed by error function factors representative of simultaneous diffusion with ...nstant D. At long times, the combination of the two terms results in ...ime differentiation gives

$$\langle v \rangle = -\frac{\mathcal{E}}{2}\left[1+\mathrm{erf}\left(\frac{x_0-\mathcal{E}t}{\sqrt{4Dt}}\right)-\left(1-\mathrm{erf}\left(\frac{x_0+\mathcal{E}t}{\sqrt{4Dt}}\right)\right)e^{\frac{x_0}{\ell}}\right].$$
(6.19)

...(6.18) and (6.19) apply for $x > 0$. The average velocity obviously begins ...e of the V-potential at the position of initial placement, i.e., has the value ...e were no diffusion, i.e., if $D = 0$, the average velocity would jump to zero ...alker reaches the attractive center as a consequence of the reverse sign of ...ntial slope on the other side of the center. Diffusion said that the jump

6.3 Comparison with the Quadratic Potential

A comparison of the V-potential results with those of the general Smoluchowski equation, Eq. (5.1) with the commonly used (see, e.g., ref. [67]) quadratic $U(x)$ given

by $(1/2)\gamma x^2$, is suggested by the use of the later in understanding various physical problems of confined random walkers [67,68] We concluded by contrasting these two cases more closely. For this purpose we compare the propagator we have derived for the case of the V-potential, Eq. (6.15), with the well-known quadratic Smoluchowski propagator [1, 2, 67]

$$\Pi(x, x_0, t) = \frac{e^{-\frac{\left(x - x_0 e^{-\gamma t}\right)^2}{4D\mathcal{T}(t)}}}{\sqrt{4\pi D\mathcal{T}(t)}}, \qquad (6.20a) \qquad \mathcal{T}(t) = \frac{1 - e^{-2\gamma t}}{2\gamma}. \qquad (6.20b)$$

The spatial dependence of the propagator is always Gaussian in the quadratic case. Consequently, the shape-shifting phenomenon we have witnessed for the V-potential case does not arise. In addition, the average displacement and velocity, $\langle x \rangle$ and $\langle v \rangle$, have forms for the quadratic case that are considerably simpler than for the V-potential. Both are calculated to be exponential in time, $\langle x \rangle = x_0 e^{-\gamma t}$, $\langle v \rangle \equiv d\langle x \rangle/dt = -x_0\gamma e^{-\gamma t}$, and thus to be related linearly to each other: $\langle v \rangle = -\gamma\langle x \rangle$. The time dependence of $\langle x \rangle$ and $\langle v \rangle$ is, on the other hand, more complex for the V-potential, see Eqs. (6.18) and (6.19). Unlike in the quadratic case, it is not straightforward at all to eliminate t from those equations to obtain a v-x relation. We found it necessary to use a numerical procedure to extract that relation. Unlike in the quadratic case there is an unavoidable dependence of the V-potential relation on the diffusion constant D and the initial location x_0.

Of particular interest is the difference between the initial slopes of the velocity versus time plots in the quadratic versus the V-potential case, given in Eq. (6.19). In the quadratic case, the slope, equal to $-x_0\gamma$, is dependent on the potential strength and is different from different initial locations. This contrasts with the V-potential case for which neither the initial location nor any potential parameter decides the initial slope; the $v(t)$ curve is initially *totally* flat in the V-potential case. Not only

the first t-derivative but *all* order derivatives of the velocity vanish initially. This is confirmed explicitly by differentiating Eq. (6.19),

$$\frac{d\langle v \rangle}{dt} = \frac{x_0 \mathcal{E}}{\sqrt{4\pi D t^3}} e^{-\frac{(x_0 - \mathcal{E}t)^2}{4Dt}},$$

and noticing that at $t = 0$, the Gaussian term vanishes faster than any purely polynomial term can grow. As repeated differentiations only result in polynomials of finite order, all derivatives of $\langle v \rangle$ vanish at $t = 0$. This vanishing provides the initially flat nature of the velocity curve. The dormant behavior comes from the presence of an isolated essential singularity and is similar to what happens in the context of Arrhenius dependence of chemical rates or the Einstein specific heat if the temperature T is the abscissa rather than the time t as here.

By multiplying Eq. (5.1) by x, integrating over all x, and invoking standard boundary conditions on $P(x,t)$ and its spatial derivatives, one can write, for any potential $U(x)$,

$$\frac{d\langle x \rangle}{dt} = \langle v \rangle = \left\langle -\frac{dU(x)}{dx} \right\rangle. \tag{6.21}$$

When the potential is quadratic the force (or velocity) $dU(x)/dx$ is linear in x; however, in the V-potential case it is proportional to $|x|/x$ and, therefore, highly nonlinear. The linearity in the former case ensures that a closed differential equation for $\langle x \rangle$ exists. In the latter case it does not exist and so D has an effect on the average velocity. It is the fact, that the relation $\langle f(x) \rangle = f(\langle x \rangle)$ is *by no means valid* for such nonlinear functions $f(x)$, that is responsible for the richer consequences of the V-potential. In the quadratic case, the linearity of the force validates the relation accidentally and thereby imposes a simple relation between $\langle v \rangle$ and $\langle x \rangle$ without any influence of the diffusion constant.

Chapter 7

Applications in Chemical and Biological Physics

We present here two illustrative applications of the results that we derived in Chapter 6 that describe the motion of a walker undergoing diffusion in a V-potential. The first is a quantum yield calculation in doped molecular crystals [28, 101, 102]. Hanson [103, 104] and others [105] have suggested methods of creating the linear confining potential that may be used. Following a brief introduction to molecular crystals, we sketch the defect technique [28, 106–111] (adapted from [111]), which accounts for the consequences of semi-isolated defects on the motion of a walker. The Laplace-domain propagator, Eq. (6.14), is then used to calculate the quantum yield for which a non-monotonic variance is found and discussed. An analysis of the position-dependent velocity of T-cell membrane receptors during immunological synapse formation [112–123] is the second illustrative application. An important experimental result in the studies of immunological synapse formation is the position-dependent average velocity [112] of the T-cell receptor proteins. We present a qualitative comparison of these results with our calculated relationship between the average position $\langle x \rangle$, Eq. (6.18), and velocity $\langle v \rangle$, Eq. (6.19), for the V-potential.

We find that it does not adequately predict the motion and propose a second linear confining potential, dubbed the 'bucket'-potential, that incorporates a central non-convective region. Its position-dependent average velocity does qualitatively replicate the receptor motion.

7.1   Quantum Yield Calculations in Doped Molecular Crystals

Doped molecular crystals [28,101,102], exemplified by aromatic hydrocarbon lattices held together via the van der Waals interaction [124], often provide a model system for the laboratory study of the magnitude and nature of exciton motion in complex biological entities such as photosynthetic systems [125]. In early experiments [126, 127], small concentrations of guest molecules, such as tetracene, were doped into a lattice, often comprised of anthracene, onto which light was made to shine. Frenkel excitations were produced and proceeded to move on the lattice, potentially being captured by the guest molecules, and finally decayed due to their a finite lifetime. The radiation emitted during this decay occurs at different frequencies which allows the amount emitted, and therefore captured, by the guest molecules to be tracked. The ratio given by the number of excitations that radiate from the host to those that were originally created is called the host yield; we label it ϕ. If no non-radiative processes exist, the guest yield would be $1 - \phi$. The ratio of these two quantities $(1 - \phi)/\phi$ relates the fraction of excitations captured by guest molecules to those left free and thus is often called the dimensionless energy transfer rate [28]. We here calculate these quantities when the motion occurs under the influence of the V-potential in a representative one-dimensional molecular crystal.

Our starting equation that describes the excitation motion is given by Eq. (5.2

with the addition of decay and capture terms,

$$\frac{\partial P(x,t)}{\partial t} + \frac{P(x,t)}{\tau} = \mathcal{E}\frac{\partial}{\partial x}\left(\frac{|x|}{x}P(x,t)\right) + D\frac{\partial^2 P(x,t)}{\partial x^2} - C\delta(x - x_r)P(x,t). \quad (7.1)$$

Here τ is the lifetime, C is the capture parameter and x_r is the trap site. This form of decay leads to a simple exponential decay of the probability independent of position in the time domain, i.e., $P(x,t) \to \exp(-t/\tau)P(x,t)$, and the transform $\epsilon \to \epsilon + 1/\tau$ in the Laplace-domain. Analysis of the capture term requires the defect technique [28, 106–111], a sketch of which we present here, adapted, essentially, from Spendier and Kenkre [111], which is a recent review of the technique used by different authors in a variety of contexts. Here, and in ref. [111], the approach and notation followed are those of Kenkre and collaborators.

7.1.1 Introduction to the Defect Technique

We consider a particle that moves on a discrete lattice of arbitrary dimension and whose probability of being on site m is given by $P_m(t)$. The coherent motion, i.e., the motion independent of the defect, is linear in the probability and otherwise left as general. The master equation that then governs the motion of the particle is given by

$$\frac{dP_m(t)}{dt} = \text{motion terms} - \sum_r{}' C'\delta_{m,r}P_m(t), \quad (7.2)$$

where C' is the discrete capture parameter and is related to C as defined in Eq. (7.1) by the standard continuous limit, $a \to 0$, $C' \to \infty$, $aC' \to C$. The trap sites are located at r with each being selected by the kronecker-delta $\delta_{m,r}$ and the prime signifies a sum over those sites. We take a single trap site for simplicity.

Following a Laplace transform of Eq. (7.2), the Laplace-domain probability $\widetilde{P}_m(\epsilon)$ becomes

$$\widetilde{P}_m(\epsilon) = \widetilde{\eta}_m(\epsilon) - C'\widetilde{\Psi}_{m,r}(\epsilon)\widetilde{P}_r(\epsilon), \quad (7.3)$$

where $\widetilde{\Psi}_{m,r}$ is the homogenous propagator from site r to site m, and $\widetilde{\eta}_m(\epsilon)$ is the full homogenous probability at site m for the particular initial condition, i.e., $\widetilde{\eta}_m(\epsilon) = \sum_n \widetilde{\Psi}_{m,n,}(\epsilon) P_n(0)$. When the motion term in Eq. (7.2) diagonalizes in the Fourier domain, e.g., the diffusive case, one can explicitly derive Eq. (7.3). In particular, the origin of the homogenous propagator in the second term on the right-hand side is self-evident. However, its origin is intuitive in all systems by considering the time-domain equivalent of Eq. (7.3),

$$\mathrm{LT}^{-1}\left\{ C'\widetilde{\Psi}_{m,r}(\epsilon)\widetilde{P}_r(\epsilon) \right\} = C' \int\limits_0^t dt'\, C'\Psi_{m,r}(t-t') P_r(t'),$$

where $\Psi_{m,n}(t)$ is the time-domain propagator. Clearly, the second term on the right-hand side of Eq. (7.3) is understood as the 'captured' probability that *would have* contributed to the total in the *absence* of the trap.

An explicit solution requires the removal of $\widetilde{P}_r(\epsilon)$ from the right hand side of Eq. (7.3). It is found by setting $m = r$ and then solving for $\widetilde{P}_r(\epsilon)$ which can then be inserted back into Eg. (7.3). This gives the solution as

$$\widetilde{P}_m(\epsilon) = \widetilde{\eta}_m(\epsilon) - \widetilde{\Psi}_{m,r}(\epsilon) \frac{\widetilde{\mu}_r(\epsilon)}{1/C' + \widetilde{\nu}_r(\epsilon)}. \tag{7.4}$$

Two new functions have been defined in Eq. (7.4) to simplify its physical understanding: $\widetilde{\mu}_r(\epsilon)$, referred to as the the μ-function, is the probability that the particle travels from the particular initial condition to the trap site in the absence of the trap; $\widetilde{\nu}_r(\epsilon)$, the ν-function [76, 109, 128], is the self-propagator for the trap site. The latter was introduced by Kenkre [76] in his studies of energy transfer in molecular crystals and photosynthetic systems and is important in understanding exciton dynamics [28, 76, 109, 128]. The quantum yield is then found by a sum over all space. It is given by

$$\phi \equiv \sum_m \widetilde{P}_m(\epsilon) = \frac{1}{\epsilon}\left[1 - \frac{\widetilde{\mu}_r(\epsilon)}{1/C' + \widetilde{\nu}(\epsilon)_r} \right], \tag{7.5}$$

where both the homogenous solution $\widetilde{\eta}_m(\epsilon)$ and the propagator $\widetilde{\Psi}_{m,r}(\epsilon)$ sum to ϵ^{-1}. Physical understanding of the consequences of Eq. (7.5) are discussed in [28, 76, 109, 128]. Relevant to the V-potential and Eq. (7.1), the continuous limit[1] of Eq. (7.5) is taken in the standard manner $a \to 0$, $C' \to \infty$, $aC' \to C$, $\widetilde{\mu}_r(\epsilon)/a, \to \widetilde{\mu}(\epsilon)$, $\widetilde{\nu}_r(\epsilon)/a, \to \widetilde{\nu}(\epsilon)$. Thus for continuous systems we give

$$\phi = \int_{-\infty}^{\infty} dx\, \widetilde{P}(x, \epsilon) = \frac{1}{\epsilon}\left[1 - \frac{\widetilde{\mu}(\epsilon)}{1/C + \widetilde{\nu}(\epsilon)}\right], \tag{7.6}$$

7.1.2 Quantum Yield Calculation and Discussion

Upon the insertion of the Laplace-domain propagator for the V-potential, Eq. (6.14), into Eq. (7.6), the quantum yield becomes

$$\phi = \begin{cases} 1 - \dfrac{e^{-\frac{|x_r|-|x_0|}{2\ell}}\left[(Q(\epsilon)-1)\,e^{-Q(\epsilon)\frac{|x_r-x_0|}{2\ell}}+e^{-Q(\epsilon)\frac{|x_r|+|x_0|}{2\ell}}\right]}{\frac{\mathcal{E}(Q(\epsilon)^2-Q(\epsilon))}{C}+Q(\epsilon)-2e^{-Q(\epsilon)\frac{|x_r|}{2\ell}}\sinh\left[Q(\epsilon)\frac{|x_r|}{2\ell}\right]} & \mathrm{sgn}(x_r)=\mathrm{sgn}(x_0), \\[4ex] 1 - \dfrac{Q(\epsilon)\,e^{-\frac{|x_r|-|x_0|}{2\ell}}e^{-Q(\epsilon)\frac{|x_r|+|x_0|}{2\ell}}}{\frac{\mathcal{E}(Q(\epsilon)^2-Q(\epsilon))}{C}+Q(\epsilon)-2e^{-Q(\epsilon)\frac{|x_r|}{2\ell}}\sinh\left[Q(\epsilon)\frac{|x_r|}{2\ell}\right]} & \mathrm{sgn}(x_r)\neq\mathrm{sgn}(x_0), \end{cases} \tag{7.7}$$

where

$$Q(\epsilon) = \sqrt{1 + \frac{4\ell}{\mathcal{E}\tau}}.$$

The two cases correspond with the trap being located on the same side and opposite sides of origin, respectively.

We take the trap site as located at $x_r = L/2$ and calculate the yield for the illustrative localized initial condition that has the excitation (initially) located at $x_0 = -L/2$. For such symmetrical positioning around the origin, the yield becomes

$$\phi = 1 - \frac{Q(\epsilon)\,e^{-Q(\epsilon)\frac{L}{2\ell}}}{\frac{\mathcal{E}(Q(\epsilon)^2-Q(\epsilon))}{C}+Q(\epsilon)-2e^{-Q(\epsilon)\frac{L}{4\ell}}\sinh\left[Q(\epsilon)\frac{L}{4\ell}\right]} \tag{7.8}$$

---

[1]Issues may arise for motion spaces of dimension greater than one. Here, we focus on those of a single dimension. As such, no problems present themselves. See Chapter 10 for a discussion.
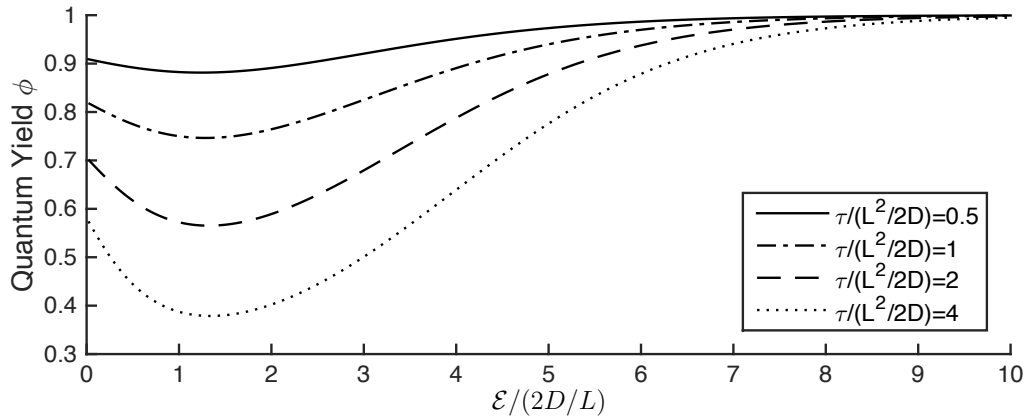
Figure 7.1: The non-monotonic dependence of the quantum yield, Eq. (7.8), on the potential strength $\mathcal{E}$ (in units of $2D/L$) for four different values of the lifetime τ (in units of $L^2/2D$). Location of the trap, x_r, and the initial location of the Frenkel excitation, x_0, are separated by a distance L symmetrically around the origin. The capture parameter, C, is set to 4 (in units of $2D/L$). Non-monotonic effects (see text) are clear from the minimum in the quantum yield located at $\mathcal{E} \approx 2D/L$.

Let us focus our attention on the effect on the observable ϕ on the degree of confinement imposed on the excitation motion by the V-potential. We depict the dependence of the quantum yield on $\mathcal{E}$ in Figs. 7.1 and 7.2. Fig 7.1, where Eq. (7.8) is plotted for four values of the lifetime τ (in units of $L^2/2D$), over a range of the potential strength $\mathcal{E}$ (in units of $2D/L$), clearly shows non-monotonic behavior: there is a minimum in the quantum yield (in Fig 7.1 it happens to appear between the values 1 and 2 of the abscissa). Since the curves rise on both sides of this value, we see that the quantum yield is non-monotonic in the confinement strength. This remarkable non-monotonicity effect has been recently reported for quadratic confinement potentials in the trapping of Smoluchowski random walkers [67] and in the transmission of infections in epidemics [68].

The non-monotonicity effect can also be seen directly in the time-domain [67, 68]. In our present context, this behavior can be noticed in the variation of the quantum yield on the lifetime of the excitation. This is clear in Fig. 7.2, where
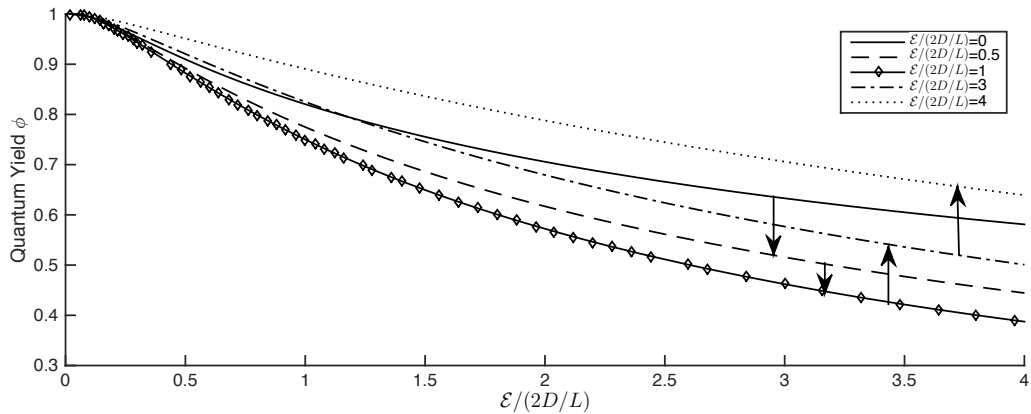
Figure 7.2: The non-monotonic dependence of the quantum yield, Eq. (7.8), on five values [0.25, 0.5, 1, 2, 4] of the potential strength $\mathcal{E}$ (in units of $2D/L$) for a range of the lifetime τ (in units of $L^2/2D$). Location of the trap, x_r, and the initial localization of the Frenkel excitation, x_0, are separated by a distance L symmetrically around the origin. The capture parameter, C, is set to 4 (in units of $2D/L$). Non-monotonicity is seen through the increase, and subsequent decrease in the normalized yield for all values of τ as $\mathcal{E}$ is increased, with the maximum occurring at $\mathcal{E} \approx 2D/L$.

the dependence of ϕ on τ is shown for five values of the confinement strength $\mathcal{E}$. The lifetime, scaled to the time the excitation would take to traverse as a random walker the distance between the initial condition and the trap site, is plotted on the x-axis. The non-monotonic dependence of the quantum yield on the potential strength is confirmed in the figure. The black arrows, whose direction corresponds to successively higher values of $\mathcal{E}$, point out this non-monotonicity as $\mathcal{E}$ is increased: initially the yield decreases, it reaches a minimum and then it increases. Intuitively this results because, for small values of $\mathcal{E}$, confinement helps trapping by limiting the probability of the excitation diffusing to $\pm\infty$ and hurts trapping at large values of $\mathcal{E}$ by strongly concentrating the probability that the excitation is very close to the origin.

7.2 Immunological Synapse Formation

Immunological synapse formation, in particular the motion of receptor proteins on the surface of the T-cells, is our second illustrative application. We discuss our findings below; our intention is to present only qualitative arguments, not quantitative predictions or explanations.

The initial event that often drives important biological processes is a binding interaction between an external target molecule and receptor proteins located on the cell membrane. This interaction leads to an appropriate cellular response. Cell surface receptors tend to be mobile with their motion influenced by interactions with intracellular molecules such as the actin cytoskeleton. In the cellular response we consider here, antigen presenting cells (APC) are initially recognized by T-cell receptors (TCRs). Groups of these receptors amalgamate into TCR microclusters which tend to move towards a central region, the contact point between the T-cell and APC, to form a spatially organized structure. These structures are called immunological synapses [113, 114] and are considered important for the function of T-cells [115]. The biological mechanism of TCR microcluster motion remains unknown; one entity that plausibly could drive their motion is the retrograde flow of actin [116–118]. The actin cytoskeleton, a filamentous network that undergirds the cell membrane, is known to transport cell surface molecules like TCRs. However, the connection between actin and TCR remain unknown (though a frictional coupling mechanism has been proposed [119, 120]). Two separate mechanisms that drive the underlying actin flow, and therefore move the coupled TCR, have appeared in the literature: actin polymerization pushing against the cell membrane [121] and myosin II pulling against the branched F-actin network [122]. Due to concentration differences between the cell periphery and the cell center [117], Myosin II contraction [122] is a distance-dependent force. The distance-dependence of the force motivates our application of linear potentials. We do not provide definitive answers to these questions;
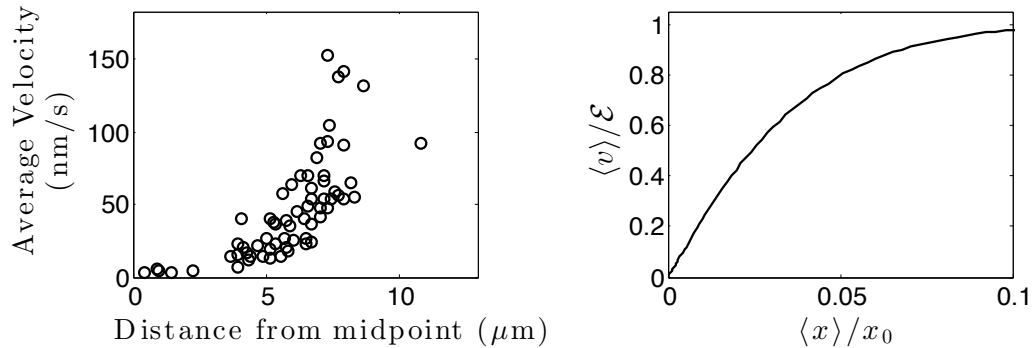
Figure 7.3: Qualitative comparison of experimental results, in the left panel, on the relation between $\langle x \rangle$ and $\langle v \rangle$ of TCR microclusters reconstructed from ref. [112] with our theoretical predictions, in the right panel, for a V-potential. The right panel shows an increase as does the left panel but the flat portion in the central region, quite obvious in the experiment, is absent in the right panel.

however, our calculations may provide a method of distinguishing between these two causes.

7.2.1 Experimental Results and V-Potential Predictions

The observations of interest focus on the time and distance dependence of velocities of the TCR microclusters on the cell surface during immunological synapse formation. We approximate their motion as being radial to allow the use of the one-dimensional results obtained in Chapter 6 directly. Following an initial period of global cellular dynamics, the time dependence of the average velocity is observed to decay towards a zero average value [118]. This is qualitatively similar to the behavior depicted in Figs. 6.4 and 6.5. Additionally, the *position*-dependence of the velocity of the TCR microclusters is provided experimentally. Reconstruction of the data found in [112], see left panel in Fig. 7.3, displays two distinct regions in which dynamics differ: a central region within 4 μm of the center and a peripheral region outside of that 8 μm diameter center. In the central region, the microclusters travel slowly, about 4

nm/s, with minimal discernible distance dependence while they move faster, about $20 - 100\ nm/s$, with a strong dependence on distance in the peripheral region. The presence of a central region, in which the behavior of the average velocity displays no distance-dependence, motivated an extension of our calculations using the results of Section 6.1. We consider a second piecewise linear potential, a composite of a central flat portion joined with V-potential pieces at the periphery. As we illustrate below, this produces a velocity-distance relation that similar to observations.

7.2.2   Extension of V-Potential to the Bucket Potential

The lack of distance dependence on the average velocity of the TCR microclusters depicted in Fig. 7.3 suggests including a central region of constant potential (no force), i.e. where the walker dynamics are solely diffusive. As discussed previously, the methods that we used to solve Eq. (5.2) are generalized by Eqs. (6.8) to any arbitrary linear potential. Here, the potential we propose is a central region of no force bracketed by linear potentials with equal and opposite potential strengths:

$$U(x) = \begin{cases} \mathcal{E}\,(x - L) & x > L \\ 0 & L < x < -L \\ -\mathcal{E}\,(x + L) & x < -L. \end{cases} \qquad (7.9)$$

Here, $\mathcal{E}$ remains the potential strength and $2L$ is the width of the central region. The propagator for this 'bucket' potential is found upon its insertion into Eq. (5.1).

For the case in which the walker is initialized on the walls of the 'bucket', i.e. $x_0 > L$ (the case of $x_0 < -L$ is solved by symmetry), the Laplace-domain propagator

is

$$
\widetilde{\Pi} = \begin{cases}
\dfrac{e^{-\frac{x-x_0}{2\ell}}}{\mathcal{E}Q(\epsilon)}\left[e^{-Q(\epsilon)\frac{|x-x_0|}{\ell}} + \dfrac{2\sqrt{\frac{4\ell\epsilon}{\mathcal{E}}}\cosh 2\sqrt{\frac{\epsilon}{D}}L}{\kappa(\epsilon)}e^{-Q(\epsilon)\frac{x+x_0-2L}{2\ell}}\right] & x > L \\[3em]
2\dfrac{e^{-(Q(\epsilon)-1)\frac{x_0-L}{2\ell}}}{\mathcal{E}\kappa(\epsilon)}\iota(\epsilon) & x < |L| \\[2.5em]
2\dfrac{e^{\frac{x+x_0}{2\ell}}}{\mathcal{E}\kappa(\epsilon)}e^{Q(\epsilon)\frac{x-x_0+2L}{2\ell}}\sqrt{\dfrac{4\ell\epsilon}{\mathcal{E}}} & x < -L,
\end{cases}
\tag{7.10}
$$

where we have suppressed the arguments of $\widetilde{\Pi}(x, x_0, \epsilon)$ and

$$
\widetilde{\iota}(\epsilon) = (Q(\epsilon)-1)\sinh\sqrt{\frac{\epsilon}{D}}(x+L) + \sqrt{\frac{4\ell\epsilon}{\mathcal{E}}}\cosh\sqrt{\frac{\epsilon}{D}}(x+L),
$$

$$
\widetilde{\kappa}(\epsilon) = \left((Q(\epsilon)-1)^2 + \frac{4\ell\epsilon}{\mathcal{E}}\right)\sinh 2\sqrt{\frac{\epsilon}{D}}L + 2(Q(\epsilon)-1)\sqrt{\frac{4\ell\epsilon}{\mathcal{E}}}\cosh 2\sqrt{\frac{\epsilon}{D}}L.
$$

The form of Eq. (7.10) in the sloped regions of the potential corresponds well with their equivalent regions when under a V-potential. They are modified by functions of L and, in the limit $L \to \infty$, reduce to Eq. (6.14). The case where $L > x_0 > -L$, i.e. the walker is initialized on the bottom of the basket, is

$$
\widetilde{\Pi}(x, x_0, \epsilon) = \begin{cases}
e^{-\left(1+\sqrt{1+\frac{4\ell\epsilon}{\mathcal{E}}}\right)\frac{x-L}{2\ell}}\dfrac{\sqrt{1+\frac{4\ell\epsilon}{\mathcal{E}}}+1}{4\ell\epsilon}\dfrac{\mathcal{P}(x_0,\epsilon)}{\mathcal{D}(\epsilon)} & x > L \\[3em]
\dfrac{\sqrt{1+\frac{4\ell\epsilon}{\mathcal{E}}}+1}{\mathcal{E}\sqrt{\frac{4\ell\epsilon}{\mathcal{E}}}4\ell\epsilon}\dfrac{\mathcal{P}(x_0,\epsilon)\mathcal{M}(x,\epsilon)}{\mathcal{D}(\epsilon)} & L > x > x_0 \\[3em]
\dfrac{\sqrt{1+\frac{4\ell\epsilon}{\mathcal{E}}}+1}{\mathcal{E}\sqrt{\frac{4\ell\epsilon}{\mathcal{E}}}4\ell\epsilon}\dfrac{\mathcal{P}(x,\epsilon)\mathcal{M}(x_0,\epsilon)}{\mathcal{D}(\epsilon)} & x_0 > x > -L \\[3em]
e^{\left(1+\sqrt{1+\frac{4\ell\epsilon}{\mathcal{E}}}\right)\frac{x+L}{2\ell}}\dfrac{\sqrt{1+\frac{4\ell\epsilon}{\mathcal{E}}}+1}{4\ell\epsilon}\dfrac{\mathcal{M}(x_0,\epsilon)}{\mathcal{D}(\epsilon)} & -L > x.
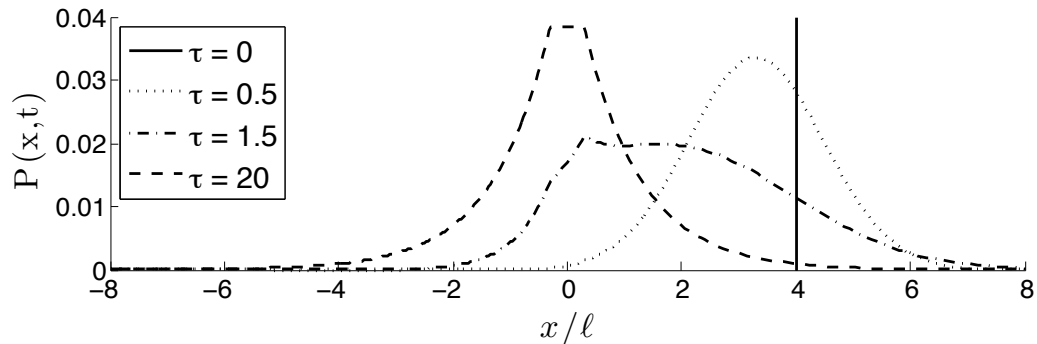\end{cases}
\tag{7.11}
$$

Figure 7.4: Counterpart of Fig. 2 for the 'bucket potential'. The time-domain propagator is plotted at four values (0,0.5,1.5,10) of the dimensionless time $\tau = t/\sqrt{2}D/\mathcal{E}^2$ for an initial location of the walker at $x_0/\ell = 4$, and the bucket width as $L/\ell = 0.3$. The propagator behaves essentially as in Fig. 2 but the steady state has a flat portion in the center. The transitioning of the intermediate Gaussian into the mod exponential with a flat central portion is already evident in the earlier time curve at $\tau = 1.5$.

Here

$$\mathcal{P}(x, \epsilon) = \left(\left(\sqrt{1 + \frac{4\ell\epsilon}{\mathcal{E}}} - 1 \right) \sinh \sqrt{\frac{\epsilon}{D}} (L + x) + \sqrt{\frac{4\ell\epsilon}{\mathcal{E}}} \cosh \sqrt{\frac{\epsilon}{D}} (L + x) \right),$$

$$\mathcal{M}(x, \epsilon) = \left(\left(\sqrt{1 + \frac{4\ell\epsilon}{\mathcal{E}}} - 1 \right) \sinh \sqrt{\frac{\epsilon}{D}} (L - x) + \sqrt{\frac{4\ell\epsilon}{\mathcal{E}}} \cosh \sqrt{\frac{\epsilon}{D}} (L - x) \right),$$

$$\mathcal{D}(\epsilon) = \sqrt{1 + \frac{4\ell\epsilon}{\mathcal{E}}} \sinh 2\sqrt{\frac{\epsilon}{D}} L + \sqrt{\frac{4\ell\epsilon}{\mathcal{E}}} \cosh 2\sqrt{\frac{\epsilon}{D}} L.$$

The presence of the Laplace variable ϵ in two different forms, $1 + 4D\ell\epsilon/\mathcal{E}$ and ϵ/D, in Eq. (7.10) requires numerical methods to invert the transform. For this purpose we use standard inversion routines [129, 130]. We exhibit the resulting time-domain propagator for a walker initially in the periphery at four different dimensionless times in Fig. 7.4. The propagator travels in a similar manner to the probability propagation of the V-potential, Fig. 6.3, traveling ballistically initially, undergoing a transition in shape, then settling into the steady state distribution. The latter consists of a central plateau of width $2L = 6$ bracketed by decaying exponentials
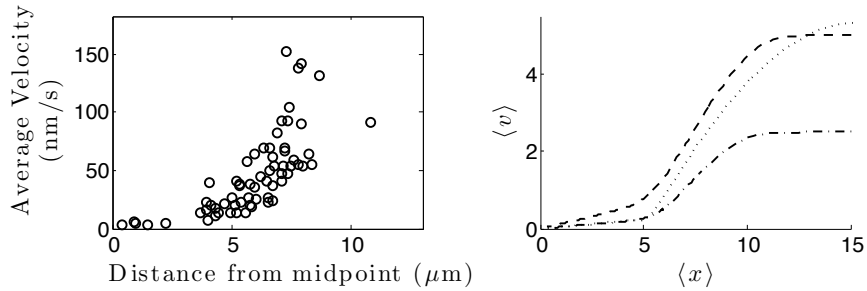
Figure 7.5: Qualitative comparison, as in Fig. 6, of experimental observations from ref. [112] (left panel is identical to that in Fig. 6) to our theoretical predictions. The latter here are for the 'bucket' potential for a few different values of its parameters (right panel). Considerable enhancement is seen in the qualitative agreement since the bucket potential is able to reproduce the central flat portion.

with characteristic width $\ell = 10$. This propagator and that of the V-potential behave similarly in the outer regions where it experiences a non-zero force. Its initial shape is Gaussian before the transition into a decaying exponential. The difference between the two occurs in the central region, where the 'bucket' propagator connects the probability values at the two points of discontinuity in an approximately linear fashion. This near linearity is due to the effects of diffusion under forced unequal boundary conditions. During the transition period, diffusion works to gradually equalize these two boundary probabilities, decreasing the steepness of the propagator.

The resulting relationship between $\langle x \rangle$ and $\langle v \rangle$ for the 'bucket' potential is depicted in Fig. 7.5. It is visually obvious that there is much better agreement of experiment [112] and our calculations with the bucket potential than with the V-potential. The former retains the initial dormant behavior characteristic of the V-potential as well as the plunge, $\langle v \rangle \to 0$, when the walker interacts strongly with the discontinuities present in both potentials. As expected, the qualitative difference between the two lies in the location of this rapid decrease in speed. For the 'bucket' potential this plunge occurs in the periphery, as opposed to at the center, resulting in the addition of a central area of small or vanishing velocity. The presence of this low-

velocity area results from the constant potential center, as the confinement increases the probability of locating the walker in the center where motion is dominated by diffusion.

7.3 Conclusion

We have presented two potential applications for the V-potential results derived in Chapter 6. The first is a quantum yield calculation in doped molecular crystals [101, 102] that are experiencing an applied electric field. Issues raised by Hanson [103, 104] and others [105] provide potential applicable systems. Exact calculations of the quantum yield are presented and a interesting non-monotonic behavior as the potential strength $\mathcal{E}$ is increased is noted. The non-monotonicity is similar to that that has recently been found for the quadratic potential in an analysis of infection transmission [67, 68]. Our second application is to receptor motion on the surface of T-cells during immunological synapse formation [112–123]. In particular the position-dependence of the average velocity. Observations made [112] suggest a central region with little positional dependence of velocity surrounded by a periphery where the velocity shows a strong dependence on position. The V-potential does not qualitatively model these systems. However, a proposed extension, the 'bucket' potential, using the methods of Section 6.1 displays qualitatively similar behavior.

The work in Chapters 6 and 7 in this thesis was done in collaboration with a co-investigator external to UNM, and has been published [131] as M. Chase, K. Spendier, and V. M. Kenkre, "Analysis of Confined Random Walkers with Applications to Processes Occurring in Molecular Aggregates and Immunological Systems", *Journal of Physical Chemistry B*, **120**, 3072-3080 (2016).

Part 3: Approach to Equilibrium in Quantum Systems

Chapter 8

Overview of Approach to Equilibrium in Quantum Systems

Our focus in this Part of the dissertation is on the manner in which an interaction with a bath influences the evolution of a quantum mechanical system towards its equilibrium state when it is disturbed from it. An experiment may begin with the system being prepared in a particular state. That system is then allowed to evolve and, due to its interaction with the bath, to return to its equilibrium state. A particularly common experimental setup uses light to excite a molecule into a higher energy state; the subsequent relaxation into thermal equilibrium may be noted and manipulated [132–148]. Recent improvements in spectroscopic techniques [149–151] have opened dynamics at very short timescales (some say even the attosecond timescale) to observation. At those extremely short times, an understanding of the effects of coherence is required to provide accurate predictions and to contextualize novel experimental results. Potential processes for which knowledge of these coherence effects may find application include unimolecular-dissociation [152] and other chemical reactions [149, 153, 154].

The manner in which an arbitrary system decoheres through a randomization of its phases [155–158] while simultaneously achieving occupation probabilities given by the Boltzmann weights is not fully understood. Take an isolated system with Hamiltonian $\mathcal{H}$ and therefore an energy spectrum given by the eigenvalues that correspond to the eigenstates of the Hamiltonian. If this system were to be placed in one of its eigenstates, the system evolution, as given by the Schrödinger equation, would simply be the periodic oscillation of its phase. In contrast, if the system were left to itself for a long time, one would invoke the postulate of equilibrium statistical mechanics [155]: the density matrix of the system is diagonal in its eigenbasis with those diagonal elements being proportional to their respective Boltzmann weights (in that basis). We wish to highlight that the postulate of equilibrium statistical mechanics is actually two postulates: one in reference to the phases (they are assumed to be random) and the second in reference to the probabilities (they are assumed to follow Boltzmann weights). This split nature is made particularly clear on pages 172-173 in ref. [155].

The invocation of the postulate therefore assumes that the system is not isolated but, in fact, interacts with a bath, i.e., the rest of the universe. The nature of this interaction must be quite specific to fulfill the requirements of equilibrium statistical mechanics. It must be strong enough that, *independent* of the initial condition of the system, one finds the equilibrium state with probabilities that are given by the Boltzmann weights as well as random phases. However, it must be weak enough that this equilibrium state respects the eigenvalues and eigenvectors of the *isolated* system. At equilibrium, therefore, the bath must not have further influence on the equilibrium state of the system. Our goal in Chapters 9 and 10 is to maintain such an interaction while correctly accounting for the influence of the coherent microscopic dynamics at short times (with respect to the equilibrium time).

When interest is in simply the long-time evolution, the use of a Master equation is

appropriate. Here, the equation of interest governs the evolution of the probabilities that the system is in an eigenstate with the transition rates between pairs of eigenstates required to satisfy the detailed balance condition. This latter requirement ensures that the system reaches the proper equilibrium state. Master equations are equations of the form

$$\frac{dP_M(t)}{dt} = \sum_N \left[F_{MN} P_N(t) - F_{NM} P_M(t) \right]. \tag{8.1}$$

In the present context we label the eigenstates of the Hamiltonian with M, their probability of occupation by $P_M(t)$ and require that the transition rates between each pair of eigenstates, i.e., F_{MN}, F_{NM}, obey the relation

$$\frac{F_{MN}}{F_{NM}} = e^{-\beta E_{MN}}.$$

Here, $\beta \equiv 1/k_B T$ is the standard thermodynamic beta (k_B being the Boltzmann constant and T being the bath temperature) and E_{MN} is the difference in energies between the two eigenstates.

To account for the effects of off-diagonal elements of the system density matrix, and thus more accurately describe the evolution of the system at short times, we turn to the fundamental research performed by Zwanzig [47, 159–161] and others [42, 44, 45, 162–164]. The formalism provides an equation that continuously links the short-time evolution of the system with its long-time evolution and eventual equilibrium in principle. The relevant equation, the Generalized Master equation (GME), is of the form [47, 159–163, 165, 166]

$$\frac{dP_M(t)}{dt} = \int_0^t dt' \sum_N \left[\mathcal{W}_{MN}(t - t') P_N(t') - \mathcal{W}_{NM}(t - t') P_M(t') \right]. \tag{8.2}$$

Despite the absence of explicit references to the off-diagonal matrix elements, their effects, and thus the influence of the bath, are accounted for through the memory

functions[1] $\mathcal{W}(t)$.

The energy spectra of the systems that we consider here in this thesis are equally spaced. Thus, each can be characterized by a single energy that identifies the difference between the eigenvalues of successive eigenstates. Here, the generic energy difference ΔE is used. Each system we discuss will be identified by a different symbol. We shall see that the bath effects can then be properly characterized through *two* memories that depend on a *single* [165] spectral function $Y(z)$.

The necessary formalism is available in earlier work by Kenkre [165, 167, 168] who generalized Zwanzig's projection operators to include coarse-graining over the bath and applied it to various physical systems. These memories, which we label $\phi_{\pm}(t)$, are then given through the Fourier-transform expressions

$$\kappa\phi_-(t) = \int_{-\infty}^{\infty} dz \ Y(z)\cos[(z-\Delta E)t], \tag{8.3a}$$

$$\kappa\phi_+(t) = \int_{-\infty}^{\infty} dz \ Y(z)\cos[(z+\Delta E)t], \tag{8.3b}$$

where $\kappa = \pi Y(\Delta E)$ is the reciprocal of a timescale associated with the Master equation transition rates. We require only two memories $\phi_{\pm}(t)$ because of the system being characterized by a single energy; the $+$ and $-$ therefore are naturally interpreted as being associated with the energetically upwards and downwards transitions, respectively. The differences between the two memories are simply due to the presence of either a $+$ or a $-$ in the argument of the cosine. More generally, additional pairs of memories would exist if the system were to possess many characteristic energies.

With the introduction of the bath spectral function in Eq. (8.3), the requirement

---

[1]We note that, in general, the bath also contributes to Eq. (8.2) a forcing term with dependence on the initial condition of the system. In the tradition of van Hove [42] and others [44, 47, 159–163], we ignore this term here by assuming an initially random phase, i.e., no coherent superpositions. This is valid, for example, if the initial condition is a single eigenstate. See ref. [165] for a discussion of the general case.

that the integrals of the memories obey the detailed balance condition can be written in a simple form. The bath spectral function must obey [34] the special condition

$$Y(-z) = Y(z)e^{-\beta z}, \tag{8.4}$$

or, equivalently,

$$Y(z) = \frac{Y_s(z)}{1 + e^{-\beta z}} \tag{8.5}$$

where $Y_s(z) = Y_s(-z)$ is symmetric in z and, again, $\beta \equiv 1/k_B T$. Baths are then completely specified by the symmetric function $Y_s(z)$, along with the temperature T. Through Eq. (8.4), they are also guaranteed to lead to memories whose integrals respect the detailed balance condition.

Chapters 9 and 10 are laid out as follows. In Chapter 9, the strength of the GME is displayed by considering the relaxation of a simple system: the non-degenerate dimer analyzed previously in our research group [169]. The necessity of the special condition on the bath spectral function is highlighted. We then introduce illustrative analytic, phenomenological bath function calculations. A physical discussion of the relevant energies, and their ratios, is given.

In Chapter 10, we discuss the effects of the memory functions in the GME on the evolution of an excited molecule that undergoes vibrational relaxation. We present the GME that naturally generalizes the Montroll-Shuler equation [141], the workhorse in the study of vibrational relaxation, to account for coherent effects. We also show, in passing, interesting results in a related condensed matter system: a charged particle in a crystal accelerated by a strong electric fields leading to the formation of Stark ladders.

Throughout Chapters 9 and 10, energies are taken to be normalized by $\hbar\kappa$.

Chapter 9

A Simple Non-Degenerate System and Explicit Calculations of Bath Spectral Functions

In this Chapter we present two items: an introduction to a simple non-degenerate system previously analyzed by Tiwari and Kenkre [169] and explicit calculations of bath spectral functions that we have performed in this thesis which are applicable to that introductory system as well as the richer systems we investigate in Chapter 10. In Section 9.1, the reader is introduced to the non-degenerate dimer, i.e., a two-state system of unequal energies, for two reasons. First, it provides a pedagogically simple system to illustrate the subtleties of the decoherence and detailed balance processes. In the manner of Eqs. 8.3, we represent the effects of these processes with the use of the bath spectral function $Y(z)$; notably, the detailed balance requirement on $Y(z)$, given in Eq. (8.4), is highlighted. Secondly, the dimer serves as a model system to which we present physically realistic extensions in Chapter 10.

Not present in ref. [169] is a discussion of particular bath spectral functions.

Thus, in Section 9.2, we present eight symmetrical bath spectral functions that can be grouped in three. The triple delta-function, and its approximation with three Lorentzian functions, is introduced to elucidate examples of the transition from coherent evolution to incoherent. Two examples of a simple truncated spectrum are provided by the flat box and the triangle. The last five consist of simple one-parameter functions with infinite support: the Lorentzian, squared Lorentzian, quartic, mod exponential and Gaussian. We end with a discussion of the three ratios of characteristic energies. We conclude in Section 9.3 with brief remarks including a comment on an alternative approach.

9.1 Relaxation of a Simple Quantum System: the Non-Degenerate Dimer

The non-degenerate dimer, a two-state system in which the states are at different energies, presents a simple case to familiarize oneself with the basic issue studied in this Part of the thesis. The Hamiltonian $\mathcal{H}_{Di}$ that defines the system is given by

$$\mathcal{H}_{Di} = \begin{bmatrix} \Delta & 0 \\ 0 & -\Delta \end{bmatrix}. \tag{9.1}$$

Here, 2Δ is the difference in energy between the two Hamiltonian eigenstates. We label the eigenstate with eigenvalue Δ as $|1\rangle$ and that with eigenvalue $-\Delta$ as $|2\rangle$. The equilibrium density matrix in the eigenbasis is then

$$\rho_{\text{therm}} = \frac{1}{2\cosh\beta\Delta} \begin{bmatrix} e^{-\beta\Delta} & 0 \\ 0 & e^{\beta\Delta} \end{bmatrix}.$$

Defining the occupation probabilities of eigenvector $|1\rangle$ and $|2\rangle$ as $P_1(t)$ and $P_2(t)$, respectively, we have at equilibrium

$$P_1(t \to \infty) = \frac{1}{2} - \frac{\tanh \beta \Delta}{2}, \quad (9.2a) \qquad P_2(t \to \infty) = \frac{1}{2} + \frac{\tanh \beta \Delta}{2}, \quad (9.2b)$$

The effect of the non-degeneracy of the system on the equilibrium state is particularly clear in Eqs. (9.2): the deviation from the degenerate is simply a decrease (increase) proportional to $\tanh(\beta \Delta)/2$ for eigenstate $|1\rangle$ ($|2\rangle$).

The starting point of our analysis is the von Neumann equation (we put $\hbar = 1$ throughout this thesis),

$$i \frac{d}{dt} \rho = [\mathcal{H}, \rho], \qquad (9.3)$$

where $\mathcal{H} = \mathcal{H}_{Di} + V$ and V represents the interaction between the bath and the system. It is taken to be of the form

$$V = \begin{bmatrix} 0 & V \\ V & 0 \end{bmatrix},$$

that is, a simple, symmetrical coupling of the two sites. The properties of the bath itself are left unspecified as is the physical origin of the interaction. In the usual manner of the GME formalism [47, 159–161, 165, 166], the interaction is taken to be weak enough that it can be treated perturbatively.

9.1.1 Generalized Master Equation for the Non-Degenerate Dimer

The simplicity of the dimer allows the general GME, Eq (8.2), to be written in terms of a single variable $p(t)$, defined as the difference in the probabilities of occupation of the two eigenstates, i.e., $p(t) = P_1(t) - P_2(t)$. The equation that governs the

evolution of $p(t)$ is then

$$\frac{d}{dt}p(t) + \kappa \int_0^t dt' \left[\phi_+(t-t') + \phi_-(t-t')\right] p(t') = \kappa \int_0^t dt' \left[\phi_+(t') - \phi_-(t')\right]. \quad (9.4)$$

Here, κ is the reciprocal time-scale that is associated with the equivalent Master equation. As in Eqs. 8.3, $\phi_-(t)$ and $\phi_+(t)$ are the memories that describe, respectively, the transition downwards and upwards in energy. With the energy difference between the two eigenstates being 2Δ the integral expression for the memories are

$$\kappa\phi_-(t) = \int_{-\infty}^{\infty} dz \ Y(z) \cos\left[(z-2\Delta)t\right], \quad (9.5a)$$

$$\kappa\phi_+(t) = \int_{-\infty}^{\infty} dz \ Y(z) \cos\left[(z+2\Delta)t\right]. \quad (9.5b)$$

To obtain the correct equilibrium value, we shall see that the bath spectral function $Y(z)$ must obey Eq. (8.4).

The GME, Eq. (9.4) with memories given by Eqs. (9.5b) and (9.5a), can be formally solved in the Laplace-domain and written as

$$\widetilde{p}(\epsilon) = \frac{1}{\epsilon}\widetilde{\xi}(\epsilon) + \frac{1}{\epsilon + \kappa[\widetilde{\phi}_+(\epsilon) + \widetilde{\phi}_-(\epsilon)]}\left[1 - \widetilde{\xi}(\epsilon)\right], \quad (9.6)$$

with

$$\widetilde{\xi}(\epsilon) = \frac{\widetilde{\phi}_+(\epsilon) - \widetilde{\phi}_-(\epsilon)}{\widetilde{\phi}_+(\epsilon) + \widetilde{\phi}_-(\epsilon)} \equiv -\frac{\widetilde{\phi}_\Delta(\epsilon)}{\widetilde{\phi}_S(\epsilon)}.$$

We have introduced here the Laplace-domain expressions for $\phi_\Delta(t)$ and $\phi_S(t)$ the sum and difference memory functions, respectively. Explicitly in terms of $\phi_\pm(t)$ they are given by

$$\kappa\phi_\Delta(t) = \kappa\left[\phi_-(t) - \phi_+(t)\right]. \quad (9.7a) \qquad \kappa\phi_S(t) = \kappa\left[\phi_-(t) + \phi_+(t)\right]. \quad (9.7b)$$

The first is product of the sine of the bath spectral function with the factor $2\sin\Delta t$ and the second the product of the cosine transform with the factor $2\cos\Delta t$. Generally, both quantities are found to be of both physical and conceptual importance.

The use of the Abelian theorem, $f(t \to \infty) = \lim_{\epsilon \to 0} \epsilon \widetilde{f}(\epsilon)$, allows the calculation of the long-time value of $p(t)$ from its Laplace-domain expression. The steady-state difference in probabilities is therefore

$$p(t \to \infty) = \frac{\widetilde{\phi}_+(0) - \widetilde{\phi}_-(0)}{\widetilde{\phi}_+(0) + \widetilde{\phi}_-(0)}, \tag{9.8}$$

One can see explicitly in Eq. (9.8) the importance of the Markoffian-approximated rates, $F_\pm = \kappa \int_0^\infty dt' \, \phi_\pm(t) \equiv \kappa \widetilde{\phi}_\pm(0)$. These two rates $F_\pm$ determine exactly the impact of the memories on the equilibrium state. Calculated explicitly, the expressions for the Markoffian-approximate rates are

$$F_- = \pi \int\limits_{-\infty}^{\infty} dz \, Y(z)\delta(z - 2\Delta) = \pi Y(2\Delta), \quad F_+ = \pi \int\limits_{-\infty}^{\infty} dz \, Y(z)\delta(z + 2\Delta) = \pi Y(2\Delta)e^{-\beta 2\Delta}.$$

The factor of $\pi Y(2\Delta)$ defines the reciprocal timescale κ in Eq. (9.6). We have used Eq. (8.4) in the right-hand equation to replace $Y(-2\Delta)$ with $Y(2\Delta)\exp(-\beta 2\Delta)$.

As expected, the requirement on $Y(z)$ results in the ratio of the two Markoffian-approximated rates,

$$\frac{F_+}{F_-} = e^{-\beta 2\Delta}, \tag{9.10}$$

satisfying the detailed balance condition. The reason for the requirement on the bath spectral function given in Eq. (8.4) is therefore made clear by Eq. (9.10). Only for this particular relation will detailed balance be satisfied for arbitrary non-degeneracy. At infinite time, the probabilities of occupation are

$$P_1(t \rightarrow \infty) = \frac{1}{2} - \frac{\tanh \beta \Delta}{2}, \qquad\qquad P_2(t \rightarrow \infty) = \frac{1}{2} + \frac{\tanh \beta \Delta}{2},$$

exactly equivalent to Eqs. (9.2).

This brief explanation of the non-degenerate dimer introduced by Tiwari and Kenkre [169] in their study of the approach to equilibrium of a quantum system shows explicitly the dual memories $\phi_\pm$ that incorporate the microscopic dynamics that describe the evolution of a system at short-times. It also sets the stage for our memory calculations below in Section 9.2 and our application to more realistic systems in Chapter 10.

9.2   Memory Functions for Specified Baths

We give here some explicit forms of the bath spectral function $Y(z)$ and their resulting memories $\phi_\pm(t)$. The detailed balance requirement, which results in bath spectral functions of the form given in Eq. (8.5), allows $Y(z)$ to be specified through the symmetrical function $Y_s(z)$. The bath can be simply characterized by two energy parameters, the width of the symmetrical spectral function, which we call w, and the thermal energy of the bath which we represent by the inverse temperature $\beta = 1/k_B T$. The system may have various characteristic energies. Let us typify them in the two-state system by the energy difference Δ between the two levels, in the Stark ladder by the energy difference Γ between neighboring sites, and in the harmonic oscillator by the frequency Ω of the oscillator. In this section, we use the symbol Ω as the characteristic energy of the system. With the exception of the delta-function triplet, each bath spectrum function is normalized such that $Y(\Omega) = 1/\pi$.

We give an illustration example of a bath spectral function in Fig. 9.1. The
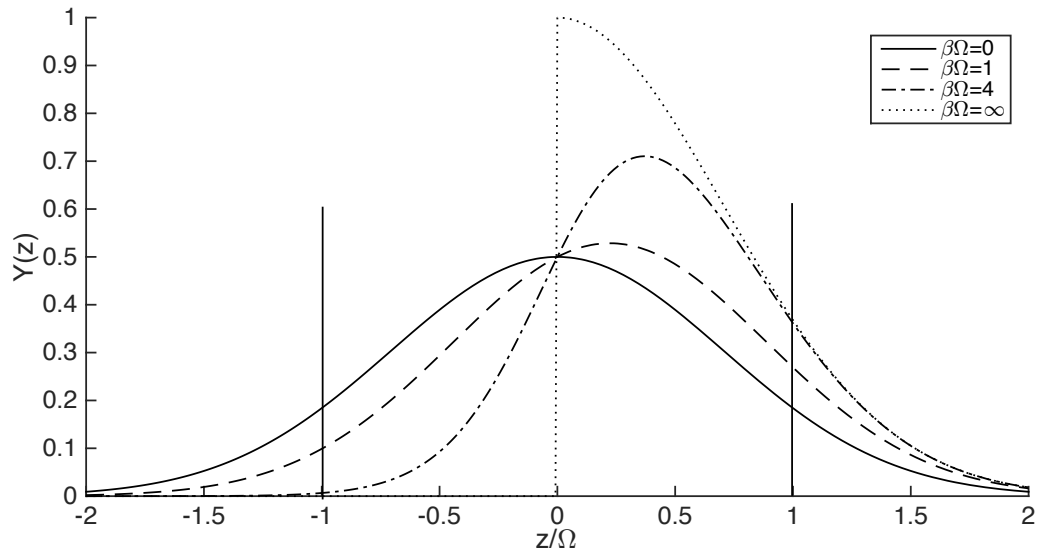
Figure 9.1: Gaussian bath spectral function $Y(z)$ is displayed for 4 values of the parameter $\beta\Omega = 0,\ 1,\ 2,\ 4,\ \infty$. The vertical lines indicate the width of the spectral function and we use Ω to normalize the horizontal axis.

Gaussian spectral function is displayed for 4 values of the dimensionless energy ratio $\beta\Omega = 0,\ 1,\ 4,\ \infty$. The solid vertical lines indicate the width of the spectral function and the horizontal axis is normalized by Ω. An increase in the parameter $\beta\Omega$ leads to a breaking of the symmetry between the left- and right-half planes and thus, the symmetry between the transition to higher energy and the one to lower energy. Small values of $\beta\Omega$ are approximately Gaussians shifted slightly leftward.

9.2.1 The Delta-Function Triplet and the Introduction of Incoherence

The delta-function triplet peaks at 0 and $\pm\Omega$. Here, in contrast to all the other cases, we have normalized $Y(z)$ by setting its integral to 1, given the presence of the

δ-function at Ω. The bath spectral function is

$$Y(z) = \frac{2}{1 + e^{-\beta z}} \left(S\delta(z) + (1 - S)\frac{\delta(z - \Omega) + \delta(z + \Omega)}{2} \right), \tag{9.12}$$

with S determining the relative strengths of the zero-energy and Ω-energy transitions. We note that the case of $S = 0$ corresponds with the vertical lines displayed at $z/\Omega = 1$ in Fig. 9.1. The memories are given by

$$\kappa\phi_{\pm}(t) = S \cos \Omega t + (1 - S) \left[\cos^2 \Omega t \mp \left(\tanh \frac{\beta\Omega}{2} \right) \sin^2 \Omega t \right]. \tag{9.13}$$

Fig. 9.2 in the left panel displays two examples each of the memories plotted against the dimensionless time κt. The dashed line is $\phi_+(t)$ and the dashed-dotted line is $\phi_-(t)$ for $\beta = 1/2$. The solid line is $\phi_+(t)$ and the dotted line is $\phi_-(t)$ for $\beta = 2$. We take the characteristic system energy $\Omega = 1$ and the spectral strength $S = 1/2$ in both. Both cases illustrate that a spectrum limited to delta-functions results in purely oscillatory memories, see Eq. (9.13), and, therefore, to completely coherent motion.

Broadening of the delta-functions in the spectrum by Lorentzians

$$\delta(z) \rightarrow \frac{1}{\pi} \left(\frac{\alpha}{z^2 + \alpha^2} \right),$$

where α is the broadening (width) parameter, leads to the damping of the memories as expected. Fig 9.2 in its right panel depicts these damped memories for two values of α. The thermal energy scale is $\beta = 1/2$ in these plots. The dotted and solid lines show the memories, $\phi_+(t)$ and $\phi_-(t)$ respectively, for $\alpha = 1/8$; the coherent oscillations persist for several periods before the memories decay. By contrast, for larger α $(= 1)$, the dashed-dotted and dotted lines depict the respective memories as damping much quicker. The delta-function spectrum and coherent memories are recovered in the limit $\alpha \rightarrow 0$.
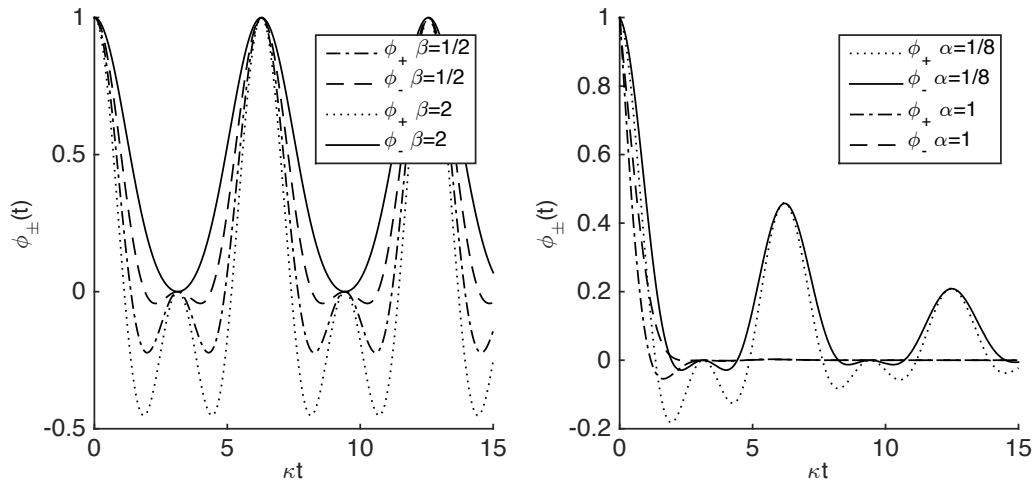
Figure 9.2: Time evolution of the memories $\phi_\pm$ for the 3-peaked spectral function. Coherent oscillations are seen for true delta-functions in the left panel while the introduction of α, which broadens the delta-functions into Lorentzians, damps the memories in the right panel. Each memory is shown for two values of the thermal energy: $\beta = 1/2, 2$. The right panel depicts the memories that result when each delta-function in Eq. (9.12) is represented with Lorentzians of finite width α: $1/8$ and 1 respectively.

9.2.2 Truncated Spectra

To satisfy detailed balance, the width w must be taken as greater than Ω for truncated spectra. The 'box' spectral function, centered at the origin, has width $2w$ and constant height $1/\pi$. The expression for $Y(z)$ is given by

$$Y(z) = \frac{1}{\pi}\left[\frac{1 + e^{-\beta\Omega}}{1 + e^{-\beta z}}\right]\Theta(w - |z|), \tag{9.14}$$

where $\Theta(z)$ is the Heaviside step function. The memories are

$$\phi_\pm(t) = \frac{1 + e^{-\beta\Omega}}{\pi}\left[\frac{\sin wt}{t}\cos\Omega t \mp \frac{1 - \cos wt}{t}\sin\Omega t \tag{9.15}\right.$$

$$\left.\mp 2\sin\Omega t\sum_{n=1}^{\infty}(-1)^n\left[\left(\frac{t}{n^2\beta^2 + t^2}\right)(1 - e^{-n\beta w}\cos wt) - \left(\frac{n\beta}{n^2\beta^2 + t^2}\right)e^{-n\beta w}\sin wt\right]\right]$$
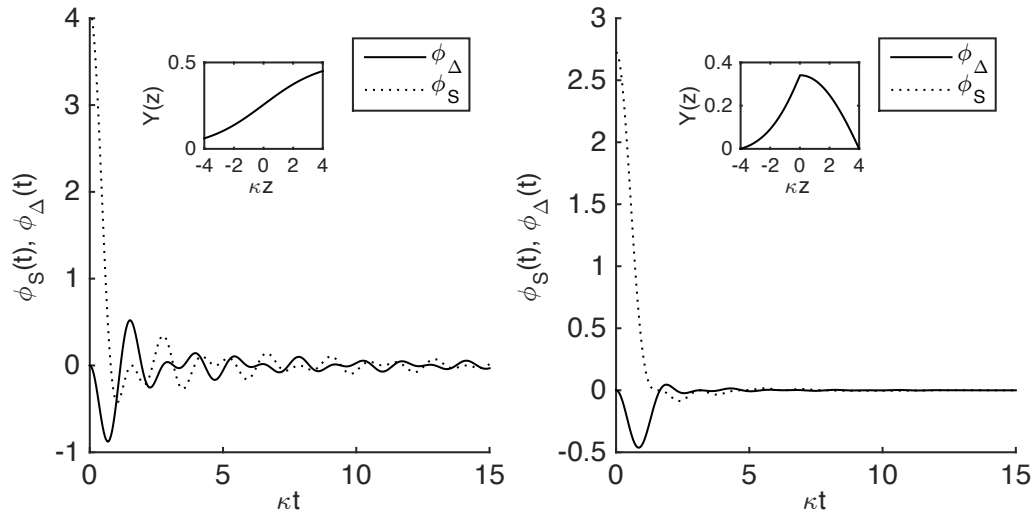
Figure 9.3: Depicted in the left panel are the sum and difference of the memories for the 'box' spectral function, given in Eqs. (9.15), with the corresponding $Y(z)$, Eq. (9.14), in the inset. Values for the characteristic energies are $\Omega = 1$, $\beta = 1/2$, $w = 4$. The sharp truncation of he 'box' spectral function results in memories with strong oscillatory behavior. In the right panel, the sum and difference of the triangular spectral function, Eqs. (9.17), are depicted with the corresponding $Y(z)$, Eq. (9.16), in the inset. The energy scales are $\Omega = 1$, $\beta = 1/2$, $w = 4$.

The sum $\phi_S(t) = \phi_+(t) + \phi_-(t)$ and difference $\phi_\Delta(t) = \phi_-(t) - \phi_+(t)$ of the memories given by Eqs. (9.15) are depicted in Fig. 9.3, left panel, while the bath spectral function for the 'box', Eq. (9.14), is shown in the inset. The chosen parameter values: thermal energy $\beta = 1/2$, the characteristic system energy $\Omega = 1$, and the spectral width $w = 4$. The discontinuous spectrum results in memories with persistent oscillations.

The triangular spectral function is centered at the origin with width $2w$, height $w/(w - \Omega)$ and constant slope. The bath spectral function is given by

$$Y(z) = \frac{1}{\pi} \left[\left(\frac{1 + e^{-\beta\Omega}}{1 + e^{-\beta z}} \right) \left(\frac{w - |z|}{w - \Omega} \right) \right] \Theta[w - |z|] \tag{9.16}$$

The expression for the memories are therefore

$$\phi_{\pm}(t) = \frac{1 + e^{-\beta\Omega}}{\pi(w - \Omega)} \left[\left(\frac{1 - \cos wt}{t^2} \right) \cos \Omega t \mp \left(\frac{wt - \sin wt}{t^2} \right) \sin \Omega t \right.$$

$$\left. \mp 2\sin\Omega t \sum_{n=1}^{\infty} (-1)^n \left[\frac{wt}{n^2\beta^2 + t^2} - 2n\beta t \left(\frac{1 - \cos wt \, e^{-n\beta w}}{(n^2\beta^2 + t^2)^2} \right) - 2t^2 \left(\frac{\sin wt \, e^{-n\beta w}}{(n^2\beta^2 + t^2)^2} \right) \right] \right]. \tag{9.17}$$

Fig. 9.3, right panel, depicts the sum and difference of the memories, Eqs. (9.15), for the triangular spectra while the spectral function, Eq. (9.14), is in the inset. Parameter values are $\Omega = 1$, $\beta = 1/2$, $w = 4$. Compared to the memories that result from the 'box' spectral function, those of the triangular $Y(z)$ have weaker oscillations; however, in both cases, the sharp truncation causes persistent oscillations.

9.2.3 Spectra with Infinite Support

The Lorentzian spectral function, centered at the origin with spectral width w, results in memories that are particularly simple. The normalized expression for the bath spectral function is given by

$$Y(z) = \left(\frac{1}{\pi} \right) \left(\frac{1 + e^{-\beta\Omega}}{1 + e^{-\beta z}} \right) \left[\frac{\Omega^2 + w^2}{z^2 + w^2} \right]. \tag{9.18}$$

The expressions for the memories that result from Eq. (9.18) are

$$\phi_{\pm}(t) = \left(\frac{1 + e^{-\beta\Omega}}{2} \right) \left(\frac{\Omega^2 + w^2}{w} \right) \left[\left(\cos \Omega t \mp \tan \frac{\beta w}{2} \sin \Omega t \right) e^{-wt} \right. \tag{9.19}$$

$$\left. \mp 4\sin\Omega t \sum_{n=0}^{\infty} \left[\frac{\beta w}{\beta^2 w^2 - \pi^2(2n+1)^2} \right] e^{\frac{-\pi(2n+1)t}{\beta}} \right]$$

Fig. 9.4, in its left panel, depicts the sum and difference of the memories, Eq. (9.19), for two sets of the parameter values: characteristic system energy $\Omega = 1$, thermal energy $\beta = 1$ and spectral widths $w = 1/4$ and 4. An increase in the spectral width leads to an increase in the damping of the memories. The inset displays Lorentzian spectral functions that correspond with the characteristic energies above. They are
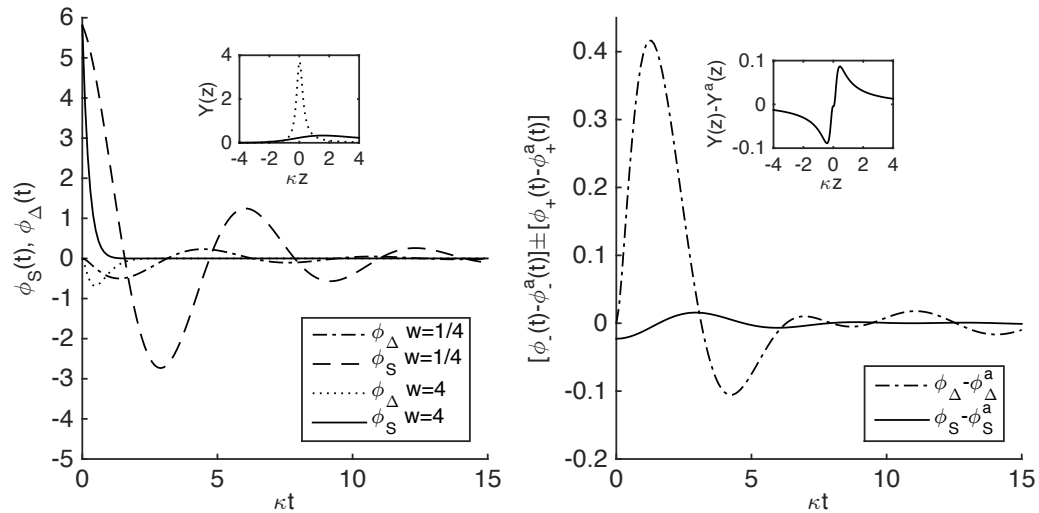
Figure 9.4: The left panel displays the sum and the difference of the memories for a Lorentzian spectral function, given in Eqs. (9.19). In the inset is the corresponding $Y(z)$, Eq. (9.18). $\Omega = 1$, $\beta = 1$ in both and two values of $w = 1/4$, 4 are shown. An increase in the spectral width leads to a broadening of the spectrum (solid line in the inset) and an increase in the damping. Depicted in the right panel are the difference between the real and approximated memories $\left[\phi_-(t) - \phi_-^a(t)\right] - \left[\phi_+(t) - \phi_+^a(t)\right]$ for a single set of parameter values: $\Omega = 1, \beta = 1, w = 1/4$. In the inset is the difference between the corresponding real and approximate bath spectral functions $Y(z) - Y^a(z)$ (inset). Note the difference in scale for the left and right panels.

represented by solid and dashed-dotted lines, respectively. An increase in the spectral width both broadens and shifts the bath spectral function.

The Lorentzian spectral function, Eq. (9.18), can be approximated for small values of βw by a shifted Lorentzian with shift parameter $\bar{z} = \beta w/4$. The width of the approximated Lorentzian spectral function $Y^a(z)$ is modified such that $w \rightarrow w(1 - \bar{z}^2)$. It is then given by

$$Y^a(z) = \left(\frac{1 + e^{-\beta\Omega}}{2\pi}\right) \frac{\Omega^2 + w^2}{(z - w\bar{z})^2 + w^2(1 - \bar{z}^2)^2}. \tag{9.20}$$

The approximate spectra from Eq. (9.20) have been introduced because they lead to memories $\phi_\pm^a(t)$ that are somewhat simpler than the true memories, Eqs. (9.19).

They are given by

$$\phi_{\pm}^a(t) = \left(\frac{1 + e^{-\beta\Omega}}{2}\right)\left(\frac{\Omega^2 + w^2}{w(1 - \bar{z}^2)}\right)\cos\left(\Omega \pm a\bar{z}\right)t\,e^{-w(1-\bar{z}^2)t}, \qquad (9.21)$$

and might be used for back-of-the-envelope calculations. The difference between the real and approximate memories, Eqs. (9.19) and Eqs. (9.21), respectively, is depicted in Fig. 9.4, right panel. Shown are $\phi_\Delta(t) - \phi_\Delta^a(t)$ and $\phi_S(t) - \phi_S^a(t)$, where $\phi_\Delta^a(t)$ is defined as in $\phi_\Delta(t)$ except with the approximate memories, $\phi_\pm^a(t)$, replacing the true memories, $\phi_\pm(t)$. The characteristic energies are taken to be the same as the first pair of memories ($\Omega = 1$, $\beta = 1$, $w = 1/4$). The approximate bath spectral function, Eq. (9.20), differ from the true Lorentzian spectral function closest to the origin (see inset).
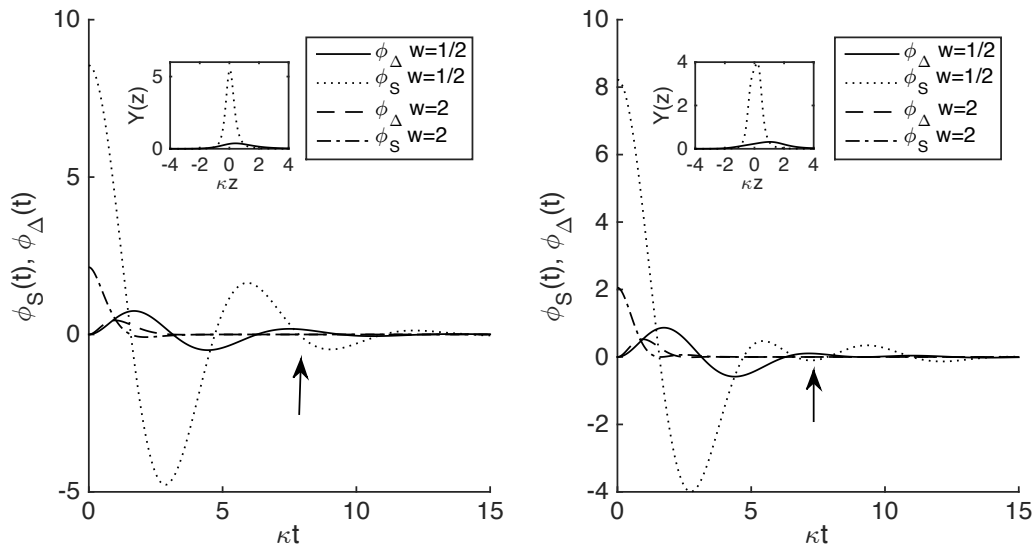
Figure 9.5: Depicted are the sum and difference of the memories that result from a squared Lorentzian (left panel) and quartic (right panel) spectral functions, Eqs. (9.24) and (9.26), respectively. Both are shown for $\Omega = 1$, $\beta = 1$ and two values $w = 1/2, 2$. The respective spectrum, Eqs. (9.23) and (9.25), are in the inset. A subtle difference in the dependence on z of either spectrum leads to similar memories with small differences at intermediate times that we have indicated with the arrow, namely, the presence of a distinct hump for the quartic spectral function.

A generalization of the Lorentzian spectral function in Eq. (9.18) is the generalized Cauchy distribution [170] specified by the parameter ν which determines the high-energy tails of the bath spectral function. The general expression is given by

$$Y(z;\nu) = \left(\frac{1}{\pi}\right)\left(\frac{1+e^{-\beta\Omega}}{1+e^{-\beta z}}\right)\left[\frac{\Omega^2 + a^2}{z^2 + a^2}\right]^{\nu}, \tag{9.22}$$

where $\nu > 1/2$ is required for $Y(z,\nu)$ to be normalizable. The Lorentzian spectral function, Eq. (9.18), reemerges when $\nu = 1$. Here, we give the case of $\nu = 2$, the square Lorentzian spectral function. This results in a z^{-4} dependence at high energies. For this case, the generalized spectral function, Eq. (9.22), is specialized to

$$Y(z) = \left(\frac{1}{\pi}\right)\left(\frac{1+e^{-\beta\Omega}}{1+e^{-\beta z}}\right)\left[\frac{\Omega^2 + w^2}{z^2 + w^2}\right]^{2}. \tag{9.23}$$

The memories that result from Eq. (9.23) are given by

$$\phi_{\pm}(t) = \left(\frac{1+e^{-\beta\Omega}}{4}\right)\left(\frac{\Omega^2+w^2}{w^{\frac{3}{2}}}\right)^2\left[\frac{(1+wt)(\cos\Omega t + \cos(\Omega t \pm \beta w)) \pm \beta w\sin\Omega t}{1+\cos\beta w}e^{-wt}\right.$$

$$\left.\mp 8\sin\Omega t\sum_{n=0}^{\infty}\left[\frac{\beta^3 w^3}{(\beta^2 w^2 - \pi^2(2n+1)^2)^2}e^{-\frac{\pi(2n+1)t}{\beta}}\right]\right] \tag{9.24}$$

The bath spectral function, Eq. (9.23), and the sum and difference of the memories, Eq. (9.24), are displayed in Fig. 9.5, left panel, for $\Omega = 1$, $\beta = 1$ and $w = 1/2, 2$. The bath spectral function (inset) shows the standard broadening and shifting as the spectral width w is increased.

As a comparison, the quartic spectral function possesses a z^{-4} dependence at high energies as well. The expression for its bath spectral function is

$$Y(z) = \left(\frac{1}{\pi}\right)\left(\frac{1+e^{-\beta\Omega}}{1+e^{-\beta z}}\right)\left[\frac{\Omega^4 + w^4}{z^4 + w^4}\right]. \tag{9.25}$$

The distinction between the squared Lorentzian spectral function, Eq. (9.23), and Eq. (9.25)) is most evident in the intermediate energy regime. The memories that

result from Eq. (9.25) are given by

$$\phi_\pm(t) = \left(\frac{1+e^{-\beta\Omega}}{\sqrt{8}}\right)\left(\frac{\Omega^4+w^4}{w^3}\right)\left[\left(\cos\frac{wt}{\sqrt{2}}+\sin\frac{wt}{\sqrt{2}}\right)\cos\Omega t\, e^{-\frac{wt}{\sqrt{2}}}\right.$$
$$\mp\left[\left(\frac{\sinh\eta+\sin\eta}{\cosh\eta+\cos\eta}\right)\sin\frac{wt}{\sqrt{2}}-\left(\frac{\sinh\eta-\sin\eta}{\cosh\eta+\cos\eta}\right)\cos\frac{wt}{\sqrt{2}}\right]\sin\Omega t\, e^{-\frac{wt}{\sqrt{2}}} \quad (9.26)$$
$$\left.\mp 4\sqrt{2}\sin\Omega t\sum_{n=0}\left[\frac{\beta^3 w^3}{\beta^4 w^4+\pi^4(2n+1)^4}e^{-\frac{\pi(2n+1)t}{\beta}}\right]\right].$$

Here $\eta = \beta w/\sqrt{2}$. The sum and difference of the quartic spectral function memories, Eqs. (9.24), are depicted for $\Omega = 1$, $\beta = 1$ and $w = 1/2$ and 2 in Fig. 9.5, right panel, with $Y(z)$, Eq. (9.23), inset. The two arrows in Fig. 9.5 point to a subtle distinction between the memories for a squared Lorentzian spectral function, Eqs. (9.24), and those of the quartic, Eqs. (9.26), at intermediate times.

The mod exponential spectral function is centered at the origin with width w. Its bath spectral function is given by

$$Y(z) = \left(\frac{1}{\pi}\right)\left(\frac{1+e^{-\beta\Omega}}{1+e^{-\beta z}}\right)e^{-\frac{|z|-\Omega}{w}}. \quad (9.27)$$

The memories that result from Eq. (9.27) are expressed as

$$\phi_\pm(t) = \left(\frac{1+e^{-\beta\Omega}}{2\pi}\right)w\, e^{\frac{\Omega}{w}}\left[\frac{\cos\Omega t\mp wt\sin\Omega t}{1+w^2 t^2}\right. \quad (9.28)$$
$$\left.\mp 4\sin\Omega t\sum_{n=1}^{\infty}(-1)^n\frac{wt}{(1+n\beta w)^2+w^2 t^2}\right]$$

The sum and difference of the memories, Eqs. (9.28), are depicted in Fig. 9.6, left panel. The parameter values $\Omega = 1$, $\beta = 1$, and two values of $w = 1/2$, 2 are considered. Inset is the mod exponential spectral function in dotted and solid lines, respectively. The discontinuity in the derivative of the exponential spectral function at $z = 0$ causes the oscillations to be persistent.

The final bath spectral function we consider is a Gaussian of width w:

$$Y(z) = \left(\frac{1}{\pi}\right)\left(\frac{1+e^{-\beta\Omega}}{1+e^{-\beta z}}\right)e^{-\frac{z^2-\Omega^2}{w^2}}. \quad (9.29)$$
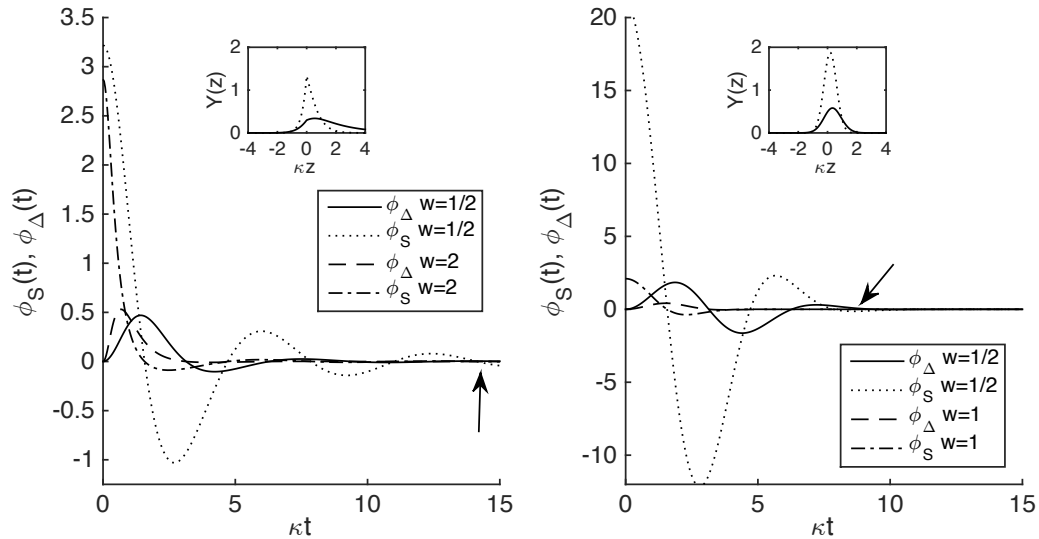
Figure 9.6: In the left panel, the sum and the difference of the memories, Eqs. (9.28), are displayed for the mod exponential spectral function while the right panel similarly displays the sum and difference of the memories, Eqs. (9.30), for the Gaussian spectral function. Inset in each is $Y(z)$, Eqs. (9.27) and (9.29), respectively. $\Omega = 1$ and $\beta = 1$ for both spectral functions while $w = 1/2$ and 2 for the mod exponential while for the Gaussian the values for the spectral width are $w = 1/2$, 1. The discontinuity in the exponential spectral density at $z = 0$ decreases the damping, resulting in the persistence of oscillations.

The magnitude of Eq. (9.29) is strongly dependent on the width. The memories that result from a Gaussian spectral function are given by

$$\phi_{\pm}(t) = \frac{1 + e^{-\beta\Omega}}{4} \frac{we^{\frac{\Omega^2}{w^2}}}{\sqrt{\pi}} \left[e^{-\frac{w^2 t^2}{4}} \cos\Omega t \pm i \left(\text{w}(\frac{wt}{2}) - \text{w}(-\frac{wt}{2}) \right) \sin\Omega t \right.$$

$$\left. + 2i \sin\Omega t \sum_{n=1}^{\infty} (-1)^n \left(\text{w}(\frac{wt + in\beta w}{2}) - \text{w}(\frac{-wt + in\beta w}{2}) \right) \right]. \qquad (9.30)$$

The Fourier transform of Eq. (9.29) results in an scaled error function of complex argument which we represent with the Faddeeva function [20], $\text{w}(iz) = \text{erfcx}(z)$. The presence of i in Eq. (9.30) should not lead the reader to conclude the memories have imaginary components. As shown in Fig 9.6, left panel, they are certainly real. Depicted are the sum and difference of the memories for $\Omega = 1$, $\beta = 1$, and two

values of $w = 1/2$ and 1 with the corresponding $Y(z)$ inset with, respectively, dotted and solid lines. The strong dependence of the Gaussian spectral function on the z results in memories with extreme quantitative dependence on the parameters.

When the dimensionless energy ratio βw is small, the Gaussian spectral function can be approximated with a shifted Gaussian centered at $w(1 - \bar{z}^2)$ where $\bar{z} = \beta w/4$. The approximation to the bath spectral function, Eq. (9.29), is given by

$$Y^a(z) = \frac{1}{\pi} \frac{1 + e^{-\beta\Omega}}{2} e^{-\frac{\Omega^2}{w^2}} e^{-\frac{(z - w\bar{z})^2}{w^2(1 - \bar{z}^2)^2}} . \tag{9.31}$$

The exact memories for the approximate spectral function, Eq. (9.31), provide analytically tractable approximation for calculations. They are given by

$$\phi^a_\pm(t) = \frac{w(1 - \bar{z}^2)}{\sqrt{\pi}} \frac{1 + e^{-\beta\Omega}}{2} e^{\frac{\Omega^2}{w^2}} \cos(\Omega \pm w\bar{z})t \, e^{-w^2(1 - \bar{z}^2)^2 t^2} \tag{9.32}$$

9.2.4 Physical Discussion of Memory Behavior

The behavior of the memories for particular bath spectral functions is intimately related to the relative values of the three (dimensionless) energies that characterize the system and the bath. They are the system energy Ω, the thermal energy of the bath $1/\beta$, and w, the energy that characterizes the spectral resolution of the bath. Physically, the effects caused by the variation of these parameters are related to the change in the ratios of the energy scales, βw, $\beta\Omega$ and Ω/w. The first ratio compares the thermal energy of the bath to its average spectral energy. For small values of this ratio the dominant energy scale of the bath is its spectral while temperature effects dominate for large values (see Fig. 9.1 for an example). The second and third ratios compare the respective bath energies to the system energy. Small values of either lead to incoherent motion whereas, the exchange of energy is suppressed when the ratios are large leading to longer coherent system evolution.

Though the ratios are the physically important quantities, their interdependence
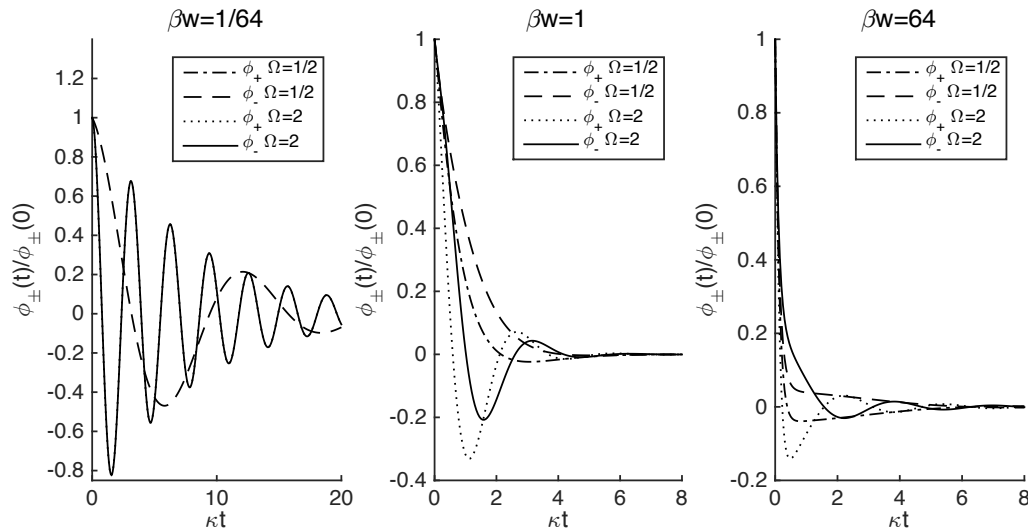
Figure 9.7: The normalized memories, $\phi_\pm(t)/\phi_\pm(0)$, for the Lorentzian spectral function are shown for two values of Ω in each of the panels. From left to right, the ratio of the characteristic bath energies, βw, takes the values $\beta w = 1/64$ ($\beta = 1/8$, $w = 1/8$), $\beta w = 1$ ($\beta = 1$, $w = 1$), and $\beta w = 64$ ($\beta = 8$, $w = 8$). The increase in Ω increases the oscillation frequency of the memories and, therefore, the coherence time of the system evolution.

on the dimensionless energies complicates a qualitative analysis of the effect of their change on the memories. Therefore, we effect change through a variation in the energies but provide commentary using the ratios. We have highlighted the salient differences in the three figures: Figs 9.7, 9.9 and 9.8. All three display memories that result from a Lorentzian spectral function, whose expression is given in Eq. (9.18). In addition, the relevant time scale is set by κ.

We display the effects of varying the characteristic energy of the system Ω in Fig. 9.7. Two values, $\Omega = 1/2, 2$, are shown for three pairs of characteristic bath energies: $\beta = 1/8$ and $w = 1/8$ (left), $\beta = 1$ and $w = 1$ (center), and $\beta = 8$ and $w = 8$ (right). The bath energies have been chosen to highlight the effect of the thermal deviation to the spectra (see Fig. 9.1 for an example of this effect). An increase in Ω generally results a decrease in the period of oscillation. In the left panel, neither of
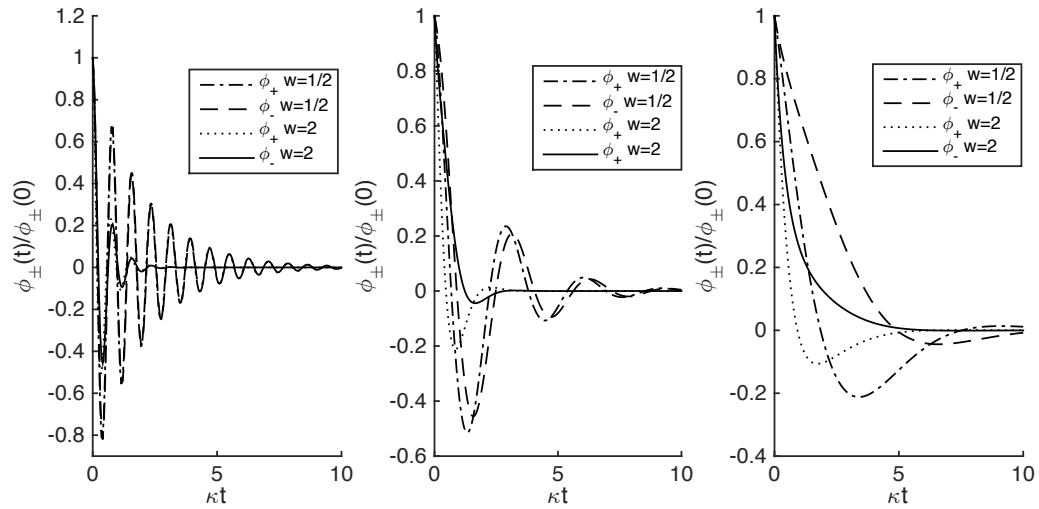
Figure 9.8: A variation to the spectral energy $w = 1/2$, 2 is displayed for the case of the Lorentzian spectral function. Three pairs of the ratio of the characteristic system energy to the thermal energy or the bath are shown: ($\Omega = 8$, $\beta = 1/4$), ($\Omega = 2$, $\beta = 1$), and ($\Omega = 1/4$, $\beta = 8$). The ratio $\Omega\beta = 2$ is held constant. An increase in the spectral width w generally results in an increase in the damping relative to the oscillation period. However, larger smaller values of βw decrease the effect as the thermal energy scale begins to dominate the dynamics.

the characteristic bath energy scales are large compared to the system energy; the oscillations of the memories therefore persist for multiple periods. An increase in the characteristic bath energies with respect to those of the system, as in the center panel, results in stronger damping, and, therefore, leads to a shorter coherence time. As seen in the right panel, however, thermal effects dominate the spectral energies when βw is large leading to re-lengthening of the coherence time scale. Across the three panels, one can observe the importance of the ratio of the characteristic bath energies in determining the coherence time scale by identifying the dominant bath energy scale.

The memories for two values of the characteristic spectral energy $w = 1/2$, 2 are displayed in each panel of Fig. 9.8. The ratio of the characteristic system energy to the thermal energy is held constant: left ($\Omega = 8$, $\beta = 1/4$), center ($\Omega = 2$, $\beta = 1$),
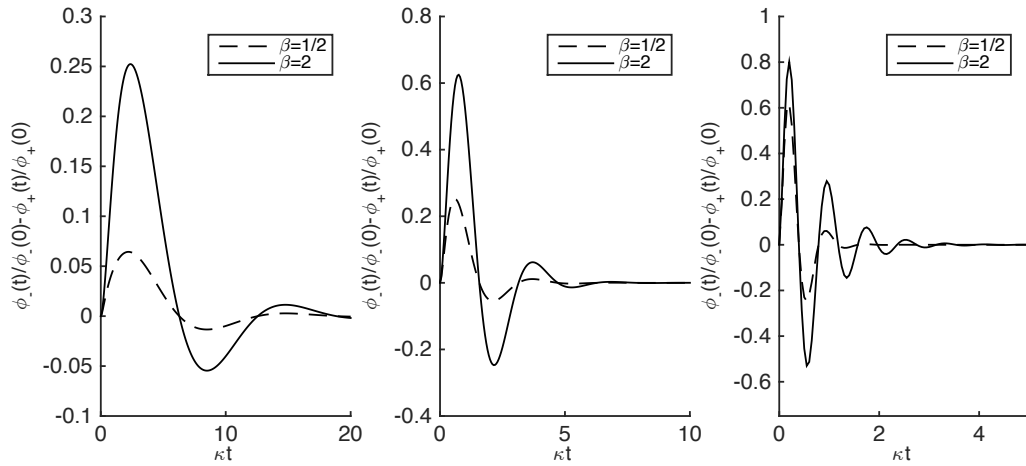
Figure 9.9: We display here the difference between the normalized memories, $\phi_-(t)/\phi_-(0) - \phi_+(t)/\phi_+(0)$ against the dimensionless time κt for two values of the thermal energy, $\beta = 1/2$. 2 and three pairs of the ratio of the system energy and spectral width: left ($\Omega = 8$, $w = 48$), center ($\Omega = 2$, $w = 1$), right ($\Omega = 1/4$, $w = 1/8$). Larger values of β result in an increase in the distinction between the memories. However, the effect itself becomes less important as βw decreases commensurate with the increase in the spectral damping.

and right ($\Omega = 1/4$, $\beta = 8$). As evidenced in Fig. 9.8, the coherent time-scale is decreased when the spectral width w is increased. Small values of w indicate a limit to the capability of the bath to dissipate energy. The effect is diminished for small values of βw when the thermal energy scale dominates the behavior of the bath.

Fig. 9.9 depicts the effect of a change in the parameter β on the difference between the normalized memories $\phi_-(t)/\phi_-(0) - \phi_+(t)/\phi_+(0)$. In each panel, two values of β (1/2, 2) are displayed while the ratio of the characteristic system energy to the spectral energy is held constant. From left to right, we use $\Omega = 8$, $w = 4$, $\Omega = 2$, $w = 1$, and $\Omega = 1/4$, $w = 1/8$. An increase in the thermal energy leads to a commensurate increase in the distinguishability of the two memories. This effect is damped, however, when its the spectral energy w that determines the energy of the bath.

9.3 Conclusion

The explicit bath spectral functions that were discussed in Section 9.2 may be used along with the simple non-degenerate dimer analyzed by Tiwari and Kenkre [169]. We use them in this thesis with systems that are richer in content and more realistic for physical applications in Chapter 10. The harmonic oscillator is one system, the state space being semi-infinite ($M = 0, 1, ..., \infty$) and the Stark Ladder system is another, for which the state space is infinite ($M = -\infty, ..., \infty$).

Chapter 10

Relaxation of Two Quantum Systems: Effects of Coherence on Vibrational Relaxation and on the Stark Ladder

In this Chapter, we study the impact of short-time coherence on the evolution of two physically interesting systems (see refs. [165, 167, 168] for a complete discussion of the formalism). An excited molecule that undergoes vibrational relaxation is our primary system of interest. The Master equation that describes the relaxation at long times, valid when the energy levels of the relaxing molecule are well-approximated by those of the harmonic oscillator, is well-known to be the Montroll-Shuler equation [141]. The details of its properties have been discussed and various extensions proposed in the literature [146, 147, 171–173]. Despite the more recent development of a number of alternative theoretical approaches [133–135, 142–144, 148, 174], however, the GME that naturally extends the Montroll-Shuler equation to the coherent domain has not

been discussed. In Section 10.1, such a generalization is one of our principal results. With its help we will describe an equation for the generating function subject to coherent effects; the equations for the moments and factorial moments; an extension into the coherent domain of the validity of the Bethe-Teller result [175], i.e., the average energy being independent of the particulars of the initial probability distribution; and give an explicit Laplace-domain solution for the special case of the system being prepared in a Boltzmann distribution characterized by a temperature T_0 given and discussed in the context of the so-called canonical invariance property [172, 173].

The Stark ladder is a second physical system that can also be considered as a natural extension to the non-degenerate dimer. It describes the motion of a charge on a lattice under strong electric fields subject to nearest neighbor coupling between lattice sites. In Section 10.2, we analyze the GME associated with such a system and give expressions for the propagator in the Laplace domain. Because the energy spectrum of this system is not bounded below, the system does not go to thermal equilibrium. Nevertheless, the time-domain dynamics of the charge are interesting enough to be discussed with reference to coherence.

10.1 Vibrational Relaxation: Coherence Effects

The Master equation that governs the relaxation of an excited molecule was constructed by Montroll and Shuler [141] as a discrete generalization of the continuum analysis given by Shuler and collaborators [138–140]. In the construction, they assume the Landau-Teller transitions [176], valid for interactions between the oscillator and the bath taken to be of sufficient weakness such that a first-order Taylor series expansion in the oscillator coordinate is appropriate. Thus, the Montroll-Shuler equation was written in ref. [141] as

$$\frac{dP_M}{dt} = \kappa \left[(M+1)P_{M+1} + Me^{-\beta\Omega}P_{M-1} - \left(M + (M+1)e^{-\beta\Omega} \right) P_M \right]. \qquad (10.1)$$

Here, $P_M(t)$ is the probability of occupation of the Mth eigenstate (M taking integer values from 0 to ∞) and both the nearest-neighbor coupling and the dependence of the transition rates on M arise from the linearity of the interaction with respect to the oscillator coordinate. As in Eq. (8.1), κ is the reciprocal time scale, β is the thermal energy scale, and Ω is the energy (or, equivalently, the frequency) characteristic of the system.

The GME that governs vibrational relaxation is derived using the generalization, devised by Kenkre [165, 167, 168], of the Zwanzig procedure of diagonalizing projection operators [47, 159–161]. It is given by

$$
\frac{1}{\kappa}\frac{dP_M(t)}{dt} = \int_0^t dt' \left[\phi_-(t-t')\left[(M+1)P_{M+1}(t') - MP_M(t')\right] \right.
$$
$$
\left. - \phi_+(t-t')\left[(M+1)P_M(t') - MP_{M-1}(t')\right] \right]. \qquad (10.2)
$$

Here, the memories $\phi_\pm(t)$ are as defined in Eqs. (8.3) and we have explicitly grouped the energetically downwards transitions (the first bracketed term) separately from the upwards transitions (the second bracketed term). The connection between the GME, Eq. (10.2), and the Montroll-Shuler equation, Eq. (10.1), becomes more evident when the terms of the latter are grouped in a similar manner. Thus, we combine the energetically downwards transitions and upward transitions into, respectively, the terms $[(M+1)P_{M+1}(t) - MP_M(t)]$ and $\exp(-\beta\Omega)[(M+1)P_M(t) - MP_{M-1}(t)]$.

Following this reorganization, Eq. (10.1) is rewritten in the form

$$
\frac{1}{\kappa}\frac{d}{dt}P_M(t) = [(M+1)P_{M+1}(t) - MP_M(t)]
$$
$$
- e^{-\beta\Omega}[(M+1)P_M(t) - MP_{M-1}(t)]. \qquad (10.3)
$$

The correspondence between the GME and the Montroll-Shuler equation, noted in Chapter 8, becomes immediately evident. When the memories $\phi_\pm(t)$ in Eq. (10.2) are replaced with their respective Markoffian approximations, i.e.,

$$\phi_-^M(t) = \delta(t) \int\limits_0^\infty dt \; \phi_-(t) = \delta(t), \qquad \phi_+^M(t) = \delta(t) \int\limits_0^\infty dt \; \phi_+(t) = e^{-\beta\Omega}\delta(t),$$

Eq. (10.3) results. The definition of $\phi_\pm(t)$ has been used to evaluate the integral in both cases. We remind the reader that the bath spectral function $Y(z)$ is normalized such that the reciprocal timescale is given by the expression $\kappa = \pi Y(\Omega)$.

Eq. (10.2) is then the generalization of the Montroll-Shuler equation accounting for coherent effects at short times. As expected for a GME, Eq. (10.2) is explicitly for the probabilities. The effects of the off-diagonal matrix elements are not neglected; however, they contribute through the memories $\phi_\pm(t)$.

10.1.1 First-Order Partial Differential Equation for the Generating Function

The analysis of Montroll and Shuler [141] owes its success to the introduction of the generating function. Defined by the transformation

$$G(z,t) = \sum_{M=0}^\infty z^M P_M(t), \tag{10.4}$$

one can use it to construct an alternative representation of the Montroll-Shuler equation. Through the transform, the original differential-difference equation, with dependence on the discrete index M, given in Eq. (10.3) is converted into a partial differential equation for the continuous variable z. The latter is given by

$$\frac{1}{\kappa}\frac{\partial G(z,t)}{\partial t} = (z-1)\frac{\partial}{\partial z}\left[(ze^{-\theta}-1)G(z,t)\right], \tag{10.5}$$

where $\theta = \Omega/k_B T$ is the ratio of the characteristic system energy to the thermal energy of the bath. The Nth probability of occupation is recovered from $G(z,t)$ by

N differentiations with respect to z and a division by $N!$ followed by setting $z = 0$. The moments are constructed directly from $G(z, t)$ by the repeated application of the operator $z\partial/\partial z$ followed by setting $z = 1$, i.e.,

$$\left(z\frac{\partial}{\partial z} \right)^n \bigg|_{z=1} = \langle M^n \rangle.$$

We note that we have maintained the Montroll-Shuler notation that the argument of the generating function is z. The reader should not confuse its use here with the use of the same variable for describing the frequency of the bath spectral function $Y(z)$ as in, for example, Section 9.2.

The power of the Montroll-Shuler analysis comes from the simple form of the solution to Eq. (10.5). Taking an arbitrary initial condition,

$$G(z, 0) = \sum_{M=0} z^M P_M(0) = G_0(z),$$

one may solve the equation for the generating function using the method of characteristics. As is common in the use of this technique, the full solution depends in a straightforward manner on the function $G_0(z)$:

$$G(z, t) = \frac{1 - e^{-\theta}}{(z - 1)e^{-\tau}e^{-\theta} - (ze^{-\theta} - 1)} G_0\left[\zeta(z)\right]. \tag{10.6}$$

Here, $\tau \equiv \kappa t \left(1 - e^{-\theta}\right)$ and the second factor in Eq. (10.6) is simply $G_0(z)$ with z substituted by the function $\zeta(z)$ given by

$$\zeta(z) = \frac{(z - 1)e^{-\tau} - \left(ze^{-\theta} - 1\right)}{(z - 1)e^{-\tau}e^{-\theta} - (ze^{-\theta} - 1)}. \tag{10.7}$$

The transformation given in Eq. (10.4) can be used in the context of the GME as well. The result is a generalization of Eq. (10.5) to account for arbitrary coherence. It is given by

$$\frac{1}{\kappa}\frac{\partial G(z, t)}{\partial t} = (z - 1)\frac{\partial}{\partial z}\int_0^t dt'\ \left[(z\phi_+(t - t') - \phi_-(t - t'))G(z, t')\right]. \tag{10.8}$$

While we have not been able to similarly solve the integro-differential equation, Eq. (10.8), for arbitrary initial conditions, we have obtained several partial results.

10.1.2 Moment and Factorial Moment Equations from the GME

One may derive a second alternative representation of the Montroll-Shuler equation (and similarly the GME) through the use of the factorial moments. They are constructed by

$$f_n(t) = \sum_M M(M-1)...(M-n+1)P_M(t), \tag{10.9}$$

where n is a positive integer (f_0 being defined as 1). The relation between the generating function, whose evolution equation is given in Eq. 10.5), and the factorial moments is

$$f_n(t) = \frac{\partial^n}{\partial z^n}G(z,t)\bigg|_{z=1}.$$

An equivalent representation of the Montroll-Shuler equation for its factorial moment is then constructed directly from the generating function equation:

$$\frac{1}{\kappa}\frac{df_n}{dt} + n(1-e^{-\theta}))f_n = n^2 e^{-\theta}f_{n-1}. \tag{10.10}$$

As compared with the equation for the probabilities of occupation, Eq. (10.3), the benefit of Eq. (10.10) lies in its hierarchical structure: the evolution equation for f_n depends only on f_n and f_{n-1}. This structure contrasts with that of the Master equation in which the evolution of P_M depends on both P_{M+1} and P_{M-1}.

One can derive an equivalent equation for the factorial moments of the GME, Eq. (10.2); being given by

$$\frac{1}{\kappa}\frac{\partial f_n(t)}{\partial t} + n\int_0^t dt'\phi_\Delta(t-t')f_n(t') = n^2\int_0^t dt'\phi_+(t-t')f_{n-1}(t'). \tag{10.11}$$

Here we see the natural appearance of the difference memory function $\phi_\Delta(t)$ defined in Eq. (9.7b). We note that its time integral from 0 to ∞ equals $1 - e^{-\theta}$, which as expected, appears in the second term of the left-hand-side of Eq. (10.10). Laplace-domain solutions can be constructed for arbitrary n using the hierarchical structure of Eq. (10.11), f_n being coupled only to f_{n-1} and f_0 being 1.

We bring our focus onto the simple moments, i.e.,

$$\langle M^n \rangle = \sum_{M=0}^{\infty} M^n P_M(t).$$

The evolution equations for a general moment is of a slightly more complicated form than that of the factorial moments. The general equation is

$$\frac{1}{\kappa}\frac{d\langle M^n\rangle}{dt} + n\int_0^t dt'\ \phi_\Delta(t-t')\,\langle M^n\rangle(t') = \int_0^t dt'\ \phi_+(t') \tag{10.12}$$

$$+\sum_{p=1}^{n-1}\binom{n}{p-1}\int_0^t dt'\left[\frac{(n+1-p(-1)^{n-p})}{p}\phi_+(t-t')-(-1)^{n-p}\phi_\Delta(t-t')\right]\langle M^p\rangle(t'),$$

When Eq. (10.12) is specialized to the case of the first ($n = 1$) and second ($n = 2$) moments, we have:

$$\frac{1}{\kappa}\frac{d\langle M\rangle}{dt} + \int_0^t dt'\phi_\Delta(t-t')\,\langle M\rangle(t') = \int_0^t dt'\phi_+(t'), \tag{10.13a}$$

$$\frac{1}{\kappa}\frac{d\langle M^2\rangle}{dt} + 2\int_0^t dt'\phi_\Delta(t-t')\,\langle M^2\rangle(t') \tag{10.13b}$$

$$= \int_0^t dt'\ [\phi_\Delta(t-t') + 4\phi_+(t-t')]\,\langle M\rangle(t') + \int_0^t dt'\ \phi_+(t').$$

We observe again both of Eqs. (10.13) depend on the memory combinations $\phi_\Delta(t)$ and $\phi_+(t)$. The results for the Montroll-Shuler equation can be found directly from Eqs. (10.13) by insertion of the Markoffian-approximated memories, i.e., the products

of $\delta(t)$ and $1 - e^{-\theta}$ and $e^{-\theta}$, respectively ($\theta = \beta\Omega$). The effects of arbitrary coherence can be gleaned from the various baths discussed in Section 9.2.

We give the solutions of Eqs. (10.13) in the Laplace-domain as

$$\widetilde{\langle M \rangle}(\epsilon) = \frac{\langle M \rangle_0}{\epsilon + \kappa \widetilde{\phi}_\Delta(\epsilon)} + \frac{\kappa \widetilde{\phi}_+(\epsilon)}{\epsilon \left(\epsilon + \kappa \widetilde{\phi}_\Delta(\epsilon) \right)} \tag{10.14a}$$

$$\widetilde{\langle M^2 \rangle}(\epsilon) = \frac{\langle M^2 \rangle_0}{\epsilon + 2\kappa \widetilde{\phi}_\Delta} + \left[\frac{\widetilde{\phi}_\Delta(\epsilon) + 4\widetilde{\phi}_+(\epsilon)}{\epsilon + 2\kappa \widetilde{\phi}_\Delta(\epsilon)} \right] \left[\frac{\kappa \langle M \rangle_0}{\epsilon + \kappa \widetilde{\phi}_\Delta(\epsilon)} \right] \tag{10.14b}$$

$$+ \frac{\kappa \widetilde{\phi}_+(\epsilon)}{\epsilon \left(\epsilon + \kappa \widetilde{\phi}_\Delta(\epsilon) \right)} + \frac{4\kappa^2 \widetilde{\phi}_+^2(\epsilon)}{\epsilon \left(\epsilon + \kappa \widetilde{\phi}_\Delta(\epsilon) \right) \left(\epsilon + 2\kappa \widetilde{\phi}_\Delta(\epsilon) \right)}$$

10.1.3 Validity of the Bethe-Teller Result in the Coherent Domain

In their investigation of the deviations from thermal equilibrium in shock waves [175], Bethe and Teller obtained a particular interesting result describing the evolution of the average energy $E(t)$ of an excited molecule coupled to a bath. They found the temporal dependence of the average energy to be given by

$$E(t) = E(0)e^{-\kappa(1-e^{-\theta})t} + E_{th}\left(1 - e^{-\kappa(1-e^{-\theta})t}\right), \tag{10.15}$$

with $E(0)$ being the initial average energy and $E_{th} = \Omega \coth \theta/2$ being its value at thermal equilibrium. Evident in Eq. (10.15) are two important properties of the relaxation of the molecule. Note that the average energy does not depend on the actual probabilities of occupation despite the dependence of their own evolution on themselves. The average energy of two systems that are prepared with identical average energy but wildly divergent probability distributions would, therefore, display identical evolution. Secondly, observe that the relaxation of the average energy is exponential at all times and, crucially, that this time dependence is independent of $E(0)$, i.e., independent of the initial average energy. The time dependence of the

evolution depends, therefore, only on the nature of the system and on the properties of the bath not on its prepared state. We study now these properties for systems of arbitrary coherence.

Using the GME, Eq. (10.2), one can extend the analysis performed by Bethe and Teller to account for coherence at short times. The average energy is essentially proportional to Eq. (10.14a), i.e., $\langle M \rangle(t)$. Following a rearrangement of the terms in Eq. (10.14a), the Laplace-domain expression for the average energy is written as

$$\widetilde{E}(\epsilon) = \frac{E(0)}{\epsilon + \kappa \widetilde{\phi_\Delta}(\epsilon)} + E_{th} \left[\frac{\widetilde{\phi_S}(\epsilon)}{\widetilde{\phi_\Delta}(\epsilon)} \tanh \left(\frac{\theta}{2} \right) \right] \left[\frac{1}{\epsilon} - \frac{1}{\epsilon + \kappa \widetilde{\phi_\Delta}(\epsilon)} \right]. \qquad (10.16)$$

As in the Bethe-Teller result, the average energy is found to be both independent of the particular distribution of the probabilities of occupation and only trivially dependent on its initial value, the latter dependence being similarly multiplicative. However, only at extremely long-times, i.e., when the Markoffian approximation becomes valid, will the time dependence of the evolution be exponential. The Bethe-Teller result is simply recovered from Eq. (10.16) by a replacement of the memories with their Markoffian-approximated equivalents.

A formal time-domain expression can be derived from Eq. (10.16) by first defining

$$\widetilde{\eta}(\epsilon) = \frac{1}{\epsilon + \kappa \widetilde{\phi_S}(\epsilon)}.$$

The first term on the right-hand-side of Eq. (10.16) is then simply $E(0)\widetilde{\eta}(\epsilon)$. Using this definition, the term proportional to E_{th} becomes a simple convolution of $1 - \eta(t)$ with $\xi(t)$, the latter being defined in the Laplace domain as

$$\widetilde{\xi}(\epsilon) = \frac{\widetilde{\phi_S}(\epsilon)}{\widetilde{\phi_\Delta}(\epsilon)} \tanh \left(\frac{\theta}{2} \right). \qquad (10.17)$$

We note that $\widetilde{\xi}(\epsilon = 0)$ is simply 1. The time-domain expression for the average energy is then given by

$$E(t) = E(0)\eta(t) + E_{th} \int_0^t dt' \xi(t - t') \left[1 - \eta(t') \right]. \qquad (10.18)$$
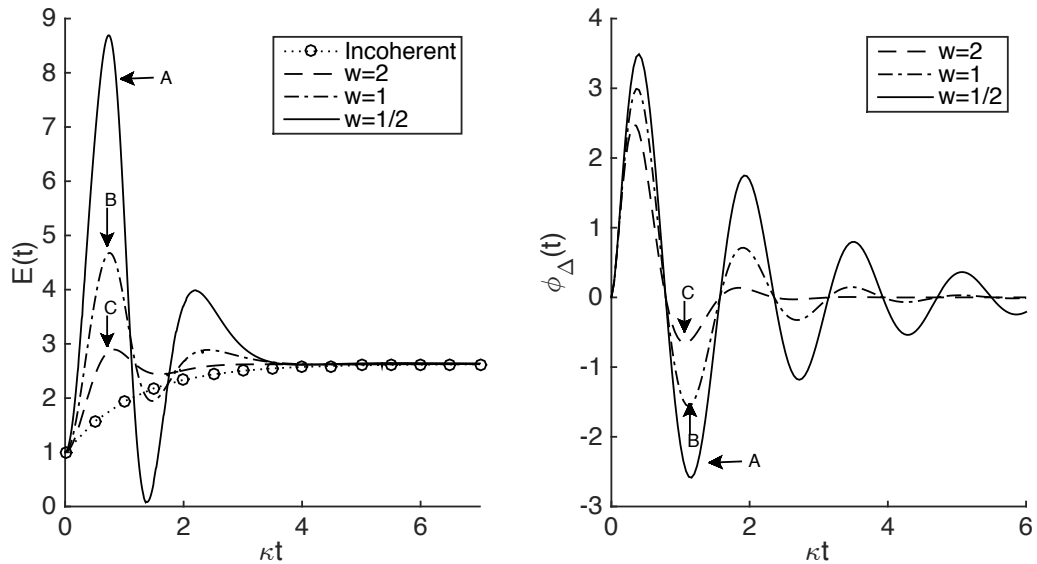
Figure 10.1: A generalization of the Bethe-Teller result to account for coherent effects is presented. The left panel displays the time evolution of the normalized average energy of the relaxing molecule, $E(t)/E(0)$, $E(0)$ being the initial energy of the particle, for the Lorentzian spectral function, Eq. (9.18). Three values of the spectral width $w = 2$, 1, $1/2$ are shown along with the incoherent limit, given by the Bethe-Teller result, Eq. (10.15), the latter being labeled by the symbol o. The values of the other parameters, $\beta = 1/2$ and $\Omega = 4$, are illustrative. Time is in units of κ. In all cases, the average energy rises from its initial value and saturates to the normalized thermal value $E_{th}/E(0)$. The incoherent limit is a simple exponential rise. Coherence, however, leads to an oscillating energy with an increase in w leading to larger amplitudes of oscillation. The right panel displays the three difference memory functions $\phi_\Delta(t)$ from Eq. (9.19) that correspond to the three examples of the coherent evolution.

By comparison with the Bethe-Teller result, Eq. (10.15), arbitrary coherence leads to two simple changes. The exponential decay $\exp(-\kappa(1 - \exp(-\theta))t)$ has become a decay whose time-dependence is determined by $\eta(t)$ and the convolution of $1 - \eta(t)$ with $\xi(t)$ has replaced the exponentially saturating factor.

In Fig. (10.1), left panel, the evolution of the average energy is displayed for the illustrative case of a Lorentzian bath spectral function, $Y(z)$ (see Chapter 9 for details). Three values of the spectral width (which defines the symmetric portion

$Y_s(z)$ of the spectral function) are chosen, $w = 1/2$, 1, 2; the equivalent Bethe-Teller result is shown as well, being labeled by the symbol o. We normalize $E(t)$ with its initial value, $E(0)$. An increase in the spectral width, equivalent to an increase in the coherence time, results in both larger and more persistent oscillations. At long times, however, the Bethe-Teller result is approached. This occurs because the factor $\xi(t \to \infty)$ approaches 1 and $\eta(t)$ becomes the standard exponential damping, i.e., $\exp(-\kappa(1 - \exp -\theta))$. For reference, the right panel of Fig. (10.1) displays the respective $\phi_\Delta(t)$. The effect in the variation of the strength of the oscillations present in $\phi_\Delta(t)$ is highlighted by the three arrows identified by A, B, and C.

10.1.4 Lack of Canonical Invariance of the GME

A general solution for the generating function of the GME, whose evolution equation is given in Eq. (10.8), is intractable. The Laplace-domain equation for the generating function of the GME, however, is essentially that of the Montroll-Shuler equation, the latter being given by

$$(z - 1) \left[\frac{\partial}{\partial z} \left[z \widetilde{\phi}_+(0) \widetilde{G}(z, \epsilon) \right] - \frac{\partial}{\partial z} \widetilde{\phi}_-(0) \widetilde{G}(z, \epsilon) \right] = \frac{\epsilon}{\kappa} \widetilde{G}(z, \epsilon) - \frac{1}{\kappa} G_0(z),$$

except with $\widetilde{\phi}_\pm(0)$ being replaced by $\widetilde{\phi}_\pm(\epsilon)$. Here, we have highlighted the connection by replacing at the appropriate places 1 and $e^{-\theta}$ with the respective time integrals $\widetilde{\phi}_\mp(\epsilon = 0)$. If the above equation is solved in an indirect manner, e.g., a Laplace transform of the solution Eq. (10.6) for a particular $G_0(z)$, then Eq. (10.5) is also solved for that particular initial condition. The factors of $\widetilde{\phi}_\pm(0)$ in the solution simply need be replaced by $\widetilde{\phi}_\pm(\epsilon)$.

As we show below, the case for an initial distribution being taken to have Boltzmann weights among the states in a manner corresponding to the "initial" temperature T_0 can be solved in this manner. Explicitly, the initial value of the generating

function is given by

$$G_0(z) = \frac{1 - e^{-\theta_0}}{1 - ze^{-\theta_0}}.$$

where $\theta_0 = \Omega/k_B T_0$. Upon the replacement of the argument of G_0 with $\zeta(z)$, and subsequent expansion of Eq. (10.6), the solution to the generating function of the Montroll-Shuler equation simplifies into

$$G(z,t) = \left[\frac{\widetilde{\phi}_+(0) - \widetilde{\phi}_-(0)}{z\widetilde{\phi}_+(0) - \widetilde{\phi}_-(0)} \right] \left[\frac{1}{1 - \frac{(z-1)(\widetilde{\phi}_+(0) - e^{-\theta_0}\widetilde{\phi}_-(0))}{(z\widetilde{\phi}_+(0) - \widetilde{\phi}_-(0))(1 - e^{-\theta_0})} e^{-\tau}} \right], \qquad (10.19)$$

Notice that the right-hand side of Eq. (10.19) is of the form $C/(1 - Ae^{-Bt})$, where A, B, and C are all constants. As such, the Laplace transform is trivially written by expanding the fraction in a power series. The Laplace transform of the solution is

$$\widetilde{G}(z, \epsilon) = \left[\frac{\widetilde{\phi}_+(0) - \widetilde{\phi}_-(0)}{z\widetilde{\phi}_+(0) - \widetilde{\phi}_-(0)} \right] \sum_k \frac{\frac{1}{\kappa}}{\frac{\epsilon}{\kappa} + k(\widetilde{\phi}_-(0) - \widetilde{\phi}_+(0))} \qquad (10.20)$$

$$\times \left[\frac{(z-1)(\widetilde{\phi}_+(0) - e^{-\theta_0}\widetilde{\phi}_-(0))}{(z\widetilde{\phi}_+(0) - \widetilde{\phi}_-(0))(1 - e^{-\theta_0})} \right]^k,$$

where the k-summation is over integers from 0 to ∞. Eq. (10.20) is the solution to the first-order differential equation w.r.t z for the generating function given above. As the solution does not depend on the argument of $\widetilde{\phi}_\pm$, we replace the 0 present in Eq. (10.20) with an ϵ. The result is

$$\widetilde{G}(z, \epsilon) = \left[\frac{\widetilde{\phi}_+(\epsilon) - \widetilde{\phi}_-(\epsilon)}{z\widetilde{\phi}_+(\epsilon) - \widetilde{\phi}_-(\epsilon)} \right] \sum_k \frac{\frac{1}{\kappa}}{\frac{\epsilon}{\kappa} + k(\widetilde{\phi}_-(\epsilon) - \widetilde{\phi}_+(\epsilon))} \qquad (10.21)$$

$$\times \left[\frac{(z - 1)(\widetilde{\phi}_+(\epsilon) - e^{-\theta_0}\widetilde{\phi}_-(\epsilon))}{(z\widetilde{\phi}_+(\epsilon) - \widetilde{\phi}_-(\epsilon))(1 - e^{-\theta_0}))} \right]^k,$$

To ensure that Eq. 10.21 is the solution to the generating function of the GME one need substitute it into Laplace-domain expression equivalent to the evolution equation given in Eq. (10.5). We have carried that out and shown that Eq. 10.21 is indeed valid.

For canonical invariance to hold, the time-domain expression of the generating function must be of the form

$$G(z,t) = \frac{1 - e^{-\Theta(t)}}{1 - ze^{-\Theta(t)}}.$$

where $\Theta(t)$ is strictly proportional to the temperature. Unfortunately, Eq. (10.21) can not be analytically transformed for an arbitrary memory. The presence of multiple factors does suggest, however, that the time-domain solution will have multiple convolutions. Thus, no $\theta(t)$ exists.

10.2   Stark Ladder: Coherence Effects

The system that underlies vibrational relaxation, the harmonic oscillator, can be considered a natural extension of the non-degenerate dimer [169] briefly discussed in Section 9.2. Compared to that of the dimer, the richness of the former's behavior stems from two sources. The system state-space is extended from two states to a semi-infinite number, i.e., $M = 0, 1, ..., \infty$ instead of simply 1 and 2, and the transitions depend on the index M, a result of the linearity with regards to the oscillator coordinate of the interaction between the system and the bath. Upon reflection, a second natural extension of the dimer suggests itself: a charged particle moving in a discrete crystal under the action of an electric field. Here, the state-space is infinite, i.e., $M = -\infty, ..., \infty$, but the transitions remain independent of the index. Known as the Stark ladder system, its GME can be solved explicitly and interesting conclusions about evolution at short times drawn. Its energy spectrum lacks a lower bound; however, so at long times the system does not approach thermal equilibrium. Our focus here is on the behavior at short times; we briefly mention in Section 10.3 an effect observed at long times that remains not fully understood.

Consider then a charged particle that moves under the influence of a strong

electric field on a 1-dimensional crystal lattice of intersite spacing a. We denote by Γ the product of the charge, the spacing and the strength of the electric field and label the sites by M. Taking the system to be of a simplified one-band form and the bath interaction to couple only nearest-neighbor sites, the eigenstates are well-known [177, 178] to be localized at the sites of the crystal. The eigenvalues correspond exactly with the site energies; the spectrum is, therefore, equally spaced as in both the non-degenerate dimer and the harmonic oscillator. Though simpler than the latter due to the lack of a dependence on M in its transition rates, the Stark ladder system still displays complex behavior because the state-space is infinite.

Using the formalism developed in refs. [165, 167, 168], the evolution equation for $P_M(t)$, the probability of occupation of the Mth site, is given by

$$\frac{1}{\kappa}\frac{d}{dt}P_M(t) = \int_0^t dt\,\phi_\Delta(t-t')[P_{M-1}(t') - P_{M+1}(t')] \tag{10.22}$$

$$+ \int_0^t dt\,\phi_S(t-t')[P_{M+1}(t') + P_{M-1}(t') - 2P_M(t')].$$

Here, we have used the sum and difference memories, $\phi_S(t)$ and $\phi_\Delta(t)$ respectively, that are defined in Eqs. (9.7). Upon first glance one may assume that Eq. (10.22) is merely the discrete version of a generalized advective-diffusion equation, i.e., an equation of the form

$$\frac{\partial}{\partial t}P(x,t) + \gamma\int_0^t dt'\,\phi_A(t-t')\frac{\partial}{\partial x}P(x,t') = D\int_0^t dt.\,\phi_D(t-t')\frac{\partial^2}{\partial x^2}P(x,t'), \quad (10.23)$$

where γ and D are constants and $\phi_A(t)$ and $\phi_D(t)$ are, respectively, the advective and diffusive memories. An attempt to take the continuum approximation ($a \to 0$, $P_M(t)/a \to P(x,t)$) of Eq. 10.22, however, immediately runs into a contradiction. The bracketed term in the upper line of Eq. (10.22) would be proportional to a,

$$[P_{M-1}(t') - P_{M+1}(t')] \to a\frac{\partial}{\partial x}P(x,t'),$$

while the bracketed term in the lower line would be proportional to a^2,

$$[P_{M+1}(t') + P_{M+1}(t') - 2P_M(t')] \rightarrow a^2 \frac{\partial^2}{\partial x^2} P(x, t'),$$

but neither $\phi_\Delta(t)$ nor $\phi_S(t)$ produces[1] a factor of a. The continuum approximation of Eq. (10.22) would therefore require both κa and κa^2 to be finite. Clearly, κ can not be taken to infinity in a manner that respects both, i.e., proportional to both a and a^2. Despite the seemingly obvious relation between Eq. (10.22) and Eq. (10.23) no procedure connects the two. We note that the Markoffian approximation of Eq. (10.22), however, *is* the discrete version of the advective-diffusion equation. The required extra factor of a appears in the transition rate, $1 - \exp(-\beta\Gamma)$, that results from the approximation of $\phi_\Delta(t)$. That is $1 - \exp(-\beta\Gamma) \rightarrow a\beta\Gamma$ where $\Gamma = \Gamma/a$ is finite.

The discrete equation, Eq. (10.22), can be solved using standard Fourier transform procedures. The propagator for an initial localized charge, i.e., $P_M(0) = \delta_{M,0}$ may be written in the Laplace-domain as

$$\widetilde{P}_M(\epsilon) = \frac{\frac{1}{\kappa}}{\left[\widetilde{\phi}_S \pm \widetilde{\phi}_\Delta\right]^{|M|}} \frac{\left[(\frac{\epsilon}{\kappa} + \widetilde{\phi}_S + \sqrt{\widetilde{\phi}_S^2 - \widetilde{\phi}_\Delta^2})^{\frac{1}{2}} - (\frac{\epsilon}{\kappa} + \widetilde{\phi}_S - \sqrt{\widetilde{\phi}_S^2 - \widetilde{\phi}_\Delta^2})^{\frac{1}{2}}\right]^{|M|}}{\left[(\frac{\epsilon}{\kappa} + \widetilde{\phi}_S)^2 + \widetilde{\phi}_\Delta^2 - \widetilde{\phi}_S^2\right]^{\frac{1}{2}}}, \quad (10.24)$$

where we have suppressed the arguments of the memories. The $\pm$ in the first term is understood to be $+$ for positive M and $-$ for negative M.

The moments of the distribution can be calculated either directly from Eq. (10.24) or from Eq. (10.22). The expression for an arbitrary moment $\langle M^n \rangle$ is

$$\widetilde{\langle M^n \rangle} = \sum_{\substack{p=0 \\ n-p \, \text{even}}}^{n-1} \binom{n-1}{p} \widetilde{\phi}_S(\epsilon) \frac{\kappa \widetilde{\langle M^p \rangle}}{\epsilon} + \sum_{\substack{p=0 \\ n-p \, \text{odd}}}^{n-1} \binom{n-1}{p} \widetilde{\phi}_\Delta(\epsilon) \frac{\kappa \widetilde{\langle M^p \rangle}}{\epsilon}. \quad (10.25)$$

---

[1] The reader may comment that the memories, being dependent on Γ (which is also taken to zero in the continuum limit), should themselves be affected by the approximation. However, both $\phi_S(t)$ and $\phi_\Delta(t)$ depend on Γ only through the argument of a cosine ($\cos(\Gamma t)$) and sine ($\sin(\Gamma t)$), respectively. As Γ multiplies the time t in both, no new parameter can be defined. One finds a similar issue when considering the fully coherent Stark ladder system, the propagator of which is $J_M^2(4V/\Gamma \sin(\Gamma t/2))$. In the continuum limit, either the effect of the electric field is removed or time must be inappropriately redefined.

The expressions for the particular cases of the first and second moments are given by

$$\widetilde{\langle M \rangle}(\epsilon) = \frac{\kappa \widetilde{\phi}_\Delta(\epsilon)}{\epsilon^2}, \quad (10.26a) \qquad \widetilde{\langle M^2 \rangle}(\epsilon) = \frac{\kappa \widetilde{\phi}_S(\epsilon)}{\epsilon^2} + 2\frac{\kappa^2 \widetilde{\phi}_\Delta(\epsilon)^2}{\epsilon^3}. \quad (10.26b)$$

Both the average displacement, Eq. (10.26a), and the average squared displacement, Eq. (10.26b), reduce to their respective values when either the coherent or incoherent limit is taken. By explicitly expanding $\widetilde{\phi}_S(\epsilon)$ and $\widetilde{\phi}_\Delta(\epsilon)$ in terms of their integral representations, given in Eqs. (9.7), one can formally invert Eqs. (10.26). Their time-domain expressions are

$$\langle M \rangle = \int_{-\infty}^{\infty} dz\, Y(z) \left(1 - e^{-\beta z}\right) t^2 \left[\text{sinc}^2\, \frac{(z - \Gamma)t}{2} \right], \qquad (10.27a)$$

$$\langle \Delta M^2 \rangle = \int_{-\infty}^{\infty} dz\, Y(z) \int_{-\infty}^{\infty} dz'\, Y(z')\, (F_2(z, z', t) - F_1(z, t) F_1(z', t)) \qquad (10.27b)$$

$$+ \int_{-\infty}^{\infty} dz\, Y(z)(1 + e^{-\beta z})\, t^2 \, \text{sinc}^2\, \frac{(z - \Gamma)t}{2},$$

where we have defined

$$F_1(z, t) = \left(1 - e^{-\beta z}\right) \left(\frac{t^2}{2}\right) \text{sinc}^2\, \frac{(z - \Gamma)t}{2},$$

$$F_2(z, z', t) = \left(1 - e^{-\beta z}\right) \left(1 - e^{-\beta z'}\right) t^2 \left(\frac{\text{sinc}^2\, \frac{(z-\Gamma)t}{2} - \text{sinc}^2\, \frac{(z-\Gamma)t}{2}}{(z' - z)(z' + z - 2\Gamma)} \right),$$

and used the symmetrical bath spectral function introduced in Eq. (8.5) and discussed in Section 9.2.

A more physically important quantity than $\langle M \rangle$, Eq. (10.27a), is the average velocity of the charge $\langle v \rangle$, i.e., its derivative $\equiv d\langle M \rangle / dt$. In Fig. 10.2, main frame, we display $\langle v \rangle$ for the illustrative case of a Lorentzian spectral function, whose expression is given in Eq. (9.18), against the dimensionless time κt. We have used the parameters
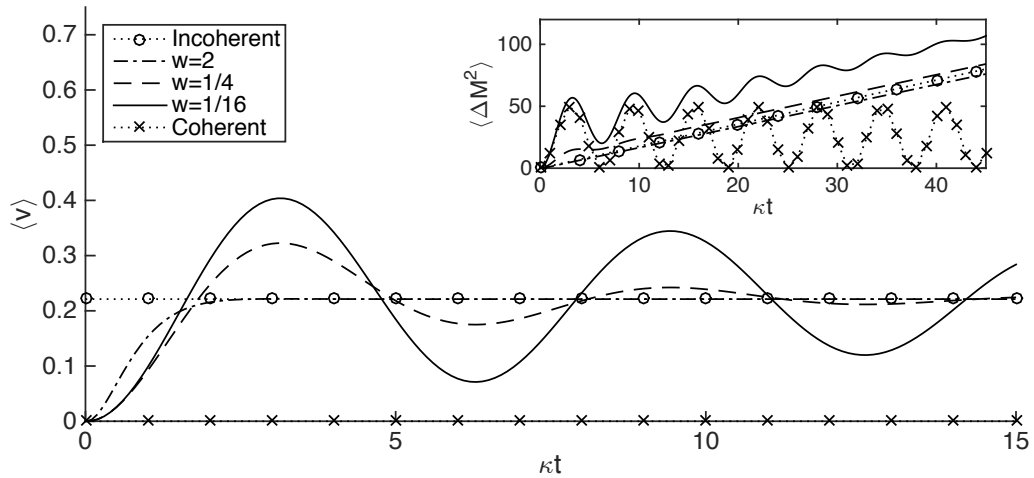
Figure 10.2: Depicted is the average velocity of the charge $\langle v \rangle$ (given by the derivative of Eq. (10.26a) w.r.t. time), main figure, and the average-squared displacement (given in Eq. (10.26b)), inset, for the dimensionless frequencies $\Gamma = 1$, $\beta = 1/4$ and three values of the spectral width $w = 1/4$, 1, 4 as well as the coherent and incoherent limits. In the case of arbitrary coherence, the charge initially remains at rest before a delayed acceleration. This contrast with its counterpart in the incoherent limit which instantaneously achieves its steady-state value $\kappa(1 - \exp(-\beta\Gamma))$. The average velocity approaches its value in the incoherent limit at long times. The effect of arbitrary coherence is similar for the average squared displacement (inset) as well: at short times the extent of the charge oscillates as in the coherent case while at long times it is purely diffusive a la the incoherent case.

$\Gamma = 1$ and $\beta = 1/4$ and have displayed three values of the spectral width $w = 1/16$, 1/4, 2 along with the relevant incoherent and coherent limits. At times short compared to κ, arbitrary coherence results in the charge behaving similar to that of its coherent counterpart; it remains essentially localized at its initial location (here, $M = 0$). This contrasts with the immediate delocalization of the charge that is evident in the incoherent limit of the system. At times large compared with κ, however, the effects of coherence are destroyed and the velocity of the charge is identical to that of its incoherent counterpart (whereas the charge remains localized for all times in the coherent limit of the system). For intermediate times, the average velocity oscillates around the incoherent steady state value, the amplitude and persistence of

these oscillations increasing as the value of the spectral width is made larger, i.e., as the coherence of system is increased.

The inset of Fig. 10.2 depicts the average squared displacement of the charge, Eq. (10.27b), for the same Lorentzian spectral function. The parameters used are as in the main figure. Similar to that of the average velocity, at times short compared with κ, arbitrary coherence results in the charge behaving similarly to its coherent[2] counterpart. In a replication of the oscillations seen in that limit, the charge displays 'breathing' dynamics in which its extent not only oscillates but actually decreases. As expected, the length of time for which the 'breathing' is observed decreases as the spectral width is decreased, i.e., as the system becomes less coherent. At times large compared with κ, the average-squared displacement displays the diffusive behavior standard to the incoherent case.

10.3   Conclusion

The derivation [42,44,47,159–163] of the GMEs briefly outlined in Chapter 8 assumed a maximally incoherent initial condition, i.e., only the diagonal elements of the initial density matrix are non-zero. The forcing term that accounts for the effect of non-zero off-diagonal matrix elements has been neglected. Though this assumption of diagonal initial conditions is common in investigations that use the GME (see ref. [166] for an exception), complete understanding of the system-bath interaction necessitates its investigation. The results presented in this Chapter can be used as a stepping stone to the more general case. The microscopic specification of baths is another issue neglected in this analysis. Such calculations would be useful in the understanding of particular experimental results especially in the context of vibrational relaxation.

---

[2]An ambiguity in the time scale for the coherent limit exists due to the appropriate limiting procedure ($w \to 0$, $\kappa \to 0$, $\kappa/w \to 1$). We chose a coherent time-scale that highlights the similarities between the general case, Eq. (10.27b), and its coherent limit.
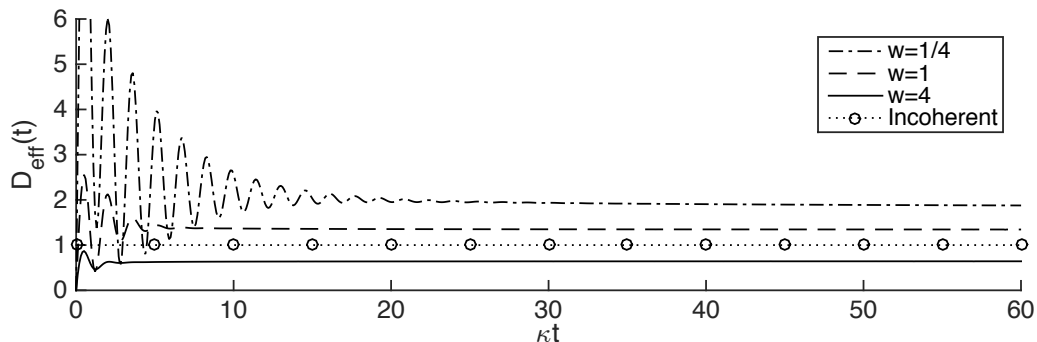
Figure 10.3: Displays effective diffusion constant, $D_{eff}(t)$ (see text for description) versus the dimensionless time κt for the Lorentzian spectral function. Three values of the spectral width are shown $w = 1/4$, 1, 4 along with the incoherent limit. The diffusion constant, i.e., the steady-state value of $D_{eff}(t)$, is seen to vary with the spectral width. Thus, properties of the bath effect steady-state quantities. Other characteristic frequencies ($\Gamma = 4$, $\beta = 2$) have been chosen to highlight the effect

Two extensions that are particular to vibrational relaxation would be of further value in such an analysis. An expansion of the interaction between the system and the bath to third-order in the oscillator coordinate leads to an effective long distance interaction. Though such an interaction remains weak, as both standard in the GME formalism and desirable in the present context, a non-local interaction could generate interesting dynamics. Of secondary interest is an extension of these results to an anharmonic oscillator, e.g., the Morse oscillator [179, 180]. An operator structure is retained in such a system but the effect of disassociation would be observed.

We briefly remark on an interesting observation in the Stark ladder system. Depicted in Fig. 10.3 is the effective diffusion constant, i.e., $D_{eff} = \langle \Delta M^2 \rangle / t$, for the Lorentzian spectral function. Three values of the spectral width are shown $w = 1/4$, 1, 4 along with the result in the incoherent limit (the other characteristic frequencies ($\Gamma = 4$, $\beta = 2$) are chosen to highlight the following effect). As is evident from the figure, the steady-state value of $D_{eff}(t)$ is different for various spectral widths; it must depend, therefore, explicitly on the properties of the bath.

An understanding of this effect is complicated by the dependence of the memories on a single bath spectral function. We instead consider the generalized advective-diffusion equation, Eq. (10.23), with arbitrary memories $\phi_A(t)$ and $\phi_D(t)$. The average displacement and the average squared displacement are essentially equivalent to those of the Stark ladder system, being given by:

$$\widetilde{\langle x \rangle}(\epsilon) = \frac{\kappa \widetilde{\phi}_A}{\epsilon^2}, \qquad\qquad \widetilde{\langle x^2 \rangle}(\epsilon) = \frac{\kappa \widetilde{\phi}_D(\epsilon)}{\epsilon^2} + 2\frac{\kappa^2 \widetilde{\phi}_A(\epsilon)^2}{\epsilon^3}.$$

Explicit calculations can then be performed by assuming a simple functional form of the memories. We take the advective memory to be exponential, i.e., $\phi_A(t) = \varpi \exp(-\varpi t)$ with damping parameter ϖ, and the diffusive memory to be a δ-function, i.e., $\phi_D(t) = \delta(t)$; we have then

$$\langle x \rangle = \gamma t - \gamma \frac{1 - e^{-\varpi t}}{\varpi}, \tag{10.29a}$$

$$\langle \Delta x^2 \rangle = -2\gamma^2 \frac{t}{\varpi} + \gamma^2 \left(\frac{5 - 4e^{-\varpi t} - e^{-2\varpi t}}{\varpi^2} \right) - 4\gamma^2 \frac{t e^{-\varpi t}}{\varpi} + 2Dt. \tag{10.29b}$$

In Eq (10.29b) we have introduced the mean square displacement $\langle \Delta x^2 \rangle = \langle x^2 \rangle - \langle x \rangle^2$. At long times, the quantities of interest are then the average velocity, which is simply γ, and the diffusion constant. The latter is defined in the standard manner

$$\mathcal{D} = \lim_{t \to \infty} \frac{\langle \Delta x^2 \rangle(t)}{2t} = D - \frac{\gamma^2}{\varpi}. \tag{10.30}$$

The diffusion constant is dependent on the parameters of the bath. The physicality of this observation remains an open question.

Investigations reported in this Chapter 10 are being submitted for publication as an article, V. M. Kenkre and M. Chase, "Approach to Equilibrium of a Quantum System and Generalization of the Montroll-Shuler Equation for Vibrational Relaxation of a Molecular Oscillator" to *Journal of Chemical Physics.*

Appendices

Appendix A

Some Subtleties in Reaction Diffusion Theory

We present in this Appendix a completely unrelated problem that is, however, broadly relevant to the other contents of the thesis. We examine a subtle, yet important, dimensional effect in the context of reaction-diffusion theory [28, 106, 108, 111, 181, 182]. Applicable in contexts as diverse as exciton trapping in molecular systems [183–188] and the coalescence of receptor clusters on cellular surfaces [85, 86, 113], reaction-diffusion theory allows one to model the motion of an object when its movement may be restricted by an external process such as capture or a chemical reaction. Of interest are situations for which one may wish to treat the so-called trapping region, in which the latter processes (the "reaction" part of the reaction-diffusion) occur, to be of a smaller dimension than the over-all motion space.

Appendix A. Some Subtleties in Reaction Diffusion Theory

A.1 Reaction-Diffusion Theory: the ν-Function

The focus here being on a particular technical problem, we only briefly outline the necessary background to reaction-diffusion theory [28,106,108,111,181,182]. We refer the reader to a recent review [111] for a complete discussion on the theory and its numerous applications. Applicable to classical systems that can be described with a continuous spatial coordinate, our starting point is given by

$$\frac{\partial}{\partial t} P(\vec{x}^m, t) = [\text{Motion Terms}] - C \int' d\vec{y}^r \delta^m(\vec{x}^m - \vec{y}^m) P(\vec{x}^m, t). \qquad (\text{A.1})$$

The particle, whose location is identified by the probability distribution $P(\vec{x}^m, t)$, moves in an m-dimensional space which contains a reaction region. Here, C is the capture rate (with units that depend on the trap dimension), $\delta^m(...)$ is the m-dimensional δ-function, the prime indicates that the integration is over the reaction region, and we leave the (homogenous) motion terms as general with $\Pi(\vec{x}^m, \vec{y}^m, t)$ being the resultant (homogenous) propagator.

While the 'reaction' in reaction region can refer to a process of essentially arbitrary nature, e.g., infection, annihilation, chemical synthesis, etc., we refer to it throughout this Section as the trapping region, or trap, for simplicity.

Using standard techniques [28, 110, 111, 181, 182], one can calculate quantities such as the survival probability of the particle using Eq. (A.1). Of particular interest to applications of reaction-diffusion theory, the Laplace-domain expression (tildes denote Laplace-transformed functions and ϵ is the Laplace variable) for the survival probability is

$$\widetilde{Q}(\epsilon) \equiv \int_{-\infty}^{\infty} dx^m \widetilde{P}(\vec{x}^m, \epsilon) = \frac{1}{\epsilon} \left[1 - \frac{\widetilde{\mu}(\epsilon)}{1/C + \widetilde{\nu}(\epsilon)} \right]. \qquad (\text{A.2})$$

In Eq. (A.2) we have introduced two important functions in the theory of reaction-diffusion: the μ-function and the ν-function. Their expression in the time-domain

are

$$\mu(t) = \int{}' d\vec{x}^m \int\limits_{-\infty}^{\infty} d\vec{x}_0^m \, P_0(\vec{x}_0^m)\Pi(\vec{x}^m, \vec{x}_0^m, t), \tag{A.3a}$$

$$\nu(t) = \frac{\int{}' d\vec{y}^m \int{}' d\vec{x}^m \, \Pi(\vec{x}^m, \vec{y}^m, t)}{\int{}' d\vec{y}^m}, \tag{A.3b}$$

As evident from the presence of the homogenous propagator in Eqs. (A.3), both are dependent on the trapping region only through its extent. The first, Eq. (A.3a), is the probability density that the particle has travelled from its initial condition, given by $P_0(\vec{x}_0^m)$, to the trapping region. Generally speaking, it is well-behaved. The latter quantity, Eq. (A.3b), was defined by Kenkre and collaborators [76, 109, 128]. It is constructed from the probability density that a particle initialized in the trapping region at the point $\vec{x}_0^m$ returns to the trapping region at time t. This probability density is then averaged over all points $\vec{x}_0^m$. Highly-symmetric trapping regions do not require this averaging. In these cases, the ν-function is exactly the probability density that a particle initialized in the trapping region returns at the time t. Even in the general case one can informally interpreted it as essentially the probability (density) of return.

A.2 A Point-Like Trap with Diffusion

We proceed with by illustrating the dimensionality issue through a specialization of Eq. (A.1) to the case of diffusive motion. While simple, pure diffusion highlights the dimensionality effect without any additional complexity that can be present in purely homogenous motion. The particular form of Eq. (A.1) that governs this situation is

$$\frac{\partial}{\partial t} P(\vec{x}^m, t) = D \frac{\partial^2}{\partial x^2} P(\vec{x}^m, t) - C \int{}' d\vec{y}^m \delta^m(\vec{x}^m - \vec{y}^m) P(\vec{x}^m, t), \tag{A.4}$$

with D being the standard diffusion constant. The (homogenous) propagator is then given by the well-known expression

$$\Pi(\vec{x}^m, \vec{x}_0^m, t) = \left(\frac{1}{4\pi Dt}\right)^{\frac{m}{2}} e^{-\frac{(\vec{x}^m - \vec{x}_0^m)^2}{4Dt}}, \tag{A.5}$$

which is exactly equal to the tensor product of m standard one-dimensional propagators. When the trapping region is taken to be a single point, located at $\vec{x}_0^m$, the ν-function is found by simply equating $\vec{x}^m$ to $\vec{x}_0^m$ in Eq. (A.5). Its time-domain expression is then

$$\nu(t) = \left(\frac{1}{4\pi Dt}\right)^{\frac{m}{2}}. \tag{A.6}$$

From Eq. (A.2), the calculation of the survival probability requires that Eq. (A.6) be Laplace-transformed. However, the Laplace transform exists only for $m < 2$. When the trapping region is taken to be a single point, the survival probability can only be calculated for a one-dimensional motion space. A point-trap in two dimensions leads to a divergence in the Laplace transform that stems from the short-time behavior of Eq. (A.6). In the next subsection, we extend these results to simple extended traps in motion spaces of low dimension.

A.3   The ν-Function for Simple Extended Traps

We catalogue here time-domain ν-functions for various simple extended traps in low-dimensional motion spaces. This serves to both provide sample calculations for further use and to illustrate that the existence of the Laplace-transformed expressions depends on its short-time behavior. We provide here both the short-time and long-time dependence of the ν-functions along with the complete expression.

We consider one- and two-dimensional motion spaces. In the former, we take trapping regions to be a single point, two points (separated a distance $2d$), and a finite line (of length l). In the latter, the trapping regions are taken to be an infinite line, a

m	Trap Style	ν-function	Short-Time	Long-Time	LT
1	Point	$\frac{1}{\sqrt{4\pi Dt}}$	$\frac{1}{\sqrt{t}}$	$\frac{1}{\sqrt{t}}$	✓
1	Two Points	$\frac{1}{\sqrt{4\pi Dt}}\left(1+e^{-\frac{a^2}{4Dt}}\right)$	$\frac{1}{\sqrt{t}}$	$\frac{1}{\sqrt{t}}$	✓
1	Finite Segment	$\mathrm{erf}\frac{l}{\sqrt{Dt}}-\frac{1}{l}\sqrt{\frac{4Dt}{\pi}}e^{-\frac{l^2}{2Dt}}\sinh\frac{l^2}{2Dt}$	1	$\frac{1}{\sqrt{t}}$	✓
2	Point	$\frac{1}{4\pi Dt}$	$\frac{1}{t}$	$\frac{1}{t}$	
2	Two Points	$\frac{1}{4\pi Dt}\left(1+e^{-\frac{a^2}{4Dt}}\right)$	$\frac{1}{t}$	$\frac{1}{t}$	
2	Line Segment	$\frac{1}{\sqrt{4\pi Dt}}\mathrm{erf}\frac{l}{\sqrt{Dt}}-\frac{1}{l\pi}e^{-\frac{l^2}{2Dt}}\sinh\frac{l^2}{2Dt}$	$\frac{1}{\sqrt{t}}$	$\frac{1}{t}$	✓
2	Infinite Line	$\frac{1}{\sqrt{8\pi Dt}}$	$\frac{1}{\sqrt{t}}$	$\frac{1}{\sqrt{t}}$	✓
2	Ring	$\frac{1}{4\pi Dt}e^{-\frac{r^2}{2Dt}}\mathrm{I}_0\left(\frac{r^2}{2Dt}\right)$	$\frac{1}{\sqrt{t}}$	$\frac{1}{t}$	✓
2	Spot	$\frac{\int_0^\rho d\rho'\,\rho'\int_0^\rho d\rho''\,\rho''e^{-\frac{\rho'^2+\rho''^2}{4Dt}}\mathrm{I}_0\left(\frac{\rho'\rho''}{2Dt}\right)}{a^2Dt}$	1	$\frac{\rho^2}{8Dt}$	✓

Table A.1: The ν-function for various simple traps in a one- and two-dimensional motion space are presented . Included are the short- and long-time behavior. A checkmark indicates that the Laplace transform (LT) exists.

ring (of radius r), and a spot (of radius ρ) in addition to the all three identified above. The results are in Table A.1. The left-most column identifies the dimensionality of the motion space, the next column displays an image of the trapping region, the left-center column gives the full ν-function calculated using Eq., the center column gives the short-time behavior, the center-right column gives the long-time behavior, and the right column indicates if the ν-function is Laplace-transformable.

For a motion space of one dimension, the ν-function can be Laplace-transformed for both point-like and finite traps. These results are recorded in the first three entries of Table A.1. The Laplace transform exists for two-dimensional motion spaces, however, only when the trap is of finite extent, e.g., a line or a spot. The finite

traps in two-dimensional motion spaces comprise the last four entries of Table A.1. Point-like traps in a two-dimensional motion space, the fourth and fifth entries in Table A.1, do *not* lead to ν-functions that possess Laplace-transformed expressions. This non-existence of the Laplace-domain expression occurs because of the short-time behavior of the ν-function; both expressions go as $1/t$ as $t \to 0$. This dependence results in the logarithmic divergence of the integral. While the factor of $\exp(-\epsilon t)$ in the transform damps long-time algebraic dependences; it provides no corresponding damping at short times. The logarithmic divergence from the short-time dependence therefore dominates the integral.

A pattern emerges from the results of Table A.1. When the trapping regions is either of equal dimension to the motion space or one dimension smaller, the Laplace transform exists. If, however, the trapping region is two dimensions smaller the Laplace transform does not. In practice, therefore, one can ensure appropriate behavior from the ν-function by taking the trapping region to be of equal dimension to the motion space. Though some complications arise in calculations due to the presence of m-integrations, having a trapping region and a motion space of the same dimensional tends to be more physically appropriate because most physical objects are space-filling. However, one may remain interested in the criteria that determines the existence of the Laplace-transform of the ν-function for arbitrary trapping region. In the next subsection, we derive this criteria for an interesting subset of allowable traps.

A.4   One-Less-Dimension for Separable Traps

The existence criteria for the Laplace transformed ν-function for an arbitrary trapping region is beyond the scope of the present discussion. However, by considering an intuitive description of trap as being points, lines, volumes, etc., one is motivated

to study the subset of trapping regions that match these descriptions. We focus then on trapping regions that can be exactly decomposed into a Cartesian coordinate system. While not as general as the intuitive descriptors given above, these special cases capture the essential idea. These traps are constructed such that their extent in all of the m-dimensions of the motion space are independent of their extent in any of the other $m - 1$-dimensions. Thus, they can be built dimension-by-dimension from the single dimension traps that we consider in Table A.1 (the first three entries). Their trapping regions can then be naturally decomposed into two distinct subspaces. In the first, a p-dimensional subspace, the trap is point-likely, i.e., the trapping region is a set of isolated points. In the second, a q-dimensional subspace, the trap is a q-dimensional hyperrectangle, i.e., the trapping region is of the same dimensionality as the subspace. Clearly, we have $m = p + q$. Though these traps represent an extremely special subset of allowable trapping regions, they provide a useful starting point to develop intuitive reasoning that can be applied to more general examples.

We take the Cartesian basis that respects this decomposition to be given by the components of the vector $\vec{x}^m$ that originally appeared in Eq. (A.1). Then the integral in Eq. (A.1) over the trapping region can itself be simply decomposed into the localized and delocalized subspaces of p and q dimensions. The integral is rewritten as

$$\int' d\vec{y}^m \rightarrow \int_{AS} d\vec{x}^m \sum_{\vec{y}^p}' \underbrace{\int \cdots \int}_{q}' d\vec{y}^q \delta^p(\vec{x}^p - \vec{y}^p)\delta^q(\vec{x}^q - \vec{y}^q). \qquad (A.7)$$

Here, the original integral over the trapping region is deconstructed into a *sum* over the localized subspace, with each trap location being identified with the points $\vec{y}^p$, and an *integration* over the delocalized subspace, identified by $\vec{y}^q$. Here, we explicitly divide the latter integration into individual integrals for each of the q dimensions to highlight the separability of the trap. Henceforth, these q integrations are collapsed into a single integral that we label with q. We also replace the prime on the sum

Appendix A. Some Subtleties in Reaction Diffusion Theory

with the label p so as to clearly indicate that it sums over the dimensions in the localized subspace. The final integral, labeled by AS, is over the full m-dimensional motion space. It, along with the δ-functions, smooths the above transition from an implied integration to a explicit sum.

We insert the integral representation for the trapping region, Eq. (A.7), into the definition of the ν-function given in Eq. (A.3b). We have then a general expression for the ν-function for a separable trap. It is given by

$$\nu(t) = \frac{\overset{p}{\underset{\vec{y}^p}{\sum}} \int^q d\vec{y}^q \, \overset{p}{\underset{\vec{x}^p}{\sum}} \int^q d\vec{x}^q \, \Pi(\vec{x}^m, \vec{y}^m, t)}{\overset{p}{\underset{\vec{y}^p}{\sum}} \int^q d\vec{y}^q}, \tag{A.8}$$

where the sums are over the isolated point-traps identified with $\vec{x}^p$. As evidenced by the results collected in Table A.1, focus should be on the short-time behavior as it determines the existence of the Laplace-domain expression for the ν-function. When $t = 0$, the propagator in Eq. (A.8) can be replaced exactly by a delta function of m-dimensions, its argument being $\vec{x}^m - \vec{y}^m$. The result is

$$\nu(t = 0) = \frac{\overset{p}{\underset{\vec{y}^p}{\sum}} \overset{p}{\underset{\vec{x}^p}{\sum}} \delta^p(\vec{x}^m - \vec{y}^p)}{\overset{p}{\underset{\vec{x}^p}{\sum}}}, \tag{A.9}$$

where the separability of the two subspaces is used to exactly cancel the double integration in the numerator with the single one that is present in the denominator. The value of $\nu(t = 0)$ is, as expected, infinite when p is a positive integer, which confirms the results found in Table A.1. By taking $t = 0$, however, we have obscured the exact short-time behavior and, therefore, the criteria for the existence of the Laplace-domain expression.

Without specifying the homogenous propagator no further progress can be made. Thus, we proceed as in Section A.2 with the illustrative example in which the motion

term is taken to describe pure diffusion. For simplicity, we take the trap in the localized subspace to be only a single point. This choice is motivated by the results in Table A.1 that suggest that the existence of the ν-function does not depend on the number of isolated points merely that there are only isolated points. Following the insertion of the diffusive propagator, Eq. (A.5), we have the time-domain expression for the ν-function as

$$\nu(t) = \frac{1}{Q}\left(\frac{1}{4\pi Dt}\right)^{\frac{p}{2}} \int^q d\vec{y}^q \int^q d\vec{x}^q \left(\frac{1}{4\pi Dt}\right)^{\frac{q}{2}} e^{-\frac{(\vec{x}^q - \vec{y}^q)^2}{4Dt}}, \qquad (A.10)$$

where $\int^q d\vec{x}^q = Q$ is the volume of the trapping region in its delocalized subspace. Eq. (A.10) simplifies by noting that the double integral of a Gaussian leads to a single integral of error functions. As $t \to 0$, these approach a constant and the remainder is simply

$$\nu(t \to 0) \propto t^{-\frac{p}{2}}. \qquad (A.11)$$

Confirming the results displayed in Table A.1, the Laplace transform of Eq. (A.11) only exists for integer values when $p = 0, 1$. Thus, only when the delocalized subspace is of equal dimension to the motion space or of one less dimension does the Laplace transform of the ν-function exist for the diffusive case.

A.5 Conclusion

We have discussed an issue with reaction-diffusion theory in dimensions higher than one. The ν-function, which is required to calculate quantities such as the survival probability, may not exist. This result has been shown explicitly for the particular case of homogenous motion described by pure diffusion; for an isolated point-trap, the Laplace-domain expression for the ν-function only exists when the motion space is one-dimensional. Higher dimension motion spaces result in Laplace integrals that diverge. Time-domain expressions for the ν-function for particularly simple low-

dimensional traps in one- and two-dimensional motion spaces are presented in Table A.1. A general trend emerges: divergences in the Laplace integral arise from the behavior of the ν-function at short times. This short-time behavior is essentially determined by the difference in the dimensionality of the motion space and that of the trapping region. The latter being at minimum only one dimension smaller than the former.

While the extension of this observation to general trapping regions is left unexplored, we analyze the one-dimension-less conjecture for an interesting subset of traps: those that can be decomposed into a localized subspace and a delocalized subspace. We motivate the specialization to these trapping regions by the intuitive description of traps as points, lines, etc. Again for the special case of of diffusive motion, we confirm that the localized trapping region can be no more than a single dimension. This result is only shown for diffusive motion. From Eq. (A.9), however, one may intuit a more general result: the short-time behavior of the ν-function depends on the dimensionality d_p of the localized trapping region such that each of these dimension can be treated as independent from the remainder. Thus, the short-time behavior of the ν-function goes as if the system were d_p copies of a simple point trap in a one-dimensional motion space. Intuition can also be developed for more complex trapping regions. For example, a line trap that is oriented not in a separable manner but in the shape of the letter M will result in a similar dependence of the ν-function at short times because both are lines.

The work reported in this Appendix is being prepared for publication by S. Sugaya, M. Chase, and V. M. Kenkre as an article "Comment on reaction-diffusion theory in dimensions higher than one", to be submitted to *Physical Review B*.

Appendix B

Derivation of Equations for the Joint Probability Distributions

We derive here the closed Fokker-Planck equations for the one- and two-time joint probability distributions.

Into the implicit equations, given in Eqs. (4.14a) and (4.14b), one inserts the time-convolutionless Langevin equation, Eq. (4.11). The resulting equations are

$$\frac{\partial}{\partial t} P_1(x,t) = -\frac{\partial}{\partial x}\langle[-A(t)x_i(t) + B(t) + \iota(t)]\,\delta\,(x_i(t) - x)\rangle, \tag{B.1a}$$

$$\frac{\partial}{\partial t} P_2(x,t;x',t') = -\frac{\partial}{\partial x}\langle[-A(t)x_i(t)+B(t)+\iota(t)]\,\delta\,(x_i(t)-x)\,\delta(x_i(t')-x')\rangle, \tag{B.1b}$$

where we have used the notation introduced in Eqs. (4.16), i.e., $A(t)$, $B(t)$, etc., and the noise $\iota(t)$. The first two terms on the left-hand-side can be trivially evaluated by noting that $\langle x_i(t)\delta(x_i(t) - x)\rangle = x\langle\delta(x_i(t) - x)\rangle$. Using the definition of the joint

Appendix B. Derivation of Equations for the Joint Probability Distributions

probability distributions, e.g., $P(x,t) = \langle \delta(x_i(t) - x) \rangle$, we have

$$\frac{\partial}{\partial t} P_1(x,t) = \frac{\partial}{\partial x} \left[A(t)x - B(t) \right] P_1(x,t) - \frac{\partial}{\partial x} \langle \iota(t) \delta\left(x_i(t) - x \right) \rangle, \tag{B.2a}$$

$$\frac{\partial}{\partial t} P_2(x,t;x',t') = \frac{\partial}{\partial x} \left[A(t)x - B(t) \right] P_2(x,t;x',t')$$

$$- \frac{\partial}{\partial x} \langle \iota(t) \delta\left(x_i(t) - x \right) \delta\left(x_i(t') - x' \right) \rangle. \tag{B.2b}$$

The noise terms can be evaluated using Novikov's theorem [7]. Using the notation in ref. [7], Novikov's theorem relates the weighted value of a functional $R[f]$, where $f(s)$ is a random Gaussian function with correlation $\langle f(s)f(s') \rangle = F(s,s')$, to the average of its functional derivative, i.e.,

$$\langle f(s) R[f] \rangle = \int_0^s ds' \, F(s,s') \left\langle \frac{\delta[R[f]]}{\delta f(s')} \right\rangle, \tag{B.3}$$

where $\delta[...]/\delta f(s)$ indicates a functional derivative.

From the noise term in Eq. (B.2a) we have:

$$\langle \iota_i(t) \delta\left(x_i(t) - x \right) \rangle = \int_0^t ds \, \langle \iota_i(t) \iota_i(s) \rangle \left\langle \frac{\delta[\delta(x_i(t) - x)]}{\delta \iota_i(s)} \right\rangle,$$

$$= \int_0^t ds \, \langle \iota_i(t) \iota_i(s) \rangle \left\langle \frac{\delta[x_i(t)]}{\delta \iota_i(s)} \frac{\delta[\delta(x_i(t) - x)]}{\delta x_i(t)} \right\rangle,$$

$$= - \int_0^t ds \, \langle \iota_i(t) \iota_i(s) \rangle \left\langle \frac{\delta[x_i(t)]}{\delta \iota_i(s)} \frac{\partial \delta(x_i(t) - x)}{\partial x} \right\rangle,$$

$$= - \frac{\partial}{\partial x} \int_0^t ds \, \langle \iota_i(t) \iota_i(s) \rangle \left\langle \frac{\delta[x_i(t)]}{\delta \iota_i(s)} \delta(x_i(t) - x) \right\rangle. \tag{B.4}$$

Between the second and the third lines the exchange property of the delta function, i.e., $\partial/\partial x[\delta(x - y)] = -\partial/\partial y[\delta(x - y)]$, has been used; between the third and the fourth lines the independence of $x_i(t)$ and x has been taken utilized.

Appendix B. Derivation of Equations for the Joint Probability Distributions

Lastly, we evaluate the functional derivative of $x_i(t)$ with respect to $\iota(s)$. It can be calculated directly from the solution, Eq. (4.8), by rewriting the latter in terms of $\iota(t)$. We have

$$x_i(t) = x_0 \lambda(t) + \lambda(t) \int_0^t ds \frac{\iota_i(s)}{\lambda(s)} + \Phi(t);$$

the functional derivative is then trivial, being given by

$$\frac{\delta[x_i(t)]}{\delta \iota_i(s)} = \frac{\lambda(t)}{\lambda(s)}. \tag{B.5}$$

With Eq. (B.5), along with correlation function, the noise term is then given by

$$\langle \iota_i(t) \delta \left(x_i(t) - x \right) \rangle = -\lambda(t)^2 \int_0^t ds \frac{d}{dt} \frac{d}{ds} \left[\int_0^s ds' \frac{\lambda(t-s')}{\lambda(t)} \frac{\lambda(s-s')}{\lambda(s')} \right] \frac{\partial}{\partial x} P_1(x,t). \tag{B.6}$$

Care must be taken to ensure that the differential operators only act on the correct functions. The result is

$$\langle \iota_i(t) \delta \left(x_i(t) - x \right) \rangle = -D\lambda(t)^2 \frac{d}{dt} \left[\int_0^t ds \, \lambda(s^2) \right] \frac{\partial}{\partial x} P_1(x,t), \tag{B.7}$$

Upon the insertion of Eq. (B.7) into Eq. (B.2a), the result is the closed Fokker-Planck equation for the one-time joint probability distribution given in Eq. (4.15a)

The process is quite similar for the two-time joint probability distribution but for

Appendix B. Derivation of Equations for the Joint Probability Distributions

the presence of a second term. The noise term in Eq. (B.2b) is simplified as

$$\langle \iota_i(t)\delta\left(x_i(t)-x\right)\delta\left(x_i(t')-x'\right)\rangle$$

$$= \int_0^t ds \langle \iota_i(t)\iota_i(s)\rangle \left\langle \frac{\delta[\delta(x_i(t)-x)]}{\delta\iota_i(s)}\delta\left(x_i(t')-x'\right)\right\rangle$$

$$+ \int_0^{t'} ds \langle \iota_i(t)\iota_i(s)\rangle \left\langle \delta\left(x_i(t)-x\right)\frac{\delta[\delta(x_i(t')-x')]}{\delta\iota_i(s)}\right\rangle,$$

$$= \int_0^t ds \langle \iota_i(t)\iota_i(s)\rangle \left\langle \frac{\delta[x_i(t)]}{\delta\iota_i(s)}\frac{\delta[\delta(x_i(t)-x)]}{\delta x_i(t)}\delta\left(x'-x_i(t')\right)\right\rangle$$

$$+ \int_0^{t'} ds \langle \iota_i(t)\iota_i(s)\rangle \left\langle \frac{\delta[x_i(t')]}{\delta\iota_i(s)}\delta\left(x_i(t)-x\right)\frac{\delta[\delta(x_i(t')-x')]}{\delta x_i(t')}\right\rangle,$$

$$= -\frac{\partial}{\partial x}\int_0^t ds\ \langle \iota_i(t)\iota_i(s)\rangle \left\langle \frac{\delta[x_i(t)]}{\delta\iota_i(s)}\delta(x_i(t)-x)\delta\left(x_i(t')-x'\right)\right\rangle \qquad (\text{B.8a})$$

$$- \frac{\partial}{\partial x'}\int_0^{t'} ds\ \langle \iota_i(t)\iota_i(s)\rangle \left\langle \frac{\delta[x_i(t')]}{\delta\iota_i(s)}\delta\left(x_i(t)-x\right)\delta(x_i(t')-x')\right\rangle. \quad (\text{B.8b})$$

As in Eq. (B.4), the derivative has been changed through the delta function and the independence of $x_i(t)$ from x and $x_i(t')$ from x' has been used.

The first term, labeled by (B.8a), is essentially identical to that of Eq. (B.7) becoming

$$-D\lambda(t)^2\frac{d}{dt}\left[\int_0^t ds\ \lambda(s^2)\right]\frac{\partial}{\partial x}P_2(x,t;x',t'), \qquad (\text{B.9})$$

when the functional derivative is evaluated. The second term, labeled by (B.8b), can

Appendix B. Derivation of Equations for the Joint Probability Distributions

be simplified as

$$- D\lambda(t)\lambda(t') \int\limits_0^{t'} ds \frac{d}{dt}\frac{d}{ds}\left[\int\limits_0^s ds' \frac{\lambda(t-s')}{\lambda(t)}\frac{\lambda(s-s')}{\lambda(s)}\right] \frac{\partial}{\partial x'}P_2(x,t;x',t')$$

$$= -2D\lambda(t)\frac{d}{dt}\left[\int\limits_0^{t'} ds \frac{\lambda(t-s)\lambda(t'-s)}{\lambda(t)}\right] \frac{\partial}{\partial x'}P_2(x,t;x',t'). \tag{B.10}$$

Inserting both Eq. (B.9) and Eq. (B.10) into Eq. (B.2b) and the result is the Fokker-Planck equation for the two-time probability distribution given in Eq. (4.15b).

Appendix C

Solution to Joint Probability Distribution Equations

We derive here the one- and two-time propagators from their respective Fokker-Planck equations, given in Eqs. (4.15).

Following a Fourier transform (dual for the two-time equation) where k (and k') is the Fourier variable that correspond with the spatial coordinates x (and x', respectively), the two equations become

$$\left[\frac{\partial}{\partial t} + A(t)k\frac{\partial}{\partial k}\right]\widehat{P}_1(k,t) = -\left(ikB(t) + k^2D(t)\right)\widehat{P}_1(k,t), \tag{C.1a}$$

$$\left[\frac{\partial}{\partial t} + A(t)k\frac{\partial}{\partial k}\right]\widehat{P}_2(k,t;k',t') = -\left(ikB(t) + kk'C(t,t') + k^2D(t)\right)\widehat{P}_2(k,t;k',t'). \tag{C.1b}$$

Here, $\widehat{P}_1(k,t)$ is the Fourier transform of $P_1(x,t)$ and $\widehat{P}_2(k,t;k',t')$ is the dual Fourier transform of $P_2(x,t;x',t')$. Both of Eqs. (C.1) are first-order partial differential equations and, therefore, amenable to the use of the method of characteristics with respect to k and t. The variables k' and t' are to be treated as parameters.

Per the method of characteristics, the variable s is defined along each of the characteristic curves. Thus, the bracketed term in both equations is treated as a

Appendix C. Solution to Joint Probability Distribution Equations

total derivative, i.e.,

$$\frac{d}{ds} = \frac{\partial}{\partial t} + A(t)k\frac{\partial}{\partial k}.$$

We have then the functional dependence of the characteristic variable s on the variables k and t as

$$s = t, \qquad k = \frac{k_0}{\lambda(s)},$$

where k_0 is the constant of integration for k-integral (that of the t-integral has been set equal to 0.)

We solve Eq. (C.1a) first. By rewriting k in terms of s along with the explicit insertion of the coefficients, whose expressions are given in Eqs. (4.16) we have

$$\frac{d}{ds}\widehat{P}_1(s) = \left[\frac{d}{ds}\left(i\left[\frac{k_0}{\lambda(s)}\right]\Phi(s) - \left[\frac{k_0}{\lambda(t)}\right]^2 D \int_0^s dr\ \lambda^2(r)\right)\right]\widehat{P}_1(s), \qquad (C.2)$$

A rearrangement of terms in Eq. (C.2) allows both sides to be rewritten in terms of a total derivative

$$d\left[\ln\widehat{P}_1(s)\right] = d\left[\left(i\left[\frac{k_0}{\lambda(s)}\right]\Phi(s) - \left[\frac{k_0}{\lambda(t)}\right]^2 D \int_0^s dr\ \lambda^2(r)\right)\right].$$

Taking the lower limit of the integral to be $s = 0$, with initial condition taken to be localized, i.e., $P_1(x,t) = \delta(x - x_0)$, and the upper limit to be $s = t$, we have

$$\widehat{\Pi}_1(s|x_0, 0) = \exp\left\{ik_0 x_0 + i\left[\frac{k_0}{\lambda(t)}\right]\Phi(t) - \left[\frac{k_0}{\lambda(t)}\right]^2 D \int_0^t dr\lambda^2(r)\right\}. \qquad (C.3)$$

Reinserting k_0 into Eq. (C.3), the expression for the one-time propagator in the Fourier-domain is

$$\widehat{\Pi}_1(k, t|x_0, 0) = \exp\left\{ik\lambda(t)x_0 + ik\Phi(t) - k^2 D \int_0^t dr\lambda^2(r)\right\}. \qquad (C.4)$$

An inverse Fourier transform of Eq. (C.4) results in the one-time propagator that we have given in Eq. (4.18a).

Appendix C. Solution to Joint Probability Distribution Equations

The procedure for the two-time propagator is slightly complicated by the presence of k' and t' as parameters. The rewriting k in terms of s and insertion of the coefficients results in

$$\frac{d}{ds}\widehat{P}_2(s;k',t') = \left[\frac{d}{ds}\left(i\left[\frac{k_0}{\lambda(s)}\right]\Phi(s) - 2\left[\frac{k_0}{\lambda(s)}\right]k'D\int_0^{t'}dr\;\lambda(s-r)\lambda(t'-r)\right.\right.$$
$$\left.\left. - \left[\frac{k_0}{\lambda(s)}\right]^2 D\int_0^s dr\;\lambda^2(r)\right)\right]\widehat{P}_2(s;k',t'). \qquad (C.5)$$

Eq. (C.5) can also be rearranged into a total derivative:

$$d\left[\ln\widehat{P}_2(s;k',t')\right] = d\left[i\left[\frac{k_0}{\lambda(s)}\right]\Phi(s) - 2\left[\frac{k_0}{\lambda(s)}\right]k'D\int_0^{t'}dr\lambda(s-r)\lambda(t'-r)\right.$$
$$\left. - \left[\frac{k_0}{\lambda(s)}\right]^2 D\int_0^s dr\;\lambda^2(r)\right].$$

Care must be taken due to the 'delayed' initial condition, i.e., $\delta(x-x')\Pi_1(x',t'|x_0,0)$, which is specified at the time t'. The lower limit of the total derivative is then evaluated at $s = t'$, with $k_0' = k_0/\lambda(t')$ being the initial k value; the upper limit is evaluated at $s = t$. We have then

$$\widehat{\Pi}_2(s;k',t'|x_0,0) = \widehat{\Pi}_1\left(\frac{k_0}{\lambda(t')}+k',t'|x_0,0\right)\exp\left\{i\left[\frac{k_0}{\lambda(t)}\right]\Phi(t)+i\left[\frac{k_0}{\lambda(t')}\right]\Phi(t')\right.$$
$$-2\left[\frac{k_0}{\lambda(t)}\right]k'D\int_0^{t'}dr\;\lambda(t-r)\lambda(t'-r)+2\left[\frac{k_0}{\lambda(t')}\right]k'D\int_0^{t'}dr\;\lambda^2(r)$$
$$\left.-\left[\frac{k_0}{\lambda(t)}\right]^2 D\int_0^t dr\;\lambda^2(r)+\left[\frac{k_0}{\lambda(t')}\right]^2 D\int_0^{t'}dr\;\lambda^2(r)\right\}. \qquad (C.6)$$

156

Appendix C. Solution to Joint Probability Distribution Equations

Reinsertion of k results in

$$\widehat{\Pi}_2(k,t;k',t'|x_0,0) = \widehat{\Pi}_1\left(k\frac{\lambda(t)}{\lambda(t')} + k', t'|x_0,0\right)\exp\left\{ik\Phi(t) - ik\left[\frac{\lambda(t)}{\lambda(t')}\right]\Phi(t')\right.$$

$$-2kk'D\int_0^{t'} dr\,\lambda(t-r)\lambda(t'-r) + 2kk'\left[\frac{\lambda(t)}{\lambda(t')}\right]D\int_0^{t'} dr\,\lambda^2(r)$$

$$\left. -k^2 D\int_0^{t} dr\,\lambda^2(r) + k^2\left[\frac{\lambda(t)}{\lambda(t')}\right]^2 D\int_0^{t'} dr\,\lambda^2(r)\right\}. \tag{C.7}$$

When the expression for the one-time propagator is inserted into Eq. (C.7), we have

$$\widehat{\Pi}_2(k,t;k',t'|x_0,0) = \exp\left\{ik(\lambda(t)x_0 + \Phi(t)) + ik'(\lambda(t')x_0 + \Phi(t'))\right.$$

$$\left. -\left(k^2 D\int_0^{t} dr\,\lambda(t)^2 + 2kk'D\int_0^{t'} dr\,\lambda(t-r)\lambda(t'-r) + k'^2 D\int_0^{t'} dr\,\lambda^2(r)\lambda^2(r)\right)\right\}. \tag{C.8}$$

Eq. (C.8) is simply the Fourier-domain expression for a bivariate Gaussian with means given by $\lambda(t)x_0 + \Phi(t)$ and $\lambda(t')x_0 + \Phi(t')$, variances given by $\sqrt{2DT(t)}$ and $\sqrt{2DT(t')}$, and covariance given by $N(t,t')$. An inverse Fourier transform of Eq. (C.8) therefore results in the two-time propagator that we have given in Eq (4.18b):

References

[1] H. Risken. *The Fokker Planck Equation, Methods of Solution and Application.* Springer Verlag, Berlin, Heidelberg, 1989.

[2] L. E. Reichl. *A Modern Course in Statistical Physics.* Wiley, Weinheim, 2009.

[3] L. Giuggioli and V. M. Kenkre. Consequences of animal interactions on their dynamics: Emergence of home ranges and territoriality. *Mov. Ecol.*, 2:20, 2014.

[4] V. M. Kenkre. Analytic formulation, exact solutions, and generalizations of the elephant and the alzheimer random walks. *arXiv preprint arXiv:0708.0034*, Aug 2007.

[5] T. J. McKetterick and L. Giuggioli. Exact dynamics of stochastic linear delayed systems: Application to spatiotemporal coordination of comoving agents. *Phy. Rev. E*, 90(4):042135, 2014.

[6] L. Giuggioli, T. J. McKetterick, and M. Holderied. Delayed response and biosonar perception explain movement coordination in trawling bats. *PLoS Comput. Biol.*, 11:e1004089, 2015.

[7] E. A. Novikov. Functionals and the random-force method in turbulence theory. *Sov. Phys. JETP*, 20:1290–1294, 1965.

[8] N. G. van Kampen. *Stochastic Processes in Physics and Chemistry.* Elsevier, Amsterdam, third edition, 2007.

[9] D. Boyer and C. Solis-Salas. Random walks with preferential relocations to places visited in the past and their application to biology. *Phys. Rev. Lett.*, 112:240601, 2014.

[10] S. Trimper and G.M. Schutz. Elephants can always remember: Exact long-range memory effects in a non-Markovian random walk. *Phys. Rev. E*, 70:045101, 2004.

References

[11] A. A. Budini and M. O. Cáceres. Functional characterization of generalized Langevin equations. *J. Phys. A: Math. Gen*, 37:5959–5981, 2004.

[12] A. A. Budini and M. O. Cáceres. Delay and memory-like Langevin equations. *Physica A*, 356:31–36, 2005.

[13] R. Metzler and J. Klafter. The random walk's guide to anomalous diffusion: a fractional dynamics approach. *Phys. Rep.*, 339:1–77, 2000.

[14] J. E. Fiscina, M. O. Cáceres, and F. Mücklich. On the spectrum behavior of vibrated granular matter. *J. Phys.: Condens. Matter*, 17:S1237, 2005.

[15] A. D. Drozdov. Fractional oscillator driven by a Gaussian noise. *Physica A*, 376:237–245, 2007.

[16] A. O. Bolivar. Non-Markovian effects on the Brownian motion of a free particle. *Physica*, 390:3095–3107, 2011.

[17] A. K. Das, S. Panda, and J. R. L. Santos. A path integral approach to the Langevin equation. *Int. J. Mod. Phys. A*, 30:1550028, 2015.

[18] M. San Miguel and J. M. Sancho. A colored-noise approach to Brownian motion in position space. corrections to the Smoluchowski equation. *J. Stat. Phys.*, 22:605–624, 1980.

[19] R. Gorenflo, A. A. Kilbas, F. Mainardi, and S. V. Rogosin. *Mittag-Leffler Functions, Related Topics and Applications*. Springer-Verlag, Berlin, 2014.

[20] M. Abramowitz and I. E. Stegun. *Handbook of Mathematical Functions*. Dover Publications, Toronto, 1970.

[21] R. E. Bellman and K. L. Cooke. *Differential-Difference Equations*. RAND Corporation, Santa Monica, CA, 1963.

[22] U. Küchler and B. Mensch. Langevins stochastic differential equation extended by a time-delayed term. *Stoc. Stoc. Rep.*, 40:23–42, 1992.

[23] F. M. Asl and A. G. Ulsoy. Analysis of a system of linear delay differential equations. *J. Dyn. Syst. Meas. Control*, 125:215–223, 2003.

[24] A. A. Budini and M. O. Cáceres. Functional characterization of linear delay Langevin equations. *Phys. Rev. E*, 70:046104, 2004.

[25] M. Chase, T. J. McKetterick, L. Giuggioli, and V. M. Kenkre. Langevin analysis for time-nonlocal Brownian motion with algebraic memories and delay interactions. *Eur. Phys. J. B*, 89:1–15, 2016.

References

[26] L. Euler. De serie lambertina plurimisque eius insignibus proprietatibus. *Acta Acad. Scient. Petropol*, 2:29–51, 1783.

[27] V. M. Kenkre. Coupled wave-like and diffusive motion of excitons. *Phys. Lett. A*, 47:119–120, 1974.

[28] V. M. Kenkre. The master equation approach: Coherence, energy transfer, annihilation, and relaxation. In *Exciton Dynamics in Molecular Crystals and Aggregates*, volume 94 of *Springer Tracts in Modern Physics*, pages 1–109. Springer, Berlin, 1982.

[29] V. M. Kenkre. Mathematical methods for the description of energy transfer. In B. di Bartolo, editor, *Proceedings of a NATO Advanced Study Institute on Energy Transfer Processes in Condensed Matter, held in Erice, Italy, June 16-30, 1983*, pages 205–249, New York, 1984. Springer.

[30] R. Kubo. Fluctuation, relaxation, and resonance. In D. Ter Haar, editor, *Magnetic Systems Scottish Universities' Summer School*, volume 2. Oliver and Boyd, Edinburgh, 1961.

[31] C. P. Slichter. *Principles of Magnetic Resonance*. Springer Series in Solid-State Sciences. Springer-Verlag, Berlin, second edition, 1978.

[32] T. Springer. *Quasielastic Neutron Scattering for the Investigation of Diffusive Motions in Solids and Liquids*. Springer Tracts in Modern Physics, Vol 64. Springer, Berlin, 1972.

[33] D. W. Brown and V. M. Kenkre. Quasielastic neutron scattering in metal hydrides: Effects of the quantum mechanical motion of interstitial hydrogen atoms. In P. Jena and C. Satterthwaite, editors, *Electronic Strucutre and Properties of Hydrogen in Metals*, pages 177–182. Plenum, New York, 1983.

[34] V. M. Kenkre and D. W. Brown. Exact solutions of the stochastic Liouville equation and application to an evaluation of the neutron scattering function. *Phys. Rev. B*, 31:2479–2487, 1985.

[35] D. W. Brown and V. M. Kenkre. Coupling of tunneling and hopping transport interactions in neutron scattering lineshapes. *J. Phys. Chem. Solids*, 46:579–583, 1985.

[36] D. W. Brown and V. M. Kenkre. Neutron scattering lineshapes for nearly-incoherent transport on non-Bravais lattices. *J. Phys. Chem. Solids*, 47:289–293, 1986.

References

[37] D. W. Brown and V. M. Kenkre. Calculation of neutron scattering lineshapes exhibiting the dynamical destruction of eigenstates. *J. Phys. Chem. Solids*, 35:456, 1987.

[38] Y. Jung, E. Barkai, and R. Silbey. Lineshape theory and photon counting statistics for blinking quantum dots: a Lévy walk process. *Chem. Phys.*, 284:181–194, 2002.

[39] V. M. Kenkre and F. Sevilla. Thoughts about anomalous diffusion: Time-dependent coefficients versus memory functions. In T. S. Ali and K. B. Sinha, editors, *Contributions to Mathematical Physics: a Tribute to Gerard G. Emch*, pages 147–160. Hindustani Book Agency, New Delhi, 2007.

[40] R. Balescu. On the approach to non-equilibrium stationary states and the theory of transport coefficients. *Physica*, 27:693–706, 1961.

[41] R.J. Swenson. A note on the formal theory of transport coefficients. *Physica*, 29:1174–1180, 1963.

[42] L. van Hove. The approach to equilibrium in quantum statistics: a perturbation treatement to general order. *Physica*, 23:441–480, 1957.

[43] I. Prigogine and P. Résibois. On the kinetics of the approach to equilibrium. *Physica*, 27:629–646, 1961.

[44] E. W. Montroll. In E. G. D. Cohen, editor, *Fundamental Problems in Statistical Mechanics (Proceedings of the NUFFIC International Summer Course in Science at Nijenrode Castle, the Netherlands, August 1961)*, page 230. North Holland, Amsterdam, 1962.

[45] R. J. Swenson. Derivation of generalized master equations. *J. Math. Phys.*, 3:1017–1022, 1962.

[46] P. Résibois. On the equivalence between two generalized Master equations. *Physica*, 29:721–741, 1963.

[47] R. Zwanzig. On the identity of three generalized Master equations. *Physica*, 30:1109–1123, 1964.

[48] V. Čápek. Stationary quantities and Markovian kinetic equations. *Czech. J. Phys. B*, 34:1246–1252, 1984.

[49] P. Allegrini, G. Aquino, P. Grigolini, L. Palatella, and A. Rosa. Generalized Master equation via aging continuous-time random walks. *Phys. Rev. E*, 68:056123, 2003.

References

[50] S. Burova, R. Metzlerb, and E. Barkai. Aging and nonergodicity beyond the Khinchin theorem. *Proc. Natl Acad. Sci. U.S.A.*, 107:13228–13233, 2010.

[51] A. Dechant, E. Lutz, D. A. Kessler, and E. Barkai. Scaling Green-Kubo relation and application to three aging systems. *Phys. Rev. X*, 4:011022, 2014.

[52] A. S. Adelman. The effective direct correlation function: An approach to the theory of liquid solutions. *J. Chem. Phys.*, 64:724–731, 1976.

[53] R. F. Fox. The generalized Langevin equation with Gaussian fluctuations. *J. Stat. Phys.*, 18:2331–2335, 1977.

[54] P. Hänggi. Correlation functions and Master equations of generalized non-Markovian Langevin equations. *Z. Phys. B Con. Mat.*, 31:407–416, 1978.

[55] P. Hänggi and P. Talkner. On the equivalence of time-convolutionless Master equations and generalized Langevin equations. *Phys. Lett. A*, 68:9–11, 1978.

[56] P. Hänggi, H. Thomas, H. Grabert, and P. Talkner. Note on time evolution of non-Markov processes. *J. Stat. Phys.*, 18:155–159, 1978.

[57] P. Hänggi. The functional derivative and its use in the description of noisy dynamical systems. In L. Pesquera and M. Rodriguez, editors, *Stochastic Processes Applied to Physics*, pages 69–95. World Scientific, Philadelphia, 1985.

[58] P. Hänggi. Colored noise in continuous dynamical systems: A functional calculus approach. In F. Moss and P. V. E. McClintock, editors, *Noise in Nonlinear Dynamical Systems*, volume 1, pages 307–328. Cambridge University Press, Cambridge, 1989.

[59] P. Hänggi and P. Jung. Colored noise in dynamical systems. In I. Prigogine and S. Rice, editors, *Advances in Chemical Physics*, volume 89, pages 239–326. John Wiley & Sons, 1995.

[60] P. Hänggi and H Thomas. Time evolution, correlations, and linear response of non-Markov processes. *Z. Phys. B Con. Mat.*, 26:85–92, 1977.

[61] L. Giuggioli, T. J. McKetterick, V. M. Kenkre, and M. Chase. Fokker?planck description for a linear delayed langevin equation with additive gaussian noise. *J. Phys. A*, 49:384002, 2016.

[62] T. Ohira and J. G. Milton. Delayed random walks. *Phys. Rev. E*, 52:3277–3280, 1995.

References

[63] S. Guillouzic, I. L'Heureux, and A. Longtin. Small delay approximation of stochastic delay differential equations. *Phys. Rev. E*, 59:3970–3982, 1999.

[64] T. D. Frank and P. J. Beek. Stationary solutions of linear stochastic delay differential equations: Applications to biological systems. *Phys. Rev. E*, 64:021917, 2001.

[65] T. D. Frank. A Markov approach to nonlinear multivariate delay systems with noise. *Phys. Scr.*, 68:333–336, 2003.

[66] T. D. Frank. Kramers-Moyal expansion for stochastic differential equations with single and multiple delays: Applications to financial physics and neurophysics. *Phys. Lett. A*, 360:552–562, 2007.

[67] K. Spendier, S. Sugaya, and V. M. Kenkre. Reaction-diffusion theory in the presence of an attractive harmonic potential. *Phys. Rev. E*, 88:062142, 2013.

[68] V. M. Kenkre and S. Sugaya. Theory of the transmission of infection in the spread of epidemics: Interacting random walkers with and without confinement. *Bull. Math. Biol.*, 76:3016–3027, 2014.

[69] T. L. Yates, J. N. Mills, C. A. Parmenter, T. G. Ksiazek, R. R. Parmenter, J. R. V. Castle, C. H. Calisher, S. T. Nichol, K. D. Abbott, J. C. Youngand M. L. Morrison, B. J. Beaty, J. L. Dunnum, R. J. Baker, J. Salazar-Bravo, and C. J. Peters. The ecology and evolutionary history of an emergent disease: hantavirus pulmonary syndrome. *J. Bioscience*, 52:989–998, 2002.

[70] M. C. Wang and G. E. Uhlenbeck. On the theory of the Brownian motion ii. *Rev. Mod. Phys.*, 17:323–42, 1945.

[71] Mr. Bayes and Mr. Price. An essay towards solving a problem in the doctrine of chances. *Phil. Trans.*, pages 370–418, 1763.

[72] L. Isserlis. On a formula for the product-moment coefficient of any order of a normal frequency distribution in any number of variables. *Biometrika*, 12:134–139, 1918.

[73] A. Hernández-Machado, J. M. Sancho, M. San Miguel, and L. Pesquera. Joint probability distribution of non-Markovian SDE. *Z. Phys. B Con. Mat.*, 52:335–343, 1983.

[74] L. M. Ricciardi and L. Sacerdote. On the probability densities of an Ornstein-Uhlenbeck process with a reflecting boundary. *J. Appl. Probab.*, 24:355–369, 1987.

References

[75] G. Wilemski and M. Fixman. General theory of diffusion-controlled reactions. *J. Chem. Phys.*, 58:4009–4019, 1973.

[76] V. M. Kenkre. A theoretical approach to exciton trapping in systems with arbitrary trap concentration. *Chem. Phys. Lett.*, 93:260–263, 1982.

[77] D. C. Torney and H. M. McConnell. Diffusion-limited reactions in one dimension. *J. Phys. Chem.*, 87:1941–1951, 1983.

[78] S. H. Park, H. Peng, S. Parus, H. Taitelbaum, and R. Kopelman. Spatially and temporally resolved studies of convectionless photobleaching kinetics: Line trap. *J. Phys. Chem. A*, 106:7586–7592, 2002.

[79] M. Hoyuelos and H. O. Mártin. Rate equation of the a+a→a reaction with probability of reaction and diffusion. *Phys. Rev. E*, 48:3309, 1993.

[80] R. C. Wade, R. R. Gabdoulline, S. K. Lüdemann, and V. Lounnas. Electrostatic steering and ionic tethering in enzyme–ligand binding: Insights from simulations. *Proc. Natl. Acad. Sci. U.S.A.*, 95:5942–5949, 1998.

[81] D. R. Livesay, P. Jambeck, A. Rojnuckarin, and S. Subramaniam. Conservation of electrostatic properties within enzyme families and superfamilies. *Biochemistry*, 42:3464–3473, 2003.

[82] B. Goldstein, C. Wofsy, and H. Echavarria-Heras. Effect of membrane flow on the capture of receptors by coated pits: Theoretical results. *Biophys. J.*, 53:405–414, 1988.

[83] C. R. F. Monks, B. A. Freiberg, H. Kupfer, N. Sciaky, and A. Kupfer. Three-dimensional segregation of supramolecular activation clusters in t cells. *Nature*, 395:82–86, 1998.

[84] V. M. Kenkre, L. Giuggioli, and Z. Kalay. Molecular motion in cell membranes: analytic study of fence-hindered random walks. *Phys. Rev. E*, 77:051907, 2008.

[85] H. W. Sohn, P. Tolar, and S. K. Pierce. Membrane heterogeneities in the formation of b cell receptor–lyn kinase microclusters and the immune synapse. *J. Cell Biol.*, 182:367–379, 2008.

[86] K. Spendier, A. Carroll-Portillo, K. A. Lidke, B. S. Wilson, J. A. Timlin, and J. L. Thomas. Distribution and dynamics of rat basophilic leukemia immunoglobulin e receptors (fcεri) on planar ligand-presenting surfaces. *Biophys. J.*, 99:388–397, 2010.

References

[87] W. Ebeling, F. Schweitzer, and B. Tilch. Active Brownian particles with energy depots modeling animal mobility. *Biosystems*, 49:17–29, 1999.

[88] L. Giuggioli, G. Abramson, V. M. Kenkre, G. Suzán, E. Marcé, and T. L. Yates. Diffusion and home range parameters from rodent population measurements in Panama. *Bull. Math. Biol.*, 67:1135–1149, 2005.

[89] L. Giuggioli, G. Abramson, V. M. Kenkre, R. R. Parmenter, and T. L. Yates. Theory of home range estimation from displacement measurements of animal populations. *J. Theor. Biol.*, 240:126–135, 2006.

[90] M. Aldana, V. Dossetti, C. Huepe, V. M. Kenkre, and H. Larralde. Phase transitions in systems of self-propelled agents and related network models. *Phys. Rev. Lett.*, 98:095702, 2007.

[91] U. Diekmann, R. Law, and J. A. J. Metz, editors. *The Geometry of Ecological Interactions: Simplifying Spatial Complexity*. Cambridge University Press, Cambridge, 2000.

[92] A. Okubo and S. A. Levin. *Diffusion and Ecological Problems: Modern Perspectives*, volume 14. Springer-Verlag, New York, 2001.

[93] A. J. McKane and T. J. Newman. Stochastic models in population biology and their deterministic analogs. *Phys. Rev. E*, 70:041902, 2004.

[94] V. M. Kenkre, L. Giuggioli, G. Abramson, and G. Camelo-Neto. Theory of hantavirus infection spread incorporating localized adult and itinerant juvenile mice. *Eur. Phys. J. B*, 55:461–470, 2007.

[95] S. Sugaya. *The Smoluchowski Equation in Population Dynamics and the Spread of Infection*. PhD thesis, University of New Mexico, 2016.

[96] M. von Smoluchowski. Drei vortrage uber diffusion, brownsche bewegung und koagulation von kolloidteilchen. *Z. Phys.*, 17:557–585, 1916.

[97] Gene Lamm and Klaus Schulten. Extended Brownian dynamics approach to diffusion-controlled processes. *J. Chem. Phys.*, 75:365–371, 1981.

[98] G. Lamm and K. Schulten. Extended Brownian dynamics. ii. reactive, nonlinear diffusion. *J. Chem. Phys.*, 78:2713–2734, 1983.

[99] G. Lamm. Extended Brownian dynamics. iii. three-dimensional diffusion. *J. Chem. Phys.*, 80:2845–2855, 1984.

References

[100] G. E. Roberts and H. Kaufman. *Table of Laplace Transforms*. W. B. Saunders Company, Philadelphia, 1966.

[101] H. C. Wolf. Energy transfer in organic molecular crystals: a survey of experiments. *Adv. At. Mol. Phys.*, 3:119–142, 1967.

[102] R. C. Powell and Z. G. Soos. Singlet exciton energy transfer in organic solids. *J. Lumin.*, 11:1–45, 1975.

[103] D. M. Hanson. Effect of an external electric field on electronic excitation energy transfer in molecular crystals: A new probe of the microscopic dynamics. *Mol. Cryst. Liq. Cryst.*, 57:243–253, 1980.

[104] J. S. Patel and D. M. Hanson. Experimental observations of the effect of an electric field on exciton motion in molecular crystals. *J. Chem. Phys.*, 75:5203–5205, 1981.

[105] C. B. Harris and D. A. Zwemer. Coherent energy transfer in solids. *Ann. Rev. Phys. Chem.*, 29:473–495, 1978.

[106] E. W. Montroll. Stochastic processes and chemical kinetics. In *Energetics in Metallurgical Phenomena*, volume 3, pages 125–187. Gordon and Breach, New York, 1967.

[107] V. M. Kenkre and Y. M. Wong. Effect of transport coherence on trapping: Quantum-yield calculations for excitons in molecular crystals. *Phys. Rev. B*, 23:3748–3755, 1980.

[108] R. J. Rubin and G. H. Weiss. Random walks on lattices. the problem of visits to a set of points revisited. *J. Math. Phys.*, 23:250–253, 1982.

[109] V. M. Kenkre and P. E. Parris. Exciton trapping and sensitized luminescence: A generalized theory for all trap concentrations. *Phys. Rev. B*, 27:3221–3234, 1983.

[110] A. Szabo, G. Lamm, and G. H. Weiss. Localized partial traps in diffusion processes and random walks. *J. Stat. Phys.*, 34:225–238, 1984.

[111] K. Spendier and V. M. Kenkre. Analytic solution for some reaction-diffusion scenarios. *J. Phys. Chem. B*, 117:15639–15650, 2013.

[112] T. Yokosuka, K. Sakata-Sogawa, W. Kobayashi, M. Hiroshima, A. Hashimoto-Tane, M. Tokunaga, M. L. Dustin, and T. Saito. Newly generated t-cell receptor microclusters initiate and sustain t-cell activation by recruitment of zap70 and slp-76. *Nat. Immunol.*, 6:1253–1262, 2005.

References

[113] C. R. F. Monks, B. A. Freiberg, H. Kupfer, N. Sciaky, and A. Kupfer. Three-dimensional segregation of supramolecular activation clusters in t cells. *Nature*, 395:82–86, 1998.

[114] J. B. Huppa and M. M. Davis. T-cell-antigen recognition and the immunological synapse. *Nat. Rev. Immunol.*, 3:973–983, 2003.

[115] M. L. Dustin, A. K. Chakraborty, and A. S. Shaw. Understanding the structure and function of the immunological synapse. *Cold Spring Harbor Perspect. Biol.*, 2:a002311, 2010.

[116] M. L. Dustin and J. A. Cooper. The immunological synapse and the actin cytoskeleton: molecular hardware for t cell signaling. *Nat. Immunol.*, 1:23–29, 2000.

[117] A. Babich, S. Li, R. S. O'Connor, M. C. Milone, B. D. Freedman, and J. K. Burkhardt. F-actin polymerization and retrograde flow drive sustained plcγ1 signaling during t cell activation. *J. Cell Biol.*, 197:775–787, 2012.

[118] Y. Yu, N. C. Fay, A. A. Smoligovets, H. J. Wu, and J. T. Groves. Myosin iia modulates t cell receptor transport and casl phosphorylation during early immunological synapse formation. *PLOS ONE*, 7:e30704, 2012.

[119] A. L. DeMond, K. D. Mossman, T. Starr, M. L. Dustin, and J. T. Groves. T cell receptor microcluster transport through molecular mazes reveals mechanism of translocation. *Biophys. J.*, 94:3286–3292, 2008.

[120] C. H. Yu, H. J. Wu, Y. Kaizuka, R. D. Vale, and J. T. Groves. Altered actin centripetal retrograde flow in physically restricted immunological synapses. *PLOS ONE*, 5:e11878, 2010.

[121] T. D. Pollard and J. Berro. Mathematical models and simulations of cellular processes based on actin filaments. *J. Biol. Chem.*, 284:5433–5437, 2009.

[122] Y. Cai, N. Biais, G. Giannone, M. Tanase, G. Jiang, J. M. Hofman, C. H. Wiggins, P. Silberzan, A. Buguin, B. Ladoux, and M. P. Sheetz. Nonmuscle myosin iia-dependent force inhibits cell spreading and drives f-actin flow. *Biophys. J.*, 91:3907–3920, 2006.

[123] Y. Yu, A. A. Smoligovets, and J. T. Groves. Modulation of t cell signaling by the actin cytoskeleton. *J. Cell Sci.*, 126:1049–1058, 2013.

[124] F. Seitz. *The Modern Theory of Solids.* McGraw-Hill, New York, 1940.

References

[125] R. K. Clayton. *Photosynthesis: Physical Mechanisms and Chemical Patterns*, volume 4. Cambridge Univ. Press, Cambridge, 1980.

[126] H. C. Wolf and H. Port. Excitons in aromatic crystals: trap states, energy transfer and sensitized emission. *J. Lumin.*, 12:33–46, 1976.

[127] D. D. Smith, R. C. Powell, and A. H. Zewail. Direct measurement of excitation transport in a highly disordered quasi-one-dimensional solid. *Chem. Phys. Lett.*, 68:309–313, 1979.

[128] V. M. Kenkre, P. E. Parris, and D. Schmid. Investigation of the appropriateness of sensitized luminescence to determine exciton motion parameters in pure molecular crystals. *Phys. Rev. B*, 32:4946–4955, 1985.

[129] D. P. Gaver Jr. Observing stochastic processes, and approximate transform inversion. *Oper. Res.*, 14:444–459, 1966.

[130] J. Abate and W. Whitt. A unified framework for numerically inverting Laplace transforms. *INFORMS J. Comp.*, 18:408–421, 2006.

[131] M. Chase, K. Spendier, and V. M. Kenkre. Analysis of confined random walkers with applications to processes occurring in molecular aggregates and immunological systems. *J. Phys. Chem. B*, 120:3072–3080, 2016.

[132] A. Laubereau and W. Kaiser. Vibrational dynamics of liquids and solids investigated by picosecond light pulses. *Rev. Mod. Phys.*, 50:605–665, 1978.

[133] S. H. Lin and H. Eyring. Stochastic processes in physical chemistry. *Annu. Rev. Phys. Chem.*, 25:39–77, 1974.

[134] D. W. Oxtoby. Vibrational relaxation in liquids. *Annu. Rev. Phys. Chem*, 32:77–101, 1981.

[135] D. D. Dlott and M. D. Fayer. Shocked molecular solids: vibrational up pumping, defect hot spot formation, and the onset of chemistry. *J. Chem. Phys.*, 92:3798–3812, 1990.

[136] A. Tokmakoff, B. Sauter, A. S. Kwok, and M. D. Fayer. Phonon-induced scattering between vibrations and multiphoton vibrational up-pumping in liquid solution. *Chem. Phys. Lett*, 221:412–418, 1994.

[137] A. Tokmakoff, B. Sauter, and M. D. Fayer. Temperature-dependent vibrational relaxation in polyatomic liquids: Picosecond infrared pump-probe experiments. *J. Chem. Phys*, 100:9035–9043, 1994.

References

[138] R. J. Rubin and K. E. Shuler. Relaxation of vibrational nonequilibrium distributions. i. collisional relaxation of a system of harmonic oscillators. *J. Chem. Phys.*, 25:59–67, 1956.

[139] R. J. Rubin and K. E. Shuler. Relaxation of vibrational nonequilibrium distributions. ii. the effect of the collisional transition probabilities on the relaxation behavior. *J. Chem. Phys.*, 25:68–74, 1956.

[140] R. J. Rubin and K. E. Shuler. On the relaxation of vibrational nonequilibrium distributions. iii. the effect of radiative transitions on the relaxation behavior. *J. Chem. Phys.*, 26:137–142, 1957.

[141] E. W. Montroll and K. E. Shuler. Studies in nonequilibrium rate processes. i. the relaxation of a system of harmonic oscillators. *J. Chem. Phys.*, 26:454–464, 1958.

[142] A. Nitzan and J. Jortner. Vibrational relaxation of a molecule in a dense medium. *Mol. Phys.*, 25:713–734, 1973.

[143] K. F. Freed and D. F. Heller. Pressure dependence of electronic relaxation: A stochastic model. *J. Chem. Phys.*, 61:3942–3953, 1974.

[144] D. J. Diestler. Theoretical studies of vibrational energy relaxation of small molecules in dense media. *Adv. Chem. Phys.*, 35:305–351, 1980.

[145] S. A. Adelman, R. Muralidhar, and R. H. Stote. Time correlation function approach to vibrational energy relaxation in liquids: Revised results for monatomic solvents and a comparison with the isolated binary collision model. *J. Chem. Phys.*, 95:2738–2751, 1991.

[146] V. M. Kenkre and V. Seshadri. Time evolution of the average energy of a relaxing molecule. *Phys. Rev. A*, 15:197–202, 1977.

[147] V. Seshadri and V. M. Kenkre. Theory of the interplay of luminescence and vibrational relaxation: A Master equation approach. *Phys. Rev. A*, 17:223–237, 1978.

[148] V. M. Kenkre, A. Tokmakoff, and M. D. Fayer. Theory of vibrational relaxation of polyatomic molecules in liquids. *J. Chem. Phys.*, 101:10618–10629, 1994.

[149] A. H. Zewail. Femtochemistry: Atomic-scale dynamics of the chemical bond. *J. Phys. Chem. A*, 104:5660–5694, 2000.

References

[150] S. K. Sundaram and E. Mazur. Inducing and probing non-thermal transitions in semiconductors using femtosecond laser pulses. *Nat. Mater.*, 1:217–224, 2002.

[151] E. Goulielmakis, Z. H. Loh, A. Wirth, R. Santra, N. Rohringer, V. S. Yakovlev, S. Zherebtsov, T. Pfeifer, A. M. Azzeer, M. F. Kling, and S. R. Leone. Real-time observation of valence electron motion. *Nature*, 466:739–743, 2010.

[152] F. P. Buff and D. J. Wilson. Some considerations of unimolecular rate theory. *J. Chem. Phys.*, 32:677–685, 1960.

[153] K. E. Shuler. On the kinetics of elementary gas phase reactions at high temperatures. *Symposium (International) on Combustion*, 5:56–74, 1955.

[154] A. Tokmakoff, M. D. Fayer, and D. D. Dlott. Chemical reaction initiation and hot-spot formation in shocked energetic molecular materials. *J. Phys. Chem.*, 97:1901–1913, 1993.

[155] K. Huang. *Statistical Mechanics*. Wiley, New York, 1987. see in particular pp. 172-3.

[156] W. H. Zurek, S. Habib, and J. P. Paz. Coherent states via decoherence. *Phys. Rev. Lett.*, 70:1187–1190, 1993.

[157] D. Giulini, E. Joos, C. Kiefer, J. Kupsch, I.-O. Stamatescu, and H. D. Zeh. *Decoherence and the Appearance of a Classical World in Quantum Theory.* Springer, Berlin, 1996.

[158] W. H. Zurek. Decoherence, einselection, and the quantum origins of the classical. *Rev. Mod. Phys.*, 75:715–775, 2003.

[159] R. Zwanzig. Ensemble method in the theory of irreversibility. *J. Chem. Phys*, 33:1338–1341, 1960.

[160] R. Zwanzig. In W. E. Brittin, B. W. Downs, and J. Downs, editors, *Lectures in Theoretical Physics*, volume 3, New York, 1961. Interscience.

[161] R. Zwanzig. Statistical mechanics of irreversibility. In P. H. E. Meijer, editor, *Quantum Statistical Mechanics*, pages 139–172. Gordon and Breach, New York, 1966.

[162] J. de Boer and G. E. Uhlenbeck. *Studies in Statistical Mechanics*, volume 1. North-Holland, Amsterdam, 1962.

References

[163] E. G. D. Cohen, editor. *Fundamental Problems in Statistical Mechanics (Proceedings of the NUFFIC International Summer Course in Science at Nijenrode Castle, the Netherlands, August, 1961)*, Amsterdam, 1962. North Holland.

[164] I. Prigogine and P. Résibois. On the approach to equilibrium of a quantum gas. *Physica*, 24:795–816, 1958.

[165] V. M. Kenkre. The generalized Master equation and its applications. In U. Landman, editor, *Statistical Mechanics and Statistical Methods in Theory and Application*, pages 441–461. Plenum, New York, 1977.

[166] V. M. Kenkre. Generalized Master equations under delocalized initial conditions. *J. Stat. Phys.*, 19:333–340, 1978.

[167] V. M. Kenkre and R. S. Knox. Generalized-Master-equation theory of excitation transfer. *Phys. Rev. B*, 9:5279–5290, 1974.

[168] V. M. Kenkre. Generalized-Master-equation analysis of a ferromagnet model. *Phys. Rev. B*, 11:3406–3412, 1975.

[169] M. Tiwari and V. M. Kenkre. Approach to equilibrium of a nondegenerate quantum system: decay of oscillations and detailed balance as separate effects of a reservoir. *Eur. Phys. J. B*, 87:1–7, 2014.

[170] P. R. Rider. Generalized Cauchy distributions. *Ann. Inst. Stat. Math.*, 9:215–223, 1957.

[171] V. M. Kenkre. Master-equation theory of the effect of vibrational relaxation on intermolecular transfer of electronic excitation. *Phys. Rev. A*, 16:766–776, 1977.

[172] H. C. Andersen, I. Oppenheim, K. E. Shuler, and G. H. Weiss. Exact conditions for the preservation of a canonical distribution in markovian relaxation processes. *J. Math. Phys.*, 5:522–536, 1964.

[173] H. C. Andersen, I. Oppenheim, K. E. Shuler, and G. H. Weiss. Nonequilibrium thermodynamics of canonically invariant relaxation processes. *J. Chem. Phys.*, 41:3012–3019, 1964.

[174] I.Tehver and V Hizhnyakov. Radiationless transfer of electronic excitation during vibrational relaxation. *Zh. Eksp. Teor. Fiz.*, 69:599, 1975. In Russian; English translation in: *Sov. Phys.-JETP* 42:305-310, 1976.

[175] H. A. Bethe and E. Teller. Deviations from thermal equilibrium in shock waves. X-117, Ballistic Research Laboratory, 1941.

References

[176] L. Landau and E. Teller. Zur theorie der schalldispersion. *Phys. Z. Sowet.*, 10:34–40, 1936.

[177] C. A. Moyer. On the Green function for a particle in a uniform electric field. *J. Phys. C*, 6:1461–1466, 1973.

[178] D. Emin and C. F. Hart. Phonon-assisted hopping of an electron on a Wannier-Stark ladder in a strong electric field. *Phys. Rev. B*, 36:2530–2546, 1987.

[179] P. M. Morse. Diatomic molecules according to the wave mechanics. ii. vibrational levels. *Phys. Rev.*, 34:57–64, 1929.

[180] J. P. Dahl and M. Springborg. The morse oscillator in position space, momentum space, and phase space. *J. Chem. Phys.*, 88:4535–4547, 1988.

[181] S. Redner and D. ben Avraham. Nearest-neighbor distances of diffusing particles from a single trap. *J. Phys. A*, 23:L1169, 1990.

[182] G. Abramson and H. S. Wio. Time behaviour for diffusion in the presence of static imperfect traps. *Chaos, Solitons Fract.*, 6:1–5, 1995.

[183] M. D. Fayer and C. B. Harris. Coherent energy migration in solids. i. band-trap equilibria at Boltzmann and non-Boltzmann temperatures. *Phys. Rev. B*, 9:748–769, 1974.

[184] D. D. Dlott, M. D. Fayer, and R. D. Wieting. Coherent one dimensional exciton transport and impurity scattering. *J. Chem. Phys.*, 67:3808–3817, 1977.

[185] D. D. Dlott, M. D. Fayer, and R. D. Wieting. Effects of impurity scattering and transport topology on exciton migration and trapping: An experimental study of quasi-one-dimensional molecular crystals. *J. Chem. Phys.*, 69:2752–2762, 1978.

[186] R. D. Wieting, M. D. Fayer, and D. D. Dlott. The effects of impurity scattering and transport topology on trapping in quasi-one dimensional systems: Application to excitons in molecular crystals. *J. Chem. Phys.*, 69:1996–2010, 1978.

[187] R. M. Shelby, A. H. Zewail, and C. B. Harris. Coherent energy migration in solids: Determination of the average coherence length in one-dimensional systems using tunable dye lasers. *J. Chem. Phys.*, 64:3192–3203, 1976.

[188] D. D. Smith, D. P. Millar, and A. H. Zewail. Energy localization in substitutionally disordered solids. ii. studies by optical and optically detected magnetic resonance spectroscopy. *J. Chem. Phys.*, 72:1187–1208, 1980.